IMPACT OF THE NON-STRUCTURAL 2 PROTEIN ON RESPIRATORY SYNCYTIAL VIRUS PATHOGENESIS

Rachael Marie Liesman

A dissertation submitted to the faculty of the University of North Carolina at Chapel Hill in partial fulfillment of the requirements for the degree of Doctor of Philosophy in the Department of Microbiology and Immunology.

Chapel Hill
2013

Approved by:

Raymond Pickles

Nancy Raab-Traub

William Goldman

Mark Heise

Barbara Sherry

ABSTRACT

Rachael Marie Liesman: Impact of the Non-structural 2 Protein on
Respiratory Syncytial Virus Pathogenesis
(Under the direction of Raymond Pickles)

Respiratory syncytial virus (RSV) infection is the major cause of bronchiolitis in young children. The factors contributing to increased propensity of RSV-induced distal airway disease compared to other commonly encountered respiratory viruses are unknown. Using a model of the well-differentiated airway epithelium, we characterized the consequences of RSV infection of ciliated epithelial cells, the primary cellular targets of RSV infection in vivo. These studies show that RSV infection results in cell rounding and degradation of the cilia apparatus, followed by active extrusion of infected cells from the epithelium, eventually resulting in a decline in the ability of the airway epithelium to perform mucociliary transport. Using recombinant respiratory viruses, we attribute these consequences to the RSV non-structural 2 (NS2) protein. Using parainfluenza virus 3 (PIV3) to deliver and express RSV NS2 in the ciliated epithelium of hamster airways, we assessed the impact of NS2 on respiratory viral pathogenesis. These studies identified the RSV NS2 protein as a unique viral genetic determinant for RSV-induced pathogenesis, resulting in two distinct effects in vivo. First, NS2 promoted epithelial cell extrusion and accelerated clearance of whole lung virus titers, presumably by clearing virus-infected cells from the airway mucosa. Second, epithelial cell extrusion promoted by NS2 resulted in accumulation of detached, pleomorphic epithelial cells in the narrow diameter bronchiolar airway lumen, resulting in acute distal airway obstruction. Finally, we identify a role for NS2 in mediating

early and robust neutrophilic influx, which may contribute to distal airway obstruction and constriction. These studies reveal a novel consequence of RSV infection of the airway epithelium, where NS2-promoted epithelial cell shedding and morphologic changes accelerate viral clearance but also cause acute distal airway obstruction. NS2-promoted epithelial cell shedding in the distal airways and the resulting obstruction of these airways represent a mechanism that may explain why RSV is the dominant virus causing bronchiolitis in young children. We identify for the first time NS2 as a pathogenesis factor for increasing the likelihood for small airway obstruction during RSV infection.

To my parents, Aaron and Joyce, and my brother, Adam. I will forever be thankful for your unwavering love, support, and confidence in me.

ACKNOWLEDGMENTS

I would like to first thank my advisor, Dr. Ray Pickles, for his mentorship and guidance throughout graduate school. I would also like to thank the members of my thesis committee, Drs. Nancy Raab-Traub, Barb Sherry, Mark Heise, and Bill Goldman, for their encouragement, guidance, and insight. I would also like to acknowledge and thank my earliest scientific mentor, Dr. Loni Walker at Illinois Wesleyan University, for introducing me to the world of scientific research and for her guidance, encouragement, and enthusiasm for teaching.

Many thanks to the members of the Pickles lab, especially Dr. Meg Scull, Dr. Nikki Worthington, Susan Burkett, Mike Tarpley, and Dr. Liqun Zhang, for their scientific contributions to this project, as well as for their advice, encouragement, and camaraderie. I would like to acknowledge and thank the members of the Department of Microbiology and Immunology and the Cystic Fibrosis Center, including the Directors and teams of the Tissue Procurement and Cell Culture Core, the Morphology and Morphometry Core, and the Michael Hooker Microscopy Facility, for their help. I would like to especially thank Dr. Robert Tarran for his guidance, advice, and friendship, and the members of the Tarran lab, who became my de facto lab mates, for their scientific support, advice, and camaraderie.

During my time in Chapel Hill, I have made so many wonderful friends and am thankful for the advice, laughter, and support that each of them has given at one time or another during my time in graduate school.

Finally, I would like to thank my family for their support and confidence in me throughout graduate school. My parents, Aaron and Joyce, are my biggest fans and their love, guidance, advice, and support is invaluable to me. My brother, Adam, has been a wonderful source of motivation, laughter, and friendship. I would also like to thank my Aunt Judy, my cousin Emily, and my entire extended family for their support, love, and encouragement. My family is an essential source of strength and love and I am incredibly thankful to have such generous and inspiring people in my life.

TABLE OF CONTENTS

LIST OF TABLES

Table

LIST OF FIGURES

Figure

LIST OF ABBREVIATIONS AND SYMBOLS

CBF	cilia beat frequency
club cell	formerly known as Clara cell
CXCL10	C-X-C motif chemokine ligand 10; also known as IP-10
dsDNA	double-stranded DNA
GFP	green fluorescent protein
HMPV	human metapneumovirus
ICAM-1	intercellular adhesion molecule 1; also known as CD54
IFN	interferon
IL-1β	interleukin 1 beta
IL-6	interleukin 6
IL-8	interleukin 8; also known as CXCL8
IRF3	IFN regulatory factor 3
IVIG	intravenous immunoglobulin
JAK	Janus kinase
MAVS	mitochondrial antiviral signaling
MCT	mucociliary transport
MOI	multiplicity of infection
NBF	neutral buffered formalin
NF-κB	nuclear factor kappa B
NS1	RSV non-structural 1 protein
NS2	RSV non-structural 2 protein
PFA	paraformaldehyde
PFU	plaque forming units

pi	post-inoculation
PIV3	parainfluenza virus 3
PIV3-NS1	parainfluenza virus 3 expressing respiratory syncytial virus non-structural 1
PIV3-NS1/2	parainfluenza virus 3 expressing respiratory syncytial virus non-structural 1 and non-structural 2
PIV3-NS2	parainfluenza virus 3 expressing respiratory syncytial virus non-structural 1
RANTES	regulated upon activation, normal T cell expressed and secreted; also CCL5
RIG-I	retinoic acid-inducible gene I
RLR	RIG-I-like receptor
RSV	respiratory syncytial virus
SeV	Sendai virus
STAT	signal transducer and activator of transcription
TCID50	50% tissue culture infectious dose
TEER	transepithelial electrical resistance
TLR	Toll-like receptor
TNFα	tumor necrosis factor alpha
ZO-1	zonula occludens 1 protein
Δ	gene deletion

CHAPTER I

INTRODUCTION

Epidemiology and Disease Burden

Human respiratory syncytial virus is the most important etiological agent of respiratory disease in children worldwide and by age 2, over 95% of individuals have experienced at least one RSV infection (1, 2). Seasonal infections of RSV generally begin in autumn and, in the US, range in duration from 13 – 23 weeks (3). Infection of adults and children most frequently results in upper respiratory tract illness (URTI) causing common cold-like symptoms, which may progress to lower repiratory tract illness (LRTI).

It has recently been estimated that 34 million new cases of RSV-associated lower airway disease occur globally in children less than 5 years of age, resulting in 66,000 – 199,000 deaths per year (4). The majority of these deaths occur in underdeveloped countries with limited access to standardized healthcare. Each year in the United States, an estimated 1.5 million outpatient visits are attributable to RSV infections in children <5 years old, resulting in 75,000-125,000 hospitalizations, of which 1.5% require admission to the pediatric intensive care unit (5-7). Average length of hospital stay for infants diagnosed with RSV bronchiolitis is 3.5 days (8-10) and hospitalization due to RSV-associated bronchiolitis results in total estimated costs of up to 700 million US dollars annually (11). RSV infections clearly represent a significant economic and health burden both globally and in the United States.

Clinical Features of RSV Infection

RSV infection results in a range of symptoms, varying from upper respiratory tract illness characterized by rhinorrhea to severe lower respiratory tract illness characterized by labored breathing necessitating oxygen supplementation. Although RSV infection often causes only URTI, 1 to 2% of infected individuals progress to severe lower respiratory tract infection, which can result in hospitalization with bronchiolitis being the most common clinical diagnosis (5, 12). RSV-associated bronchiolitis is known to be more severe and results in prolonged hospitalization compared to non-RSV associated bronchiolitis, resulting in a mortality rate of 0.01 – 0.5% annually (6, 9, 10, 13, 14). Studies of young children found that RSV infection results in twice as many visits to the emergency department, six times as many hospitalizations, and nine times as many deaths compared to seasonal influenza infections (15, 16). The most important risk factor for the development of RSV bronchiolitis is very young age (< 6 months). Other risk factors include congenital heart defects, immunodeficiency, neurodevelopmental deficits, familial history of atopy, chronic lung disease, and bronchopulmonary dysplasia (7, 9, 17, 18). Low body weight at time of hospitalization is most significantly associated with all measures of severe disease, with premature infants being the largest at-risk population (19). Despite identification of numerous factors associated with elevated rates of hospitalization, ~50% of RSV-associated hospitalizations occur in healthy children born at term with no additional identifiable risk factors (17).

Natural infection by RSV does not induce lifelong immunity to reinfection and recurring infections are common despite no significant antigenic change of the virus (1). RSV infection among the elderly and immunocompromised populations is recognized as a significant health problem. In community-dwelling US adults over age 65, RSV is the etiological agent in 3-15% of incidences of acute respiratory illness per year (20-23). Among elderly patients admitted to the hospital with acute cardiopulmonary disease, 7 – 10% were

identified as RSV-induced illness and, in one study, 18% of RSV-infected patients were admitted to the intensive care unit (24, 25). RSV associated mortality rates are higher in the elderly population than among young children (16). Additionally, RSV causes increased morbidity and mortality in immunocompromised patients, particularly in transplant patients (especially lung and bone marrow transplants) and patients with leukemia. In nosocomial outbreaks among bone marrow transplant patients, RSV has been detected in 2 – 20% of patients, resulting in a pneumonia-associated mortality rate of 55 – 80% (26-28). Aggressive treatment using aerosolized ribavirin and intravenous immunoglobulin (IVIG) is frequently initiated at the onset of upper respiratory tract illness, although this treatment regime is costly and cumbersome (29, 30). Recently, clinical efficacy and tolerance of oral ribavirin has demonstrated, representing a promising, cost-effective therapeutic strategy for RSV infection in immunocompromisd patients (31, 32).

Although the majority of infants infected by RSV eventually resolve infection and disease, history of RSV infection can be associated with long-term abnormalities in pulmonary function, including asthma, airway hypersensitivity, and recurrent wheezing (33-35). It is well accepted that severe LRTI is associated with an increased risk of wheezing, though a causal relationship to RSV infection remains controversial. An RSV-neutralizing antibody treatment (Palivizumab) used as prophylaxis for RSV infection also reduces recurrent wheeze in preterm infants, implicating RSV infection as an important cause of post-bronchiolitis wheeze (36, 37). Risk factors for development of wheeze following RSV infection include severity of disease as well as allergic risk factors, such as familial history of atopy or asthma, and predisposition to airway hypersensitivity (33, 35, 38-40). The association of severe RSV disease to long-term airway morbidity further highlights the need for effective treatment strategies to reduce the severity of clinical disease.

Treatment Strategies and Vaccine Development

Despite the significant impact of RSV bronchiolitis on infant health, therapeutic treatment options to reduce the severity of distal airway disease are limited to poorly efficacious anti-viral and anti-inflammatory therapies, supplemental oxygen, or mechanical ventilation. There remains a significant clinical need to reduce the severity of RSV-induced distal airway disease in infants and young children as well as elderly and immunocompromised populations.

Treatment with the RSV-neutralizing monoclonal antibodies palivizumab or motavizumab caused a slight reduction in viral shedding, yet no clear clinical benefit has been demonstrated (41-43). Prophylactic use of these antibodies, however, has shown to significantly reduce the severity of disease, although treatment as prophylaxis relies on expensive monthly injections and is therefore restricted to at-risk populations (14, 44-48).

Ribavirin is the only anti-viral drug currently approved for treatment of RSV infection. Although exhibiting anti-viral efficacy in tissue culture models and experimentally infected animals (49), studies of clinical use of ribavirin in RSV-infected infants and young children have failed to show significant reduction in disease outcome (50-53). Due to efficacy concerns, difficulty of delivery (aerosol), and potential side-effects in neonates, ribavirin is not currently used for routine clinical treatment of RSV in infants and young children (54). Clinical efficacy, however, has been shown for treatment of RSV infection in immunocompromised patients and nebulized, oral, or intravenous ribavirin treatment remains widely used, despite concerns for tolerance and safety (31, 32, 55).

In the absence of efficacious anti-viral therapies, bronchodilators and anti-inflammatory steroids remain widely used to dampen the inflammatory consequences of RSV bronchiolitis despite sufficient evidence these treatments provide no clinical benefit. Meta-analysis of corticosteroid use in hospitalized non-intubated patients demonstrated only at 0.5-day decrease in duration of hospital stay with steroid use (56). Steroids have also

shown no clinical effect on hospital admission rates, concentration of proinflammatory cytokines in tracheal aspirates, or length of mechanical ventilation (57-59). A more comprehensive, multi-center placebo controlled trial demonstrated no effect of dexamethasone on clinical outcome of disease (60). In spite of these studies, corticosteroid treatment for RSV infection is still used in conjunction with bronchodilators.

Despite decades of study and an obvious need, licensed RSV vaccines are currently unavailable. Because of the early age of first RSV infection, vaccination should occur within the first weeks of life. The likely need for multiple doses at such an early age further complicates the development of a pediatric RSV vaccine. In the 1960s, a formalin-inactivated RSV vaccine (FI-RSV) was developed and evaluated. Though immunogenic, this vaccine demonstrated poor protection against natural RSV infection and vaccinated individuals experienced immune-mediated enhancement of disease resulting in hospitalization of nearly 80% of infected vaccinated individuals, including two fatalities (61). The failure of this vaccine has been attributed to an aberrant immune response to FI-RSV that did not result in the production of neutralizing antibodies and induced an immune response inherently different to that induced by a natural RSV infection (61-63). As a result, inactivated whole-virus vaccine development has largely been abandoned and current vaccine development strategies are focused on live-attenuated vaccines, subunit vaccines, and virus-like particle vaccines. Biologically-derived RSV vaccines, such as vaccines based on cold-passaged viruses and temperature sensitive mutants, have been evaluated clinically but discontinued due to insufficient attenuation in infants (64). Live-attenuated vaccines were revisited with the introduction of RSV reverse genetics technology, and novel combinatorial mutations in several different RSV genes have yielded promising vaccine candidates currently in pre-clinical and clinical trials (65-69).

RSV Virology

RSV is classified within the family *Paramyxoviridae*, subfamily *Pneumovirinae,* and has a negative-sense, single-stranded RNA genome with 10 genes encoding 11 proteins. RSV encodes for 3 transmembrane glycoproteins: the fusion protein F, the attachment protein G, and the small hydrophobic protein SH. The matrix M protein is essential for the structure and assembly of the virion. The RNA genome associates with 4 proteins within the virion: the nucleoprotein N, the phosphoprotein P, the transcription processivity factor M2-1, and the large polymerase protein L. M2-2 is encoded by a small ORF within the M2 mRNA and may play a role in RNA synthesis. Two non-structural proteins, NS1 and NS2, are encoded by the virus and are not packaged within the virus particle. Replication occurs in the cytoplasm and the RNA genome is transcribed sequentially to produce 10 separate 5' capped mRNAs. Each individual gene begins with a highly conserved gene start signal that initiates mRNA synthesis and ends with a semi-conserved gene end signal that directs termination and polyadenylation of the mRNA. Dissociation of the viral polymerase after the gene end signal results in a gradient of transcription, whereby genes proximal to the 3' region are transcribed first and at a greater abundance than genes more distal to the leader sequence. RSV assembly and budding occur at the plasma membrane resulting in spread of infection.

Attachment and Entry: G Glycoprotein

The RSV glycoprotein (G) and fusion protein (F) mediate attachment and entry of RSV to the target cell. RSV binding and entry is a two-step process, whereby the virion first attaches to the cell membrane followed by a fusion event. In cell line models of infection, the F protein is sufficient for binding and entry of RSV and, although the G protein enhances attachment and syncytia formation, G is not considered required for entry (70-73). Attachment and entry of RSV likely involves interactions between cellular proteins and the

RSV F and G protein. A specific cellular receptor for RSV has yet to be identified, though the discovery of interactions between the cell surface nucleolin protein and RSV F suggest promising avenues of research (74, 75). G-mediated attachment to cultured cells is dependent on glycosaminoglycans (GAGs) on the cell surface (76, 77). GAGs are repeating disaccharide units of hexuronic acid and hexosamine that form unbranched polysaccharide chains. Heparan sulfate (HS) is the GAG most commonly associated RSV entry into HEp2 cells, and G-mediated attachment likely involves electrostatic interaction between G and HS, though requirements for GAG structural elements have been noted (76-79). Although interactions between G and HS have been well documented, HS is not detectable on the surface of primary well-differentiated models of the human airway epithelium (80, 81). Several other GAGs have been detected on the surface of the airway epithelium, including keratan sulfate, chondroitin / dermatan sulfate, and hyaluronan (82), though it is unclear what the role of GAGs are for attachment of RSV to target cells in the human airway epithelium.

A small hydrophobic region near the N-terminus of the G protein serves as a membrane anchor, resulting in insertion of G into the cell membrane and incorporation into the viral envelope. G is an extensively glycosylated protein, with the external component of the protein containing 4 predicted N-linked glycosylation sites and 24-25 predicted O-linked glycosylation sites (83). N-linked carbohydrate groups are added first in the ER, increasing to size of G from 32 kDa to an apparent 45 kDa processing intermediate form, which are then converted to complex sugars in the trans-Golgi network. O-linked oligosaccharides are also added in the Golgi compartment and O-linked sugars are estimated to comprise ~50% of the total mature 90 kDa form of G (84, 85). The glycosylation profile is cell-type specific, as G produced in different cells lines exhibits different electrophoretic mobility (86, 87). Due to heavy glycosylation and a lack of secondary structure, the ectodomain is referred to as

having a “mucin-like” structure, which may help shield the virion from antibody recognition (84).

Translation from a second initiation site within the G open reading frame results in a truncated G that is further cleaved to completely lack the membrane anchor, and this truncated protein is secreted (88, 89). Secreted G (sG) is rapidly secreted in cell culture, comprising 80% of total G protein released within 24h post inoculation (88). While the contributions of sG in productive infection remains to be fully elucidated, evidence indicates a role for immune evasion and antibody decoy (90, 91).

Immune Evasion Strategies: NS Proteins

RSV encodes 2 non-structural proteins, NS1 and NS2, at the 3’ beginning of the genome immediately following the leader sequence. These genes are expressed to high levels immediately upon infection, with both proteins being detectable 5h post-infection of A549 cells (92). NS1 and NS2 have primary roles as type I and III interferon (IFN) antagonists and deletion of one or both of these genes from recombinant RSV resulted in a large increase in type I IFN expression and signaling in infected human epithelial cell cultures and macrophages (93, 94). The magnitude of increase was greater following deletion of the NS1 gene as compared to deletion of NS2, though deletion of both genes produced the greatest effect (93). Co-immunoprecipitation studies indicate these proteins form a heterodimer, although expression of both proteins together does not appear to be essential to function (95). The mechanisms by which these proteins inhibit type-I interferon are complex, involving both coordinated and independent functions.

The signal transduction pathways involving IRF3 activation are significant targets for antagonism by both NS1 and NS2. IRF3 is a major interferon regulatory factor which, upon activation, dimerizers and transports to the nucleus to activate transcription at IFN-response elements (ISREs). Activation of IRF3 can occur downstream of Toll-like receptor (TLR) and

RIG-I-like receptor (RLR) activation, including TLR3 and RIG-I which are known to activate upon RSV infection (96, 97). NS2 has been shown to bind RIG-I, preventing interactions between RIG-I and MAVS to block signal transduction and prevent activation of IRF3 (98). Additionally, expression of either NS1 or NS2 resulted in a decrease in TRAF3 protein levels, which is downstream of MAVS along the signal transduction pathway leading to IRF3 activation (95). In the same study, NS1, but not NS2, was shown to decrease activation of IKKε, a protein kinase involved in activation of IRF3 (95).

Type I IFN-mediated signal transduction is also strongly suppressed by RSV through the JAK/STAT pathway. Both NS1 and NS2 have been shown to decrease protein levels of STAT2 (99, 100), likely via the proteosomal degradation pathway. Indeed, NS1 can function as an E3 ligase due to the presence of an elongin C and cullin 2 binding domain, resulting in ubiquitination and degradation of STAT2, and mutation of this domain results in degradation of the NS1 protein and attenuation of the virus (101, 102). Additional studies, however, indicate a primary role of NS2 in degradation of STAT2, where expression of both NS1 and NS2 together enhanced STAT2 degradation over NS2 expression alone, though expression of NS1 had no effect on STAT2 degradation (95, 99, 100).

RSV also inhibits activation of the type III IFN pathway in human epithelial cells and macrophages (93). The observed effects of NS1 and NS2 on type III IFN induction were similar to those demonstrated for type I IFN induction (93). The induction of the type I and III pathways occurs through different receptors, though both receptors signal through the JAK/STAT pathway and utilize STAT2 (103), which may account for similar effects of NS1 and NS2 on type I and III IFN induction. Type III IFN receptors are expressed primarily in epithelial cell types, suggesting a potentially important role for immune regulation in pulmonary epithelial cells (103).

Pro-survival roles via activation of NF-kB by the NS proteins have also been demonstrated in cell lines. Deletion of NS1 or NS2 reduced RSV-mediated activation of NF-

kB (104). Knockdown of NS1 or NS2 using siRNA also resulted in a reduction in several anti-apoptotic functions, including activated forms of NF-kB and phosphorylation of AKT, leading to early apoptosis (92). Suppression of apoptosis by the NS proteins also occurs in Vero cells which lack IFN-α and –β genes, suggesting anti-apoptotic functions of the NS proteins may be IFN independent (92).

Predictably, deletion of the NS1 or NS2 genes from a recombinant RSV results in reduced titer in cultured interferon-competent cell lines (93). In seronegative chimpanzees, NS1 and NS2 deletion mutants are highly attenuated (105-107), further emphasizing the role of NS1 and NS2 in RSV replication and pathogenesis.

Human Airway Epithelia

The human respiratory epithelium is the primary target of RSV infection. The conducting airways extend from the nose to the terminal and respiratory bronchioles and serve as a protective physical barrier between the external environment and host tissues as well as controlling the temperature and humidity of inspired air. The alveolar regions occupy the greatest internal surface area of the lung and facilitate gas exchange.

The cartilaginous conducting airways are lined by a pseudostratified ciliated epithelium consisting of basal, ciliated, and secretory cell types. The columnar cell superficial epithelium attaches to a sublayer of cuboidal basal epithelial cells, which serve as an attachment point to the basement membrane and function as progenitor cells (108, 109). Ciliated cells are the predominant columnar cell-types throughout the conducting airways (110). Goblet cells can extend into but not distal to the bronchiolar regions and secrete mucus into the airway essential for mucociliary clearance. Club (Clara) columnar cells are located predominately in the distal airways in humans, although regional distribution of this cell type is species dependent (111, 112). Club cells play important roles in detoxifying

noxious inhalants and maintaining distal airway defense by secreting proteases, anti-microbial peptides, surfactants, anti-proteases, and anti-inflammatory proteins (113).

In vitro models of well-differentiated airway epithelia indicate that RSV primarily infects columnar ciliated cells while sparing goblet and basal cells (114, 115). RSV infection of ciliated epithelial cells, but not basal cells, was noted throughout the respiratory tract of RSV-infected individuals post-autopsy and in calves experimentally infected with bovine RSV (116, 117). In the smaller, non-cartilaginous airways, RSV infection was also noted in non-ciliated columnar and cuboidal cells. In the larger airways, infection was evident in non-contiguous clumps of epithelium, while circumferential airway infection was often noted in smaller airways (117). Infection did not cause overt cytopathogenesis, as intact RSV-positive epithelial layers are found in vivo and airway epithelial models note no obvious deterioration of the epithelium (115, 117-119). In polarized models of epithelial cells, RSV sheds from the apical surface of infected cells into the apical lumenal space with no infectious virus detectable in the basolateral compartment (8, 114, 115).

Due to constant contact with the external environment, including insults from environmental toxicants, allergens, and pathogens, the respiratory mucosa employs a multitude of innate defense mechanisms, both physical and biological, to preserve the integrity of the epithelium and ensure efficient gas exchange. Epithelial cells play a critical role in regulating the immunological homeostasis of the airway. These cell types are also are common targets of respiratory viruses and these viruses have evolved diverse mechanisms to subvert the inter- and extracellular levels of innate airway defense. Our current knowledge of innate airway defense mechanisms and the methods by which RSV subverts these to establish respiratory infection are summarized in the following section.

Airway Defense Mechanisms: Protective Barrier

The columnar airway epithelium, existing at the interface of the external environment and the internal milieu, serves a critical role in airway defense by providing a physical barrier to systemic penetration of pathogens crucial to maintaining lung sterility. Barrier integrity is established and maintained by tight junction proteins, the most apically located of the epithelial junction complexes. Occludin, claudin, and junctional adhesion molecule (JAM) proteins form tight junctions, in addition to the family of scaffold PDZ-domain expression proteins, including zonula occludens (ZO)-1 (120). Tight junctions primarily serve to inhibit water and solute flow through intercellular spaces between cells and to establish the polarity of columnar epithelial cells (121-123).

Studies of the effects of RSV infection on membrane barrier integrity have largely concluded that RSV does not have a gross cytopathic impact on barrier integrity of the epithelial membrane. Infection of well-differentiated models of the columnar airway demonstrate no changes in staining intensity or location of ZO-1, a protein integral to tight junctions of airway epithelial cells (114). Measurements of transepithelial electrical resistance (TEER), an index of tight junction and barrier integrity, in well-differentiated cultures infected with RSV show only modest decreases in TEER compared to control, indicating no significant compromise of barrier integrity (124, 125).

Airway Defense Mechanisms: Epithelial Cell Response

The ciliated cell is the site of first contact with invading pathogens and acts as both a target and an effector cell to mediate the cellular response to viral infection. This response includes production of anti-viral and pro-inflammatory cytokines but may lead to the initiation of apoptosis and eventual extrusion of the infected cell from the epithelium into the airway lumen.

Interferon: Interferon (IFN) production and release is an integral component to the cellular antiviral response. Three classes of IFN have been described and are designated type I, type II, and type III. Type I inteferons include IFN-α, IFN-β, and IFN-ω and are the major class of IFN expressed in mammalian cells. Type II IFN, or IFN-γ, is produced by natural killer cells and activated T cells. Type III interferons include the IFN-λ family and signal via downstream pathways similar to the type I IFN signal transduction pathway, though the type III IFN receptor is restricted to epithelial cell types (103). Ciliated columnar cells signal through both the type I and type III IFN, though the type I IFN signal transduction pathway is thought to be more important. Secretion of type I IFN from virally infected cells acts in both autocrine and paracrine fashion by binding the type I IFN receptor at the cell surface and stimulating signaling through the JAK/STAT pathway, whereby STAT signaling complexes translocate to the nucleus to initiate transcription at numerous IFN-stimulated response elements (ISREs). The RSV NS proteins subvert type I IFN signaling via interactions with the JAK/STAT arm of the signaling pathway and IFN-α/β secretion is significantly reduced or absent in infants and adults infected with RSV (93, 95, 99, 100, 126-128). Interestingly, a recent study identified type III IFN as the predominant IFN secreted in nasal epithelial cells infected with RSV and demonstrated suppression of viral replication in the presence of IFN-λ (129).

Cytokines: Virally infected epithelial cells also release a diverse array of cytokines and chemokines that function as both pro- and anti-inflammatory mediators to modulate the pulmonary immune response. Production of cytokines following RSV infection has been characterized in epithelial cell lines and well-differentiated models of the airway epithelium, as well as in vivo in nasal aspirates, bronchoalveolar lavages, and blood from RSV-infected infants.

IL-1β, IL-6, and TNF-α release mediate a wide range of proinflammatory processes and are implicated in the immunoregulation of RSV disease. IL-1β is secreted from RSV

infected epithelial cells and well-differentiated models of RSV infection (130, 131) and is detectable in infants experiencing RSV bronchiolitis (118, 132). Elevated IL-1β levels in nasopharyngeal secretions have been directly associated with severity of RSV disease (133). TNF-α is increased in tissue culture models of infection as well as infants with RSV-induced bronchiolitis (104, 118, 132, 134-136). IL-6 is also detected in cell lines and airway epithelium models infected with RSV (114, 124, 131, 137) and in nasophyngeal secretions and bronchoalveolar lavage fluid from RSV-infected infants (118, 132, 134-136, 138).

Cytokine secretion is an important mechanism for recruitment of immune effector cells to sites of infection. IL-8 and CXCL10 are a major chemoattactants for neutrophils and are produced by both epithelial cells and macrophages in response to RSV infection (104, 114, 124, 131, 137, 139, 140). IL-8 levels are elevated in serum, nasophyngeal secretions, and bronchoalveolar lavage samples from infants with severe RSV bronchiolitis (118, 132, 138, 141-143). Elevated IL-8 levels in nasophyngeal aspirates are also associated with RSV disease severity (144). RANTES is a major chemoattractant for eosinophils and expression is upregulated following RSV infection of cell lines (104, 145) and airway models of infection (114, 124, 131, 140), and is detectable in RSV-infected infants (138, 143, 146).

The list of cytokines reviewed in this section is not exhaustive and many other cytokines have been detected in studies of RSV infection of cell lines, airway models, animal models, and humans. Emphasis was placed on cytokines secreted from airway epithelial cells, cytokines associated with leukocyte recruitment at early times after infection, and cytokines associated in increased severity of RSV disease.

Club cell secretory proteins: In human airways, club (Clara) cells are located in the terminal-respiratory bronchiolar regions and are the major type of non-ciliated secretory cells in the bronchial region, comprising10 – 25% of cells in the human epithelia (113, 147, 148). RSV-positive club cells have been observed in the distal airways of calves, lambs, and infants infected with RSV, suggesting that RSV can target this cell type for infection and

replication (116, 117, 149). Club cells participate in the innate defense of the airway by secreting several anti-inflammatory proteins, including CC10 (also known as CCSP, secretoglobin, and uteroglobin), surfactant protein A (SP-A), and surfactant protein-D (SP-D). Damage to club cells is associated with exacerbated lung injury and inflammation after exposure to irritants (150). Few studies have investigated the role of club cells in the context of RSV infection. CC10- and SP-D-deficient mice, when challenged with RSV, show increased viral persistence and lung inflammation (151, 152). SP-A and SP-D gene expression was increased in RSV-infected neonatal lambs, suggesting an important role for club cells during RSV infection (153).

Apoptosis and cell extrusion: Though infected epithelial cells initiate numerous anti-viral and pro-inflammatory signaling cascades, cell death can be the final outcome of viral infection. Cell shedding induces anoikis, a process defined as induction of apoptosis by disruption of cell-cell interactions (154, 155). Induction of anoikis serves to limit both viral replication and cytokine release, ridding the epithelium of cytokine-producing infected cells to dampen pro-inflammatory signals (156, 157). Furthermore, regulation of cell death and shedding helps to preserve the integrity of the epithelial barrier and reduce damage caused by infiltrating immune cells (158). Shed cells are then available for clearance from the airway lumen by mucociliary clearance mechanisms.

Anoikis and cell shedding are likely consequences of RSV infection of the airway epithelium. Increased numbers of cells are detected in the apical compartment of RSV infection of well-differentiated airway epithelial cell cultures, suggesting that infected cells are sloughed from the epithelium (114, 124, 125). Sloughed, antigen positive cells have been noted in the airway lumen of experimentally infected animals and, in addition to inflammatory debris, these cells contribute to airway obstruction and narrowing of the airway lumen, suggesting a potential role for cell shedding in RSV pathogenesis (116, 153, 159, 160). Histological examination of tissue sections from infants infected with RSV have also

documented RSV-antigen positive epithelial cells within the airway lumen (117, 118, 161). Despite the frequent appearance of RSV-infected cells in the airway lumen, the process of airway epithelial cell death and shedding following RSV infection has yet to be fully characterized and the importance of this process in development or limitation of RSV-associated disease is unknown.

Airway Defense Mechanisms: Mechanical Clearance

Several types of mechanisms mediate clearance of airway debris following viral infection, including immune-cell mediated and mechanical clearance, and these mechanisms work in tandem to facilitate clearance of viral infection and resolution of disease. In immune-cell mediated clearance, macrophages, dendritic cells, T cells and neutrophils migrate to the airway parenchyma to kill and clear infected cells via phagocytosis. Mechanical clearance includes both mucociliary clearance and cough clearance mechanisms. Cough clearance, including cough and sneeze, occurs when sensory nerves imbedded in the tracheobronchial region are stimulated, either by mechanical or inflammatory stimulation (162, 163). During periods of viral replication and shedding, coughing or sneezing likely aids the dissemination of viral particles to subsequent hosts.

Pathogens that settle on the airway surface encounter a complex mesh of mucins, decorated with a diverse library of carbohydrate side chains that are able to interact non-specifically with particles within the respiratory tract. Mechanical clearance of mucus serves to clear material trapped in the mucus gel via mucociliary transport. Mucociliary clearance is dependent upon tight regulation of the viscoelastic properties of the mucin layer and rapid, unidirectional, coordinated cilia beat, resulting in an “escalator” function to clear particles deposited in the mucus layer from the small airways to the proximal airways and larynx (164-167). Disruption of either of these clearance mechanisms has profound impact on the

ability of the host to clear respiratory pathogens. Maintenance of a hydrated airway surface is crucial to the function of cilia and individuals with diseases characterized by depletion in airway surface liquid volume, such as cystic fibrosis (CF), suffer impaired cilia beat. The dehydrated and static mucus layer may then adhere to the epithelial cell surface, resulting in impaired mucociliary clearance and contributing to increased bacterial infections and airway obstruction (168-170). Individuals primary ciliary dyskinesia (PCD), characterized by defects in cilia beat and coordination, experience increased respiratory tract infection and sinusitis resulting from a significant reduction in cilia dependent mucus clearance (171, 172). Cough clearance remains normal in these patients, possibly accounting for the less severe disease pathogenesis of PCD compared to CF (173).

Pathogenic effects of RSV infection on cilia structure and function have been noted in well-differentiated models of the human airway epithelium, animal models of infection, and infants naturally infected with RSV. RSV infection of airway models results in an overall decrease of cilia, as determined by β-tubulin staining, and increase in ciliary dyskinesia (114, 174, 175). RSV-infected ciliated cells demonstrate abnormal beat pattern as early as 24 hours pi and uninfected cells show no changes in cilia structure or function, suggesting that cilia degradation is a direct effect of RSV infection, rather than resulting from release of a soluble factor (175). Studies of calves infected with bovine RSV noted disruption of the cilia apparatus, where infected ciliated cells have fewer intact cilia than uninfected cells, basal bodies are disorganized within infected ciliated cells, and ciliary fragments are present in the airway lumen (116). Nasal biopsies from infants with RSV-associated bronchiolitis showed decreased numbers of ciliated cells within the epithelium, increased numbers of cells detached from the epithelium, and abnormalities in ultrastructural features of cilia as compared to uninfected controls (176).

Disruptions in cilia function may impair mucociliary clearance of shed cells and debris in the airways, potentially leading to acute airway obstruction. Air-trapping and

reduced pulmonary function are characteristic of acute obstructive disease and are associated with severe RSV disease in both infants and animals models (5, 177). Effective mechanical clearance mechanisms are important for clearance of shed cells and debris in the distal airways of infants or animals experiencing RSV infection. Impairment of mucociliary clearance may contribute to the distal airway obstruction noted in experimental models of RSV disease, which likely contributes to early pulmonary function changes following RSV infection. Although the clinical implications of RSV-mediated disruptions in mucociliary clearance are not yet defined, the inability to clear infection may be associated with more severe disease. In otherwise healthy infants with naturally occurring RSV infection, inability to clear RSV, as measured by higher viral loads in nasal washes at later timepoints, was associated with prolonged hospitalization, increased disease severity, and increased risk of requiring intensive care in RSV infected infants (19). In experimentally infected adults, viral load correlated with symptom severity, intranasal cytokine secretion, and nasal mucus output, further highlighting the importance of viral clearance on disease outcome (178).

Airway Defense Mechanisms: Cellular Immune Response

In addition to mediating infection through both biological and physical mechanisms, the columnar airway epithelium plays a major role in recruitment of inflammatory cells that contribute to the antiviral response of the airway. Neutrophils are the most common leukocyte associated with RSV bronchiolitis and, in RSV infected infants, neutrophils represent 80 – 93% of cells in upper airway aspirates (nasalphyrangeal aspirates) and 76 – 83% of cells in lower airway lavage fluid (bronchial lavage) (179-182). Neutrophilic infiltrates have also been noted in animal models of RSV infection. Histological examination of calves infected with bovine RSV demonstrated neutrophils associated and occasionally fused with infected epithelial cells (116). The recently developed neonatal lamb model for RSV

infection has also demonstrated neutrophil influx into the airway lumen following infection with RSV, with neutrophils located below the basement membrane as well as within the infected airway lumen (153, 183, 184). IL-8, the major chemoattractant of neutrophils, is released by airway epithelial cells in vitro and is detectable in prenatal lambs and infants infected with RSV (143, 184-187).

To arrive in the airway lumen, neutrophils leave systemic circulation and must migrate across the respiratory mucosa (188, 189). Adherence to the epithelium is mediated by interaction between CD11b/CD18 on the surface of neutrophils with ICAM-1 on the apical surface of epithelial cells and is important in neutrophil mediated cytotoxicity and phagocytosis (190, 191). Upregulation of ICAM-1 has been noted in epithelial cells infected with RSV and increased neutrophil adherence has been demonstrated on epithelial cell monolayers infected with RSV (191-194). Release of soluble mediators following neutrophil-epithelial cell interactions, such as neutrophil elastase and matrix metalloproteinases, contribute to neutrophil mediated epithelial damage. Although neutrophils are present in large numbers following RSV infection, the impact of the dual functions of viral clearance and epithelial damage on development and severity of RSV-mediated disease is not yet completely understood.

Dissertation Objectives

Respiratory syncytial virus is the most frequent cause of bronchiolitis and severe lower respiratory tract illness in infants and children. Despite being first identified in 1955, treatment options to reduce severity of disease remain limited and no vaccine currently exists. Although epidemiologic risk factors of RSV disease have been well characterized, an understanding of the underlying mechanisms of severe disease remains elusive. Specifically, the role of the columnar airway epithelium in modulating RSV disease and the

underlying viral and epithelial processes responsible for initiation of bronchiolitis remain to be explored.

Tissue culture cell line models have provided valuable information on RSV virology and pathogenesis, however, these cells are non-polarized and may not accurately reflect interaction of RSV with the polarized, pseudostratified airway epithelium, the host target of RSV infection. Rodent models of RSV infection, especially mice, show limited permissiveness to RSV lower airway infection and pathological and immunological changes can differ from clinical observations of RSV infected infants. Infection with closely related, species-specific pneumoviruses such as bovine RSV (bRSV) or ovine RSV (oRSV) has provided valuable information on pathology, but these studies are severely limited by expense, space, and ethical concerns. Autopsy and biopsy studies of human RSV infection are often confounded by co-morbidity with additional respiratory illness (e.g. viral or bacterial coinfection or underlying genetic disease) and treatment (e.g. mechanical ventilation) that greatly impact histopathological findings of these studies. As a result, we currently have a poor understanding of the pathogenic mechanisms of lower respiratory tract infection that lead to severe disease outcomes. The use of a well-differentiated polarized airway model of RSV infection is integral to understanding the response of ciliated airway epithelial cells to RSV infection. Connecting mechanisms of epithelial cell pathogenesis to pathogenic findings of early RSV infection in an in vivo model will contribute to an understanding of the early features of RSV mediated disease.

The purpose of this dissertation was to explore interactions between RSV infection and ciliated airway epithelia. The overarching goals of these studies were to understand the interaction of the RSV virion with the ciliated cell, determine the consequences of RSV infection of the ciliated cell, track the fate of ciliated cells following RSV infection, and explore the role of the NS2 protein in RSV infection of ciliated cells. To that end, we utilized recombinant RSV and PIV3 viruses and in vitro well-differentiated airway model and in vivo

hamster model of infection. We demonstrate the importance of ciliated cells in mediating RSV infection, as the ciliated cell upregulated pro-inflammatory and anti-viral modulators and participated in controlled extrusion from the airway epithelium to clear viral infection while maintaining the integrity of the epithelium. We identify a novel function of the NS2 protein to cause morphological rounding of columnar epithelial cells upon infection with RSV. Using an in vivo model, we demonstrate two consequences of NS2 induced cell rounding and shedding. In the larger airways, NS2 enhances clearance of viral titer and infected cells from the airway. In the smaller airways, NS2-mediated cell rounding and shedding causes acute bronchiolar obstruction, which may play a role in initiation of bronchiolitis.

CHAPTER II

THE ROLE OF THE G GLYCOPROTEIN IN EFFICIENT RSV INFECTION OF HUMAN CILIATED AIRWAY CELLS

2.1 Overview

The G glycoprotein on the surface of human respiratory syncytial virus serves as an attachment protein to enhance infectivity of RSV in cell line monolayers. Here, we demonstrate a requirement for the G protein for efficient RSV infection of a primary, well-differentiated model of the human airway epithelium (HAE). We also describe differences in electrophoretic mobility of G produced in different cell lines, where virions grown in Vero cells primarily display a 55 kDa G protein, likely representing a processing intermediate, while virions grown in HEp2 cells display a 90 kDa protein. A novel, 180 kDa form of G is identified from virions grown in ciliated cells of HAE. Vero-cell grown virus infected HAE 600-fold less efficiently than HEp2 grown virus, suggesting an important role G glycosylation and processing in infection of ciliated cells. Finally, we report on the generation of a HEp2 cell line that expresses a viral IFN antagonist and cannot respond to IFN. This HEp2-V cell line supports replication of attenuated viruses to high yields and practical applications of this reagent are discussed.

2.2 Introduction

Human respiratory syncytial virus (RSV) is a negative-sense, single-stranded RNA virus in the family *Paramyxoviridae*, subfamily *Pneumovirinae*. RSV causes mild-to-moderate upper respiratory disease, which can progress to severe or fatal lower respiratory tract disease primarily in infants and the elderly population. Currently no licensed vaccine is available and treatment generally consists of anti-viral and anti-inflammatory therapies with limited efficacy and supportive therapy.

RSV expresses three glycoproteins on the virion surface. The large glycoprotein (G) plays a role in attachment (195), the fusion (F) glycoprotein mediates virion fusion to the target cell membrane (196), and the small hydrophobic (SH) glycoprotein may attenuate apoptosis (197). Of these glycoproteins, only the F protein is absolutely required for infection of cell-lines, although the G protein enhances infection and syncytia formation (77, 198). G functions by attaching to glycosaminoglycans (GAGs) on the surface of immortalized cells (76, 199, 200). GAGs are repeating disaccharide units of hexuronic acid and hexosamine that form unbranched polysaccharide chains and are expressed on the surface of most mammalian cells. Several types of GAGs have been characterized and heparan sulfate (HS) is the most important GAG for RSV infection of HEp2 cells (78, 79).

The G protein is a type II integral membrane protein with a cytoplasmic N-terminus and an extracellular C-terminal ectodomain. A small hydrophobic region near the N-terminus serves as a membrane anchor. The ectodomain of G contains several predicted N- and O-linked glycosylation sites. The unglycosylated protein is predicted to be 32 kDa in size and is modified by addition of N-linked sugars while in the endoplasmic reticulum, increasing the predicted size of G to 45 – 60 kDa (84). G proteins of this size are likely partially glycosylated processing intermediates and are found in cell lines and on virions at low levels. Within the Golgi compartment, maturation of N-linked sugars and addition of O-linked

carbohydrates result in a predicted 84-92kDa fully maturated protein (201). Given the extensive glycosylation of the G protein, it is unsurprising that the carbohydrate groups influence virus infectivity (85, 202) and cell-type specific glycosylation of G has been documented to affect the electrophoretic mobility of the G protein (86, 87).

In the present study, we determine the requirement for G for efficient infection of a primary, well-differentiated human airway epithelial culture (HAE) and show that deletion of G impairs infectivity and spread of RSV. Next, we examine virus produced in HEp2 and Vero cells, both of which are commonly used to amplify RSV in the laboratory. We show that ability to infect HAE cultures differs greatly based upon cell line used to amplify virus. Biochemical comparison of virus grown in these two cell lines reveals a smaller form of the RSV G protein in virions produced by Vero cells. These results demonstrate the importance of the G protein and suggest that the cell lines used to produce a virus can alter its infectivity. Because Vero cells are necessary for growth of RSV mutants, yet virions derived from Vero cells are less able to infect HAE, we produced a HEp-2 cell line stably expressing an interferon antagonist and show that RSV mutants grow to high titers in this cell line.

2.3 Results

Requirement for RSV G in infection of human airway epithelial cultures

We and others have demonstrated that the RSV glycoprotein (G) is not required for infectivity in tissue culture cell lines (70). Because deletion of G has been shown to attenuate RSV in vivo (203), we determined the requirement of G for RSV infection of a primary well-differentiated model of the human airway epithelium (HAE). RSVΔG infected fewer numbers of cells at 24 hours pi compared to RSV and analysis of percentage of GFP-positive epithelium demonstrated a 20-fold decrease in initial infection of HAE (Figure 2.1). RSVΔG was also attenuated for secondary infection and spread in HAE, reaching peak

titers at a later time compared to RSV (4 days vs 3 days, respectively) and infecting only 37% of the surface epithelium at the time of peak infection compared to 83% GFP positive epithelium at peak infection with RSV (Figure 2.1B).

Impact of G phenotype on infection of HAE

Post-translational processing and glycosylation is important for the attachment functions of G and processing intermediates ranging from an immature 45 kDa form to the fully O-glycosylated, mature 90 kDa form of G have been described in infected cells (86, 87). To assess the size of G on virus grown in HAE, we purified virus from apical washes of HAE infected with RSV and compared the electrophoretic mobility to virus grown in HEp2 or Vero cells. As predicted, the mature 90 kDa form of G was detectable on HEp2-derived virus. Vero-derived virus, however, primarily contained the 55 kDa G protein. Western blotting of HAE-grown virions reveals a novel form of G migrating at approximately 180 kDa, in addition to a smaller amount of the 90 kDa form found in HEp2-derived virus (Figure 2.2A). This larger form of G is likely either a dimer of the 90 kDa form found in HEp2 cells or represents additional post-translational modification and more extensive glycosylation unique to the maturation of G in ciliated cells.

Differences in post-translational modification of G have been noted in in cell lines to affect the attachment function of G and infectivity of RSV (85, 202). HEp2 and Vero cell lines are most frequently used to amplify RSV, although the size of G is smaller from Vero-derived virus compared to HEp2-derived virus. To assess if this difference in G impacts RSV infection of HAE, we infected HAE cultures with equal inoculums of RSV amplified in HEp2 cells or Vero cells. Initial infection of HAE with Vero-derived RSV was significantly decreased compared to HEp2-derived RSV (Figure 2.2B). At 1 day pi, <1% of the HAE surface infected with Vero-derived RSV was GFP positive, compared to 40% GFP positive surface epithelium infected with HEp2-derived RSV at the same timepoint. After a single

round of infection, however, Vero-derived RSV replicated and spread with kinetics similar to HEp2-derived RSV. Although attenuated at 1 day pi, Vero-derived RSV reached infection levels almost equal to HEp2-derived RSV, resulting in ~70% GFP positivity of the HAE apical surface at the time of peak infection compared to ~80% GFP positive epithelium at the time of peak infection with HEp2-derived RSV (Figure 2.2B). Similar infection kinetics following the first round of infection is expected, as the form of G on the virion surface of virus produced by HAE cells would be similar, regardless of the cell line used to amplify the original inoculum.

Development and characterization of HEp2-V cell line

Vero cells, which lack the genes encoding IFN-α and –β, are frequently used to grow viruses containing attenuating mutations. RSV encodes two major IFN antagonist proteins, NS1 and NS2, and deletion of either or both of these genes results in severe attenuation of the virus in cell lines (104). Similarly, infection of HAE with these viruses results in severe attenuation of replication and spread (Figure 2.3). RSVΔNS1 infection results in only 1-4% of GFP positive apical surface area during 8 days of infection, while 16% of the airway surface was GFP positive at peak infection of RSVΔNS2. In contrast, RSV infected and replicated efficiently in HAE, resulting in 73% GFP positive surface area at 3 days pi, the time of peak infection.

Vero cells are commonly used to amplify the RSVΔNS1 and RSVΔNS2 mutant viruses to sufficiently high titer for study. However, we have demonstrated that amplification of virus in Vero cells results in initial attenuation of infection. We have therefore identified a need for a cell line capable of producing virus with the mature form of G while also able to amplify RSV lacking the type I IFN antagonism genes to high titers. To this end, we stably transformed HEp2 cells with the IFN antagonist V protein from SV5. HEp2 cells stably expressing SV5 V (HEp2-V cells) were assessed for V expression and inhibition of type I

IFN signal transduction. V was detected at high levels in whole cell lysates of HEp2-V cells, confirming robust expression (Figure 2.4A). To characterize type I IFN signal transduction in HEp2-V cells, we measured IFNβ gene message levels following treatment of HEp2 and HEp2-V cells with exogenous recombinant IFNβ for 24 hours. Exogenous IFNβ treatment stimulated a 8-fold increase in IFNβ message in HEp2 cells, while no changes were detected in HEp2-V cells (Figure 2.4B). To assess the type I IFN response of HEp2-V cells to viral infection, we infected HEp2 and HEp2-V cells with Sendai virus (SeV), a virus known to stimulate a robust type I IFN response. SeV infection resulted in a 30-fold increase IFNβ gene expression in HEp2 cells compared to mock inoculated cells (Figure 2.4C). Type I IFN secretion following SeV infection was also measured by bioassay (Figure 2.4D). HEp2 cells secreted high levels of type I IFN 24h following SeV inoculation, while no significant increases in IFN secretion from SeV-infected HEp2-V cells was detected. SeV infection resulted in equal numbers of infected cells in both HEp2 and HEp2-V cells (data not shown). We therefore conclude that stable expression of V in HEp2 cells significantly reduces the type I IFN response of this cell line.

RSV and RSV deleted for the NS1 and NS2 genes, individually (RSVΔNS1 and RSVΔNS2) and together (RSVΔNS1/2), were amplified in HEp2 cells, HEp2-V cells, and Vero cells and concentration of virus recovered, expressed as plaque forming units (PFU) per ml, was assessed for each cell line (Table 2.1). In HEp2 cells, RSVΔNS2 replicated to titers 1.5 logs lower than RSV. RSVΔNS1 and RSVΔNS1/2 grew to even lower titers and $>10^3$ PFU/ml was recovered in HEp2 cells. In Vero cells, all viruses were amplified to roughly equal levels, producing 2-6 $x10^6$ PFU/ml. In HEp2-V cells, all viruses were amplified to ~1-log greater concentration compared to amplification in Vero cells. RSV was recovered at the highest titer in HEp2-V cells ($9x10^7$ PFU/ml). Greater than 4 logs more virus was recovered when RSVΔNS1 and RSVΔNS1/2 were amplified in HEp2-V cells compared to

HEp2 cells. The ability to amplify attenuated RSV mutants to high titers in a cell line that produces a G protein conducive to efficient initial infection will allow for future studies with attenuated RSV mutants in HAE. Importantly, these findings confirm that inactivation of the type I IFN response is essential for productive RSV infection and that the NS1 and NS2 proteins are required for attenuation of this response.

2.4 Discussion

The RSV glycoprotein (G) and fusion protein (F) mediate attachment and entry of RSV to the target ciliated cell. RSV binding and entry is a two-step process, whereby the virion first attaches to the cell membrane followed by a fusion event. In cell line models of infection, the F protein is sufficient for binding and entry of RSV and, although the G protein enhances attachment, G is not considered required (71). In HAE, we demonstrated that RSV deleted for the G protein is significantly attenuated for initial infection and subsequent spread throughout the culture, suggesting a heightened requirement for RSV G for efficient in vivo infection. G-mediated attachment to cultured cells is dependent on glycosaminoglycans (GAGs) on the cell surface, most notably heparan sulfate (HS), and likely involves electrostatic interaction between G and GAGs, though requirements for GAG structural elements have been noted (76-79). Although interactions between G and HS have been well documented, HS is not detectable on the surface of primary well-differentiated models of the human airway epithelium (81), suggesting that G may interact with other GAGs present at the apical cell surface, such as keratan sulfate, or that GAG binding is not important for the attachment function of G in vivo.

In these studies, biochemical characterization of G on the surface of virus produced by Vero cells, HEp2 cells, and HAE cultures demonstrated different electrophoretic mobility of G, suggesting differences in the maturity and processing of G during infection of these

cell-types. G contains 7 N-linked glycosylation sites and 24-25 O-linked glycosylation sites and it has been estimated that approximately half of the final 90 kDa molecular mass of mature G is due to O-linked glycosylation (85). Cell-type specific differences in electrophoretic mobility of G have been documented and associated with differences in glycosylation patterns (86, 87). We found that the 55 kDa form of G is predominant on virus derived from Vero cells and likely represents a processing intermediate, although differential cleavage of G may also result in this form. The 90 kDa protein on virus derived from HEp2 cells is the mature, fully glycosylated form. Interesting, these studies reveal a larger form of G on virus produced by ciliated cells in HAE cultures. This 180 kDa form of G may be a homodimer of the same form of G found on HEp2-grown virus. An unglycosylated region in G contains four cysteines held together by disulfide bonds followed by a predicted heparin-binding domain (204-206). Dimerization via this region may make the G homodimer resistant to reduction during Western blot analysis, allowing for electrophoretic mobility in the 180 kDa range. Alternatively, the 180 kDa form of G may have additional or more extensive O-linked carbohydrate chains added during processing of G in the ciliated cell.

Maturation of G is associated with infectivity in cell lines (76, 85). Similarly, we found that the size of G greatly impacted RSV infectivity of HAE cultures, as viruses containing mature G derived from HEp2 cells are more infectious than viruses containing the smaller form of G derived from Vero cells. The impact of the increased size of G from viruses grown in HAE was not evaluated and future studies will aim to determine the glycosylation pattern of G and infectivity of virus from HAE.

Vero cells are the only cell line approved by the World Health Organization for production of live-attenuated or inactivated vaccines. However, we found that infectivity HAE with RSV grown in Vero cells was significantly reduced compared to that of RSV grown in HEp2 cells. It is reasonable to speculate that attenuated vaccine candidates amplified in

Vero cells might infect humans inefficiently as well. In trials of attenuated vaccine candidates, escalating doses are used to identify the lowest dose that induces an adequate antibody response. Although Vero cell-grown attenuated vaccine candidates induce neutralizing antibodies in infants, we predict that vaccine candidates produced in a different cell line would require less inoculum to induce an equal antibody response. A lower inoculum may reduce side effects and respiratory symptoms that have plagued similar vaccine candidates and resulted in discontinuation. Lower inoculum would reduce exposure to non-replicating viral antigens, cell culture derived cytokines and chemokines, and other possible contaminants that may contribute to inflammation and respiratory symptoms of vaccinated infants. Attenuating changes in processing and glycosylation of viral attachment proteins of viruses produced in Vero cells may impact infectivity and immunogenicity of additional respiratory viral vaccine candidates as well.

Due to the absence of IFN-α and –β genes, Vero cells are also extensively used in the laboratory to amplify viruses containing attenuating mutations. Indeed, we use Vero cells to amplify RSVΔNS1, RSVΔNS2, and RSVΔNS1/2 to sufficiently high inoculum for study in cell lines and HAE. These studies, however, indicate that RSV gene deletion mutants derived from Vero cell may be doubly attenuated. First, the G protein on these viruses does not allow for efficient initial infection of HAE cultures, resulting in fewer cells infected at day 1 pi. Second, deletion of the NS proteins results in attenuated replication due to loss of type I IFN antagonism, leading to decreased replication and spread. Such low numbers of infected cells hamper studies of these deletion mutants in HAE. Thus, a cell line that would result in proper processing of G, allowing for efficient initial infection, while also supporting replication of attenuated viruses to high titers is needed.

To address this need, we engineered Hep2 cells to be nonresponsive to IFN by stable expression of the IFN antagonist V protein of SV5, which blocks type I IFN signaling

by promoting degradation of STAT1 (207, 208). The engineered cell line HEp2-V demonstrated decreased IFN responses to exogenous recombinant IFNβ or infection with Sendai virus and supported viral replication, producing high viral yields of all RSV mutant viruses.

Generation of cell lines which cannot respond to IFN may have direct relevance for vaccine development and laboratory amplification of viruses. Such IFN-nonresponder cell lines yield significantly higher titers of viruses, especially those that grow poorly in tissue culture due to attenuating mutations, and may be useful for production of live attenuated vaccine candidates. While Vero cells are currently used for this purpose, generation of an alternative cell line may produce higher yields and more infectious virus. Additionally, the IFN response is a major constraint preventing animal viruses from replicating in human cells, where function of IFN resistance genes is hindered due to species differences. For example, bovine RSV (bRSV) shows increased sensitivity to human IFN compared to human RSV and functional differences have been identified in the IFN antagonist proteins of bRSV compared to human RSV (209, 210). Therefore, cell lines nonresponsive to IFN may be used to isolate and amplify animal viruses or cultivate viruses that grow suboptimally in currently available cell lines.

In summary, optimal RSV infection of the human airway epithelium requires the mature G protein and initial infection of HAE with viruses derived from Vero cells is inefficient due the predominance of a smaller form of G on the virus surface. To facilitate efficient infection of attenuated mutants of RSV, we engineered the HEp2-V cell line, which produced high yields of RSV NS deletion viruses and may be used to effectively amplify IFN-sensitive viruses for future study. Finally, these studies confirmed the importance of the RSV NS1 and NS2 proteins in circumventing the type I IFN response during the RSV life-

cycle, as the attenuated replication phenotype of RSV NS1 or NS2 deletion mutants was almost completely rescued in IFN nonresponsive cell lines.

2.5 Materials and Methods

Cells

Human airway epithelial cells were isolated by the UNC Cystic Fibrosis Center Cell Culture and Tissue Procurement Core from tracheobronchial airway specimens obtained from patients provided by the National Disease Research Interchange (NDRI, Philadelphia, PA) or as excess tissue following lung transplantation. All protocols were approved by the University of North Carolina at Chapel Hill Institutional Review Board. Primary epithelial cells derived from single patient sources were plated on permeable Transwell-Col supports (12-mm diameter, Corning, Inc.) and grown in custom media at an air-liquid interface for 8 to 10 weeks to form differentiated, polarized cultures as previously described (211). HEp-2 (ATCC, Manasass, VA) cell lines were grown in MEM (Gibco), 10% fetal bovine serum (FBS) and Vero cell lines in DMEM (Gibco), 10% FBS. Cells were incubated at 37^{o}C in 5% CO2.

Viruses

Recombinant GFP-expressing RSV used in these experiments were RSV (strain A2) and mutants of this virus lacking the G glycoprotein genes designated RSVΔG (71). These viruses were provided by Drs. Mark Peeples and Steve Kwilas. Recombinant RSVΔNS1, RSVΔNS2, and RSVΔNS1/2 are derivatives of the A2 strain and were constructed and described previously (105, 106, 212, 213). These viruses were provided by Dr. Peter Collins. Each of these constructs express the green fluorescent protein (GFP) gene as an additional gene inserted between the RSV phosphoprotein (P) and matrix (M) genes. Recombinant Sendai virus (SeV) expressing GFP were described previously (214). All virus stocks and cells tested negative for mycoplasma by PCR (Intronbio, Seongnam-Si, Korea).

Virus inoculation and titer

HAE cultures were rinsed with PBS 3 times over a 30 min period to remove apical secretions, and supplied with fresh basolateral media prior to inoculation. The virus inoculum was diluted to 6.2 x 10^6 pfu in100 µl HBSS (MOI ~10), applied to the apical surface of the HAE cultures for 2 hr at 37^{o}C, after which the inoculum was removed by aspiration and cultures were incubated at 37^{o}C. At indicated times post-inoculation, images were obtained using a Leica DMIRB inverted fluorescence microscope equipped with a cooled-color charge-coupled-device digital camera (Retiga 1300; QImaging, Burnaby, BC, Canada). The proportion of the epithelium positive for GFP was determined by pixilating a black and white image, inverting the image, and calculating the percent black pixels by computer for 5 images per culture and averaging.

For growth of viruses in different cell types, monolayers of Vero, HEp2, or HEp2-V cells in 10cm dishes were washed with PBS and infected at a multiplicity of infection of 0.01 PFU per cell for 2 hours at 37^{o}C. Inoculum was aspirated, cells were washed and 10ml fresh media was added, and cells were incubated at 37^{o}C for 3 days. To harvest virus, cell monolayers were scraped and combined with cell supernatant and vortexed at high speed to release cell-bound virus. Supernatant was clarified of cell debris by centrifugation and concentration of virus was determined on Vero cells by titration and counting GFP-positive cells 24 h post-inoculation.

Construction of HEp2-V cells

HEK 293 cells were transfected with the plasmids pdlNot1'SV5V'IRESpuro (described in (210)), pCMVR8.91, and pMD.G and, after 2 days, lentivirus in the supernatant was collected and purified by centrifugation. HEp2 cells were transformed with SV5V lentivirus and cultured in the presence of 1.25ug/ml puromycin to select for transformed

cells. HEp2-V cells were maintained in MEM (Gibco) supplemented with 10% FBS and 1ug/ml puromycin. Plasmids were provided by Drs. Richard Randall and Daniel Young.

Western blot

Virus produced from HEp2 and Vero cells was collected in tissue culture supernatants. Virus produced from HAE cultures was collected by performing apical surface washes with 300 µl of serum-free DMEM (Gibco) harvested at 30 min at 37^{o}C. Samples were cleared of cell debris by low speed centrifugation, then lysed and reduced. Proteins were separated by electrophoresis on a 10% polyacrylamide gel containing sodium dodecyl sulfate (SDS-PAGE) (Invitrogen). Proteins were transferred to a nitrocellulose membrane (Invitrogen) and blocked with 5% non-fat milk-0.1% Tween 20. G protein was visualized by probing with the L9 antibody that recognizes the conserved central region of the G protein (215), followed by HRP-conjugated secondary (Jackson ImmunoResearch) and developed with SuperSignal West Pico Chemiluminescent Substrate (Pierce) and exposed to film. The L9 antibody was provided by Dr. Edward Walsh.

IFN bioassay

Type I IFN secretion produced by HEp2 and HEp2-V cells was determined by IFN bioassay as previously described (125). Briefly, clarified cell culture supernatants were treated at pH 2.0 at 4^{o}C for 24h to inactivate virus and acid-labile type II IFN, and the pH was adjusted to 7.0. Type I IFN concentration was determined by measuring the restriction of replication of EMCV on A549 cell line monolayers after 24h in comparison to a known concentration of recombinant human IFNβ (Invitrogen). IFNβ standard and supernatants were serially diluted in duplicate in 96-well plate of A549 cells. At 24h pi, cells were washed and infected with EMCV at MOI = 5. After 24h of infection, bioassay plates were scored for 50% cytopathic effect as an indicator of IFN concentration. The deduced IFN concentrations in test samples were expressed as international unit (IU) per ml.

qRT-PCR

The levels of IFNβ mRNA in cells infected with SeV or treated with rhIFNβ were determined by quantitative reverse transcription (qRT)-PCR. Total intracellular RNA was extracted using the RNAeasy total RNA cell isolation kit (Qiagen). RNA was reverse transcribed using an oligo (dT) primers and SuperScript II reverse transcriptase (Invitrogen). Real-time PCR was performed using Taqman gene expression assays and an Applied Biosystems 7500 Fast Real-Time PCR System (Applied Biosystems). Each sample was internally normalized to GAPDH housekeeping gene. Signals from virus-infected or IFNβ-treated samples were expressed as fold change over mock-inoculated or untreated samples.

Statistical analysis

Unpaired t-test and one-way analysis of variance (ANOVA) with Tukey's post-test was performed as indicated. Statistical significance was defined as $P<0.05$ unless otherwise noted.

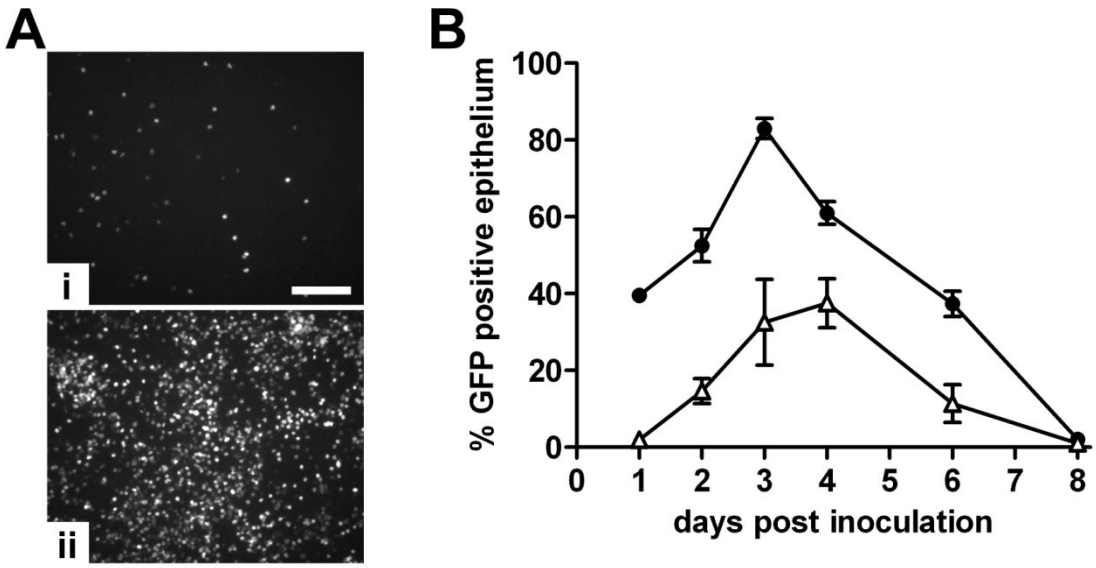

Figure 2.1. RSV requires the G protein for efficient infection of HAE. (A) Representative *en face* fluorescent images of HAE infected with RSVΔG (i) or RSV (ii) at 1 day pi. Both viruses express GFP. Scale bar represents 10 μm. **(B)** The number of cells in HAE infected over time by RSV (closed circles) or RSVΔG (open triangles), quantified as the percentage of the epithelium surface area positive for GFP fluorescence. Data (mean ± SEM) are n = 4 cultures.

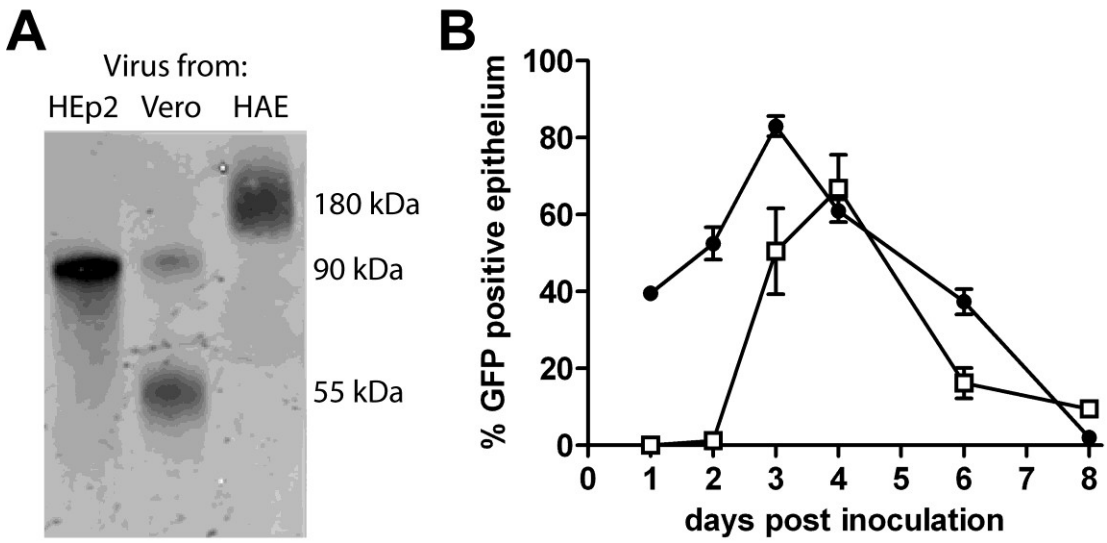

Figure 2.2 Infection of HAE with RSV amplified in Vero cells or HEp2 cells. (A) Western blot assay of virus released from HEp2 cells, Vero cells, or HAE cultures, probed with the L9 antibody to detect G. **(B)** The number of cells in HAE infected over time by RSV amplified in HEp2 cells (closed circles) or RSV amplified in Vero cells (open squares), quantified as the percentage of the epithelium surface area positive for GFP fluorescence. Data (mean ± SEM) are n = 4 cultures.

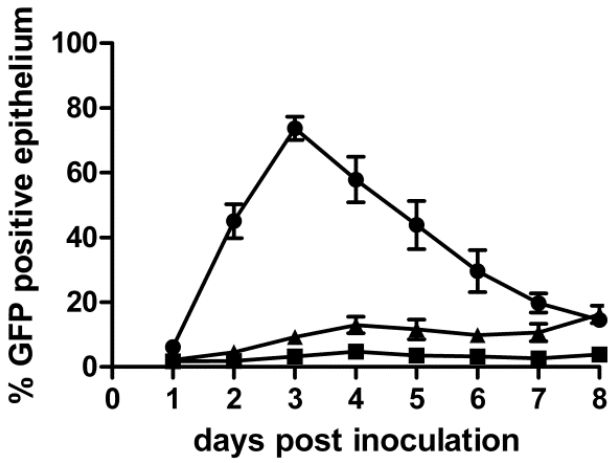

Figure 2.3 Infection of HAE with RSV NS deletion mutants. The number of infected cells over time was quantified as the percentage of the epithelium surface area positive for GFP fluorescence in HAE inoculated with RSV (circles), RSVΔNS1 (squares), or RSVΔNS2 (triangles). All viruses express GFP. Data (mean ± SEM) are representative of independent experiments utilizing n = 3-4 cultures per donor obtained from 3 different donors.

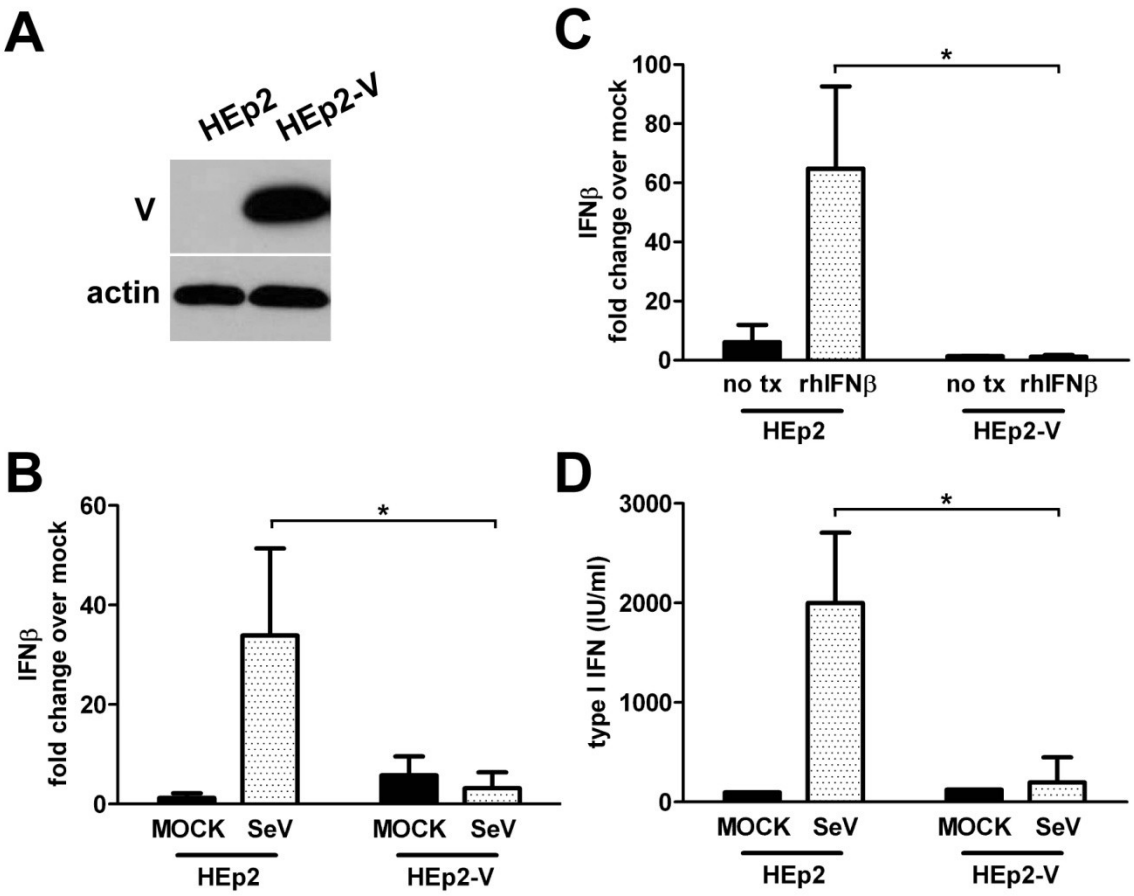
A
HEp2
HEp2-V
V
actin
B
IFNβ
fold change over mock
60
40
20
0
*
MOCK
SeV
MOCK
SeV
HEp2
HEp2-V
C
IFNβ
fold change over mock
100
80
60
40
20
0
*
no tx
rhIFNβ
no tx
rhIFNβ
HEp2
HEp2-V
D
type I IFN (IU/ml)
3000
2000
1000
0
*
MOCK
SeV
MOCK
SeV
HEp2
HEp2-V

Figure 2.4 Characterization of HEp2-V cells. HEp2 cells were stably transfected with V from SV5. **(A)** Western blot analysis of whole cell lysates from HEp2 cells or HEp2-V cells probed with an antibody to detect the V protein. Detection of actin was used as a loading control. **(B)** Expression levels of IFNβ from HEp2 and HEp2-V cells treated with exogenous recombinant human IFNβ (rhIFNβ). Total RNA was extracted from cells without treatment or treated for 24 hours with 1000 IU rhIFNβ and gene expression levels were measured by qRT-PCR. Each sample was normalized to GAPDH and is expressed as fold change compared to untreated samples. Data (mean ± SD) represent n = 3 experiments. **(C)** IFNβ expression was measured as in (A) following infection with Sendai virus (SeV) at 24h pi. Data (mean ± SD) represent n = 3 experiments. **(D)** Type I IFN secretion from HEp2 and HEp2-V cells was determined by IFN bioassay following infection with SeV at 24h pi. Data (mean ± SD) represent n = 2 experiments For (B) – (D) significant changes in mRNA or secreted type I IFN between treated HEp2 compared to treated HEp2-V cells were determined by unpaired *t* test. **P*<0.05

Table 2.1 Amount of infectious virus produced from HEp2, Vero, or HEp2-V cells.

Virus	Concentration of virus (PFU/ml) produced from:		
	HEp2	Vero	HEp2-V
RSV	5×10^6	2×10^6	9×10^7
RSVΔNS1	$< 10^3$	6×10^6	3×10^7
RSVΔNS2	2.5×10^5	5×10^6	5×10^7
RSVΔNS1/2	$< 10^3$	2×10^6	3×10^7

CHAPTER III

THE RSV NS2 PROTEIN PROMOTES CYTOPATHIC EFFECT OF COLUMNAR CILIATED AIRWAY EPITHELIAL CELLS FOLLOWING RSV INFECTION

3.1 Overview

Respiratory syncytial virus (RSV) infection is the most important cause of bronchiolitis in infants and young children worldwide. However, the mechanisms by which RSV causes more severe disease compared to other commonly encountered respiratory viruses are poorly understood. In this study, we use a primary well-differentiated model of the human airway epithelium (HAE) to investigate the consequences of RSV infection of ciliated cells, the target cell population in HAE. These results show striking resemblance to RSV infection in infant lungs. Namely, infection was restricted to ciliated cell types, induced gene transcription of antiviral cytokines, caused rounding of infected cells, and resulted in shedding of infected cells from the airway epithelium. We further identify the RSV non-structural 2 (NS2) protein as a unique viral genetic determinant for RSV-induced cell rounding, cilia degradation, and cell shedding. Sloughing of infected cells has been noted in infants with severe RSV-bronchiolitis, indicating that cell shedding occurs in vivo to enhance RSV disease and suggesting a previously unrecognized role for NS2 in RSV pathogenesis.

Sections of this chapter are under review for publication in the Journal of Clinical Investigation.

3.2 Introduction

RSV is the most common virus causing acute and severe lower airway disease in infants and young children. RSV infection is responsible for spectrum of diseases ranging from upper respiratory tract illness resulting in common cold-like symptoms to severe lower respiratory tract illness resulting in bronchiolitis and pneumonia. In ~2% of cases, lower airway disease is severe enough to require hospitalization (5). Globally, an estimated 34 million new pediatric cases of RSV-associated lower airway disease occur annually accounting for approximately 200,000 deaths, almost all occurring in developing countries with reduced access to standardized care (4). Despite the obvious impact of RSV infection on infant morbidity and mortality, treatment options remain limited to supportive care and no licensed RSV vaccine is currently available. The high incidence of RSV infection and the potential for severe distal airway disease in vulnerable young children combined with limited availability of therapeutic options identifies a significant clinical global need to reduce the burden of RSV-associated disease.

RSV infects the mucosal epithelium lining the human respiratory tract, predominantly targeting the columnar epithelial cells of the conducting airways. In addition to providing a physical barrier to prevent penetration of pathogens, the columnar airway epithelium serves a mechanical innate defense function for clearing airways of inhaled pathogens by generating unidirectional mucus transport out of the airways, facilitated by synchronous cilia beat and regulated mucin secretion. Precisely how RSV infection affects innate function of the columnar airway epithelium and how infection of columnar epithelial cells relates to subsequent RSV-associated disease is poorly defined.

Severe RSV-associated bronchiolitis is characterized by wheezing, increased airway resistance, atelectasis, and hyperinflation (216). Increased proinflammatory cytokines, especially IL-8 and IL-1β, in nasophyngeal secretions and bronchoalveolar washes

positively correlated with disease severity (118, 133, 144). Histologic analyses of autopsy lung tissues from RSV-infected infants described epithelial cells sloughed into the airway lumen (117, 119, 161). Although the contribution of these sloughed cells to exacerbation of RSV-associated bronchiolitis was unclear, it was speculated that these intralumenal accumulations of infected and necrotic epithelial cells could contribute to airway obstruction and inflammation.

The majority of studies on RSV pathogenesis utilized tissue culture cell lines or small animal models. Although these studies have provided valuable insight into RSV biology, the majority of animal models are only semi-permissive to RSV infection and cell lines do not accurately represent the highly polarized and structured nature of the ciliated cell, the target of RSV infection. Therefore, there is a need for a more complete understanding of the effects of RSV on the human airway epithelium. We have previously described an in vitro model of RSV infection of human cartilaginous airway epithelium (HAE) that recapitulates the cellular distribution and physiology of the human differentiated airway epithelium. Using this model, we and others have shown that RSV preferentially infects ciliated epithelial cells in HAE yet we are unable to detect infection of mucin-containing Goblet cells and basal cells (114, 115). Histologic studies of upper airways from RSV-infected patients also demonstrate the preferential tropism of RSV for ciliated cells, supporting our in vitro findings (117).

Our previous studies demonstrated RSV infection of human ciliated cells in HAE was minimally cytopathic, at least within the first 48h of infection (115). The lack of direct RSV-induced cytopathology was in contrast to the rapid and robust cytopathology documented in HAE infected by influenza viruses (217). We now expand our earlier studies with RSV to track the fate of RSV-infected ciliated cells over time to determine consequences of infection potentially important for pathogenesis. By determining the fate of RSV-infected ciliated cells in vitro, we identify a unique consequence of RSV infection whereby infected ciliated cells

rapidly transition from a columnar to a rounded cell morphology and are then extruded from the otherwise intact epithelium, resulting in detached, viable, virus-infected epithelial cells in the lumenal secretions of HAE. Using RSV gene deletion mutants, we attribute the function of cell rounding to the RSV non-structural 2 (NS2) protein. Gain-of-function experiments using recombinant parainfluenza virus (PIV3-GFP) engineered to express RSV NS2 (PIV3-NS2) demonstrated that ciliated cells infected by PIV3-NS2, but not PIV3, became rounded and morphologically indistinguishable from RSV-infected ciliated cells. These studies provide the first description of the unique fate of RSV-infected columnar airway epithelial cells and identify the expression of a single RSV protein, RSV NS2, as promoting this event.

3.3 Results

Kinetics of RSV replication in HAE

The kinetics of RSV infection of HAE were measured by inoculating the apical surface of cultures with a recombinant RSV expressing GFP inserted between the P and M genes ($3x10^5$ PFU; MOI ~1), and the numbers of GFP-positive cells and titers of released virus were determined every 24 h for 8 days. Representative *en face* images of GFP-positive cells and quantification of the percentage of epithelium surface area positive for GFP across HAE obtained from multiple tissue donors are shown in Figure 3.1A and 3.1C, respectively. At 1 day post-inoculation (pi), RSV infection resulted in 5% of the epithelium surface area positive for GFP and over time the extent of infection steadily increased as virus infection spread, with 53% of the epithelium surface area being GFP-positive by day 4 pi. Beyond 4 days pi, the numbers of GFP-positive cells declined rapidly and by day 8 pi, the extent of infection approximated the level of infection at 1 day pi. In agreement with previous studies, throughout infection, only ciliated cells expressed GFP, confirming RSV tropism for ciliated cells in this model. On average, ciliated cells represented ~90% of the surface

columnar epithelial cells in HAE, indicating ~60% of available ciliated cells were infected by RSV at the time of maximal infection (day 4).

RSV titers in washes harvested from the apical surfaces of HAE paralleled the numbers of GFP-positive cells (Figure 3.1D). RSV titers steadily increased proportionate to the numbers of GFP-positive cells during the first 3 days of infection, reaching maximal titers by 4 days pi ($2.6x10^6$ PFU/ml). Once maximal, virus titers declined proportionate to the loss of GFP-positive cells and, by 8 days pi, virus titers had fallen by 2 logs compared to those at 4 days pi (Figure 3.1D). The rapid net loss of RSV infection from HAE between 4 and 8 days pi suggests most of the RSV-infected ciliated cells were cleared from the epithelium during this period and, as HAE are pure populations of epithelial cells, that clearance of infected ciliated cells occurred in the absence of immune cell-mediated clearance mechanisms.

HAE cultures remained intact based on gross visual inspection, as previously described (115, 125). ZO-1 staining on uninfected and RSV infected ciliated cells indicated that tight juctions and membrane barrier integrity remained intact (Figure 3.1B).

IFN and cytokine message following RSV infection

To characterize the innate immune response of the ciliated airway epithelium, we analyzed IFNβ and cytokine message levels over time following RSV infection of HAE compared to inoculation with UV-inactivated RSV. Because these cytokines are increased in RSV infection of both tissue culture cells lines as well as infants with severe disease (118, 136, 142, 143), we chose to analyze IFNβ, CXCL10, IL-1β, IL-8, RANTES, and TNF-α (Figure 3.2). At 1 day pi, IFNβ, CXCL10, and RANTES were significantly increased compared to UV RSV, and by day 2 pi, all genes except IL-1β were significantly upregulated. Transcription of all genes analyzed peaked at 4 days pi, correlating with the time of peak infection of HAE, and began to decrease by 5 days pi, correlating with the decline in GFP positive epithelium.

A distinctive morphologic change in RSV-infected columnar airway cells

To investigate how RSV-infected (GFP-positive) ciliated cells were cleared from HAE, we tracked the fate of infected ciliated cells over time in histologic sections of cultures. These studies revealed that RSV-infected ciliated cells underwent a distinctive morphologic transition from the native columnar cell morphology to a rounded cell morphology, with infected rounded ciliated cells visibly embedded among non-infected columnar cells (Figure 3.3A). Ciliated epithelial cells in human cartilaginous airway epithelium and in HAE cultures are characteristically columnar with individual ciliated cells spanning the depth of the epithelium and the ciliated cell tail intercalating into the underlying basal epithelial cell layers. We speculate that transition of RSV-infected ciliated cells from columnar to rounded cell morphology likely involves release of the ciliated cell tail from the basal epithelial cell layer, resulting in the infected cell assuming a rounded shape. Only those ciliated cells that were GFP-positive (i.e., infected with RSV) exhibited rounded cell morphology, and no GFP-positive cells were observed that retained the native columnar shape of ciliated cells, suggesting that ciliated cell rounding was a direct consequence of RSV infection.

Ciliated cells infected by RSV also, over time, began to bulge from the epithelial layer into the lumenal compartment (Figure 3.3A). The bulging apical membranes of RSV-infected cells also progressively lost apical structural markers characteristic of ciliated cells, including cilia, as demonstrated by loss of beta-tubulin IV immunoreactivity (Figure 3.3Aiv-vi) and a marked thinning of the cytoskeletal terminal web of ciliated cells (see arrows, Figure 3.3Ai and iii). Despite significant disruption of apical membrane structures in these bulging ciliated cells, the cells retained GFP fluorescence, suggesting plasma membrane permeability was not overtly compromised (Figure 3.3Aiv-vi). High power transmission electron microscopy (TEM) studies of non-infected and RSV-infected HAE, fixed to preserve the hydrated external environment of the HAE lumenal surface, confirmed that RSV infection

resulted in the disintegration of apical membrane structures, most notably cilia shafts and microvilli (Figure 3.3B). Cytoplasmic cilia basal bodies, usually organized directly below emerging cilia shafts, were often disorganized in RSV-infected ciliated cells (Figure 3.3Biii, star). Clouds of particulate matter in the external lumenal environment were composed of fragmented cilia and microvilli directly above bulging RSV-infected ciliated cells (Figure 3.3Bii). It is reasonable to presume that these particulate clouds also contain progeny RSV virions and, on occasion, structures resembling RSV virions could be detected (Figure 3.3Biii, arrow). More direct identification of RSV virions in these clouds was technically challenging, as immunogold labeling of virus proteins would not discriminate between infectious progeny virions and virus proteins associated with fragmented cellular debris.

Shedding of epithelial cells from RSV-infected HAE

To assess the fate of cells extruded from the epithelium, we examined histologic sections of non-infected and RSV-infected HAE fixed to preserve airway surface secretions that had accumulated over a 5-day period. These studies revealed that accumulated mucus secretions in non-infected HAE contained only low numbers of detached epithelial cells (Figure 3.4Ai). In contrast, RSV-infected cultures displayed a marked increase in the numbers of detached epithelial cells that were embedded in an increased layer of lumenal surface mucus secretions (Figure 3.4Aii). Although rounded and extruding epithelial cells showed no obvious morphologic evidence of cell death while associated with the epithelium, upon becoming fully detached from the epithelium shed cells showed evidence of apoptosis, characterized by morphologic criteria including pyknosis, karyorrhexis, and karyolysis. In addition to the increased cell content of the lumenal secretions, the epithelium of RSV-infected cultures became irregular in appearance, largely due to the rounded morphology of infected ciliated cells remaining in the intact epithelium. An overall decrease in cilia also was noted in the RSV-infected epithelium.

We quantified the extent and kinetics of epithelial cell shedding from RSV-infected HAE cultures by determining the amount of double-stranded DNA (dsDNA) present in daily washes of the lumenal surfaces of non-infected and RSV-infected HAE (Figure 3.4B). Apical washes consistently contained an increased amount of dsDNA at day 1 pi for both non-infected (mock-inoculated) and RSV-infected HAE, which we attribute to consequences of the inoculation procedure. However, by day 3 pi, there was a clear separation in the amount of dsDNA present in apical washes between RSV-infected and non-infected HAE, with amounts of dsDNA consistently increasing in the RSV-infected HAE cultures and reaching maximal levels at 5-7 days pi. In contrast, the amounts of dsDNA in apical washes from non-infected HAE remained low and constant over the same time period. The increased dsDNA in apical washes closely correlated with the loss of GFP-positive epithelial cells from HAE (Figure 3.1B), indicating the usefulness of dsDNA as a marker for the numbers of shed epithelial cells in airway secretions in vitro.

Overall, these observations suggest that the loss of GFP-positive cells from RSV-infected HAE is predominately due to extrusion or shedding of the infected ciliated cells from the airway mucosa. While our studies clearly show that epithelial cells display signs of cell death after being shed, we were unable to determine the precise kinetics of cell death upon detachment of individual cells from the epithelium. We propose that RSV-infected ciliated cells remain viable during the shedding process and, once shed, undergo the process of detachment-induced apoptosis known as anoikis. Since the reduction of RSV titers in HAE paralleled the loss of GFP-positive cells, we propose that RSV-induced shedding of ciliated cells represents a primary mechanism for clearing RSV infection from a differentiated airway epithelium, at least in vitro.

Effects of RSV infection on mucociliary transport

Extensive shedding of cells onto the lumenal surface of RSV-infected HAE suggests that, in vivo, this cellular material may be cleared from the airway lumen by mechanical clearance mechanisms, such as mucociliary transport and cough clearance. In vitro, we often observed GFP-positive cells shed into the HAE lumenal secretions being be transported across the surface of cultures. Since directional transport of airway secretions in HAE is dependent on coordinated cilia beat, the potential impact of RSV infection on the effectiveness of cilia function is an important consideration when assessing the contribution of mechanical clearance to resolution of infection. We tested the ability of HAE to perform directional transport of particulates present in airway secretions by measuring mucociliary transport (MCT) rates of 1 μm fluorescent beads transported across the lumenal surface of HAE (Figure 3.4C). For non-infected HAE, MCT rates of ~40 μm/sec were maintained for 6 consecutive days of experimental analysis. For RSV-infected HAE, MCT rates approximated those of non-infected HAE during the first 2 days of RSV infection, despite infection of ~20% of the epithelium surface. However, by 3 days pi, RSV-infected HAE demonstrated a significant decline in MCT rate and by day 4 pi, when typically ~60% of the epithelium surface was infected, MCT rates had fallen drastically to below 5 μm/sec. By 5 days pi, bead transport in RSV-infected HAE had ceased.

To determine whether loss of MCT after RSV infection was directly associated with loss of cilia function, we also quantified the percentage of the epithelium surface which displayed beating cilia at each time-point (Figure 3.4D). In non-infected HAE, ~90% of the epithelium surface displayed active cilia and this level was maintained over 6 consecutive days of analysis. A similar extent of cilia activity was measured during the first 2 days of RSV infection, indicating that cilia activity of infected cells was not affected early during infection, similar to our previous findings (115). However, beginning at 3 days pi, the area of

active cilia progressively declined, resulting in only 38% of the epithelium surface displaying active cilia by 5 days pi and 10% by 6 days pi. Combined, these results show that within the first few days of infection, RSV does not significantly impact the ability of the ciliated epithelium to perform MCT. However, as increased numbers of cells were infected and infection of individual cells resulted in apical membrane cytopathology, RSV infection can abolish MCT. We noted that at 3 and 4 days pi, although the area of cilia activity was high, MCT rates had rapidly declined. Such declines in MCT rate prior to significant losses in cilia activity may be explained by subtle but deleterious effects of RSV infection on coordinated cilia beat, such as cilia beat asynchrony in infected ciliated cells, and subsequent disruption of unidirectional transport. Taken together, these data suggest that, at least up until 3 days pi, RSV-infected HAE cultures maintain sufficient MCT to transport infected cells shed on to the airway surface and that cell shedding followed by MCT may represent a previously unidentified mechanism by which RSV infection is cleared from the airways.

Cell rounding is unique to RSV among a number of common paramyxoviruses

We also investigated whether the rounding of ciliated cells following RSV infection occurs following infection with other respiratory viruses known to infect ciliated cells in HAE. Ciliated cells infected by parainfluenza virus (PIV) serotypes 1, 2, 3, or 5, Sendai virus (SeV), or human metapneumovirus (HMPV) failed to exhibit ciliated cell rounding (Figure 3.5A and data not shown). As an index of cell rounding, we measured the height of GFP-positive cells using confocal microscopy xz sections. Ciliated cells infected by RSV were significantly shorter, due to cell rounding, than those infected by the other GFP-expressing respiratory viruses that were tested (Figure 3.5Aiv). Although we noted ciliated cells infected with PIV3 were somewhat shorter than those infected with PIV5, SeV, or HMPV, PIV3-infected cells did not exhibit RSV-like rounding of infected cells, and instead appeared to remain associated with the underlying basal epithelial cells. Since our studies utilized a

recombinant RSV A2 strain expressing GFP, we confirmed that cell rounding was not an artifact of the recombinant virus or expression of GFP, as a recombinant RSV without GFP (GP1), the biologically-derived RSV from which the recombinant was generated (HEp-4), and a wild-type RSV strain of subgroup B all caused rounding of infected ciliated cells identical to the recombinant GFP-expressing virus (data not shown). Because studies have described phenotypic differences between highly passaged RSV strains and clinical isolates, we confirmed that a recently isolated, minimally passaged, clinical strain of RSV (RSV Memphis 37) caused infected ciliated cells to round with morphology indistinguishable from those cells infected by recombinant GFP-expressing RSV (Figure 3.5Ai and ii). Overall, these data suggest ciliated cell rounding is a unique consequence of RSV infection.

Columnar cell rounding is associated with expression of the NS2 gene

We speculated that the unique morphologic phenotype induced in ciliated cells by RSV infection might be due to the expression of specific RSV genes. We explored this possibility by infecting human ciliated cells with recombinant, GFP-expressing RSVs from which individual viral genes had been deleted. These studies revealed that infection of ciliated cells by a mutant RSV with deletion of the two non-structural genes, NS1 and NS2 (RSVΔNS1/2), failed to cause rounding of infected ciliated cells (Figure 3.5Biv). Instead, ciliated cells infected with this mutant retained the native columnar morphology and resembled the morphology of ciliated cells infected by other respiratory viruses, such as PIV3. Evaluation of RSV mutants deleted individually of NS1 or NS2 genes (RSVΔNS1 and RSVΔNS2) showed that RSVΔNS1 infection induced ciliated cell rounding in a manner indistinguishable from that of RSV expressing a full complement of RSV genes, suggesting NS1 was not responsible for the cell rounding phenotype (Figure 3.5Bii and iv). In contrast, ciliated cells infected by RSVΔNS2 did not round and instead maintained a columnar morphology identical to that after RSVΔNS1/2 infection (Figure 3.5Biii and iv). These

differential effects of the NS deleted viruses were not due to significant differences in mutant virus replication, as both RSVΔNS1 and RSVΔNS2 were similarly attenuated for replication compared to RSV in cell-lines (104) and HAE (Figure 2.3). Overall, these experiments indicate that expression of NS2, in the context of RSV infection, is necessary for RSV-induced ciliated cell rounding.

To determine if a specific, known domain in the NS2 protein was associated with rounding, we infected HAE with a series of mutants containing deletions in the NS2 protein. Serial 5 – 10 amino acid deletions were introduced into the NS2 protein, and an N-terminal HA tag was added to facilitate detection of the NS2 protein (Figure 3.6B). Deletion of the first 20 amino acids of the N-terminus of NS2 had no effect on the ability of the virus to cause cell rounding, and cells infected by these mutants were morphologically identical to cells infected by wild-type RSV (Figure 3.6A, C NΔ10, NΔ20, NΔ10-20). However, deletion of the first 5 amino acids of the C-terminus or deletions within the internal section of NS2 ablated the ability of RSV to cause infected cell rounding, and the morphology of cells infected by these mutants resembled RSVΔNS2-infected cells (Figure 3.6A, C NΔ30-40, NΔ40-50, NΔ50-60, NΔ84-94, CΔ10, CΔ5). All deletion mutants were attenuated for replication in HAE. Expression of NS2 was confirmed in HEp-2 cells by western blot (data not shown).

Expression of NS2 by recombinant PIV3 mimics RSV-induced cell morphology

To investigate whether RSV NS2, in the absence of other RSV genes, was sufficient to induce rounding of virus-infected ciliated cells, we took advantage of our findings that ciliated cells infected by PIV3 retained columnar morphology. Since PIV3, like RSV, exclusively infects ciliated cells in HAE cultures, we used PIV3 to deliver RSV NS1, NS2, or both genes to ciliated cells in the absence of other RSV genes. We engineered recombinant PIV3 containing the GFP gene to express NS2 (PIV3-NS2), NS1 (PIV3-NS1), or both NS1

and NS2 (PIV3-NS1/2) and assessed consequences of infection compared to PIV3 expressing GFP alone. In each case, GFP was inserted between the P and M genes, and the RSV gene(s) were inserted between the HN and L genes. These recombinants were readily recovered, and infection and growth was assessed in non-polarized epithelial cell-lines and HAE cultures. In non-polarized epithelial cell-lines, recombinant PIV3 viruses expressing RSV NS genes and GFP were slightly attenuated for growth compared to PIV3 expressing GFP alone (data not shown). Similar to the phenotype observed in cell lines, in HAE, all 3 PIV3 viruses expressing RSV NS genes exhibited modest growth attenuation compared to PIV3, despite similar levels of infection at 1 day pi (Figure 3.7A). PIV3-NS2 and PIV3-NS1 exhibited similar growth attenuation in HAE, replicating to ~1-log lower titers than PIV3 at 3 days pi, the time of peak replication. PIV3-NS1/2 was more severely attenuated, producing 2-logs lower titers than PIV3 at the time of peak replication. This observed attenuation presumably reflected the increased genome length and gene number of the PIV3 viruses with inserted RSV NS genes, although the formal possibility exists that the RSV NS proteins had direct inhibitory effects on replication.

In HAE cultures, ciliated cells infected by PIV3 or PIV3-NS1 maintained native columnar morphology, whereas ciliated cells infected by PIV3-NS2 or PIV3-NS1/2 underwent cell rounding, with significantly shortened cell heights (Figure 3.7B, C). The observation that PIV3-NS1/2 and PIV3-NS2 caused cell rounding indistinguishable from that caused by RSV suggested NS2 mediated this effect independent of the expression of NS1 or other RSV proteins.

NS2 expression adversely affects lumenal surface structures and functions of ciliated cells

Closer examination of ciliated cells infected by PIV3-NS2 or PIV3-NS1/2 showed that the ultrastructural features of the apical domains of infected ciliated cells were altered in a

manner similar to RSV-infected cells. Characteristics of RSV-infected ciliated cells such as bulging apical membranes, thinning of the terminal web, and loss of cilia and microvilli were evident in, and indistinguishable between, cells infected with RSV, PIV3-NS2, and PIV3-NS1/2 (Figure 3.8A).

Functional studies were performed to measure the extent of cilia activity in HAE infected by recombinant viruses. These results demonstrated that, for the first 4 days pi, PIV3-NS2 and PIV3-NS1/2 infection resulted in a marked decline in the surface area of epithelium displaying cilia activity (Figure 3.8B). In contrast, PIV3 infection did not cause a decline in cilia activity until 5 days pi. PIV3-NS1, despite robust replication, had little effect on cilia activity within the 6 days of experimental analysis. These data suggest PIV3 infection is not as cytopathic to cilia activity as PIV3-NS2, indicating NS2-promoted cell rounding may also be associated with disruption of cilia or cilia scaffolding complexes in infected cells. We also noted the reduced cilia cytopathology observed with PIV3-NS1 infection compared to PIV3, suggesting NS1 may further reduce even the moderate cytopathology evident after PIV3 infection. These findings are intriguing as they point to divergent effects of RSV NS1 and NS2 on ciliated cell cytopathology.

IFNβ and cytokine changes in HAE infected by PIV3, PIV3-NS1, and PIV3-NS2

PIV3 encodes viral proteins to block cellular innate immune responses, although infection of HAE induces cytokine secretion at later timepoints (218). We therefore determined if addition of NS1 or NS2 into wild-type PIV3 would have an additive effect on suppression of IFN and cytokine expression. Due to subtle but potentially significant differences in replication and spread of these viruses, we focused on the early timepoint 18 hours pi, accounting for changes in gene expression in cells infected prior to several rounds of replication and spread.

At 18 hours pi, message for PIV3-N was detectable in HAE infected by PIV3, PIV3-NS1, and PIV3-NS2, confirming active replication of the virus (Figure 3.9A). Interesting, N levels were significantly higher in PIV3-NS2 infected cultures compared to PIV3 despite equal inoculum. It is unclear from these studies whether greater numbers of cells were infected by PIV3-NS2 or whether PIV3-NS2 message is expressed at greater levels within individual cells compared to PIV3 or PIV3-NS1. Infection with each virus resulted in IFNβ message levels elevated over mock-infected cultures, although there were no significant differences between PIV3, PIV3-NS1, or PIV3-NS2 (Figure 3.9B). IL-8 message levels were not elevated over mock-inoculated cultures following infection with PIV3 or PIV3-NS1 (Figure 3.9C). However, PIV3-NS2 infection resulted in a 15-fold increase in IL-8 message. While it is possible that the increase in IL-8 message was a direct result of increased PIV3-NS2 replication, normalization of IL-8 signal to PIV3 N signal in PIV3-NS2 infected cultures resulted in over a 6-fold increase in message. We also found CXCL10 message levels were increased following infection with all viruses, though PIV3-NS2 resulted in increased message levels compared to PIV3 or PIV3-NS1 (Figure 3.9D)

3.4 Discussion

In this study, we used cultures of primary human pseudostratified airway epithelial cells (HAE), which closely resemble the epithelium of authentic airway tissue, and show that RSV infection of human ciliated cells resulted in the development of a rounded cell morphology and distinct apical surface cytopathology, followed by extrusion of the infected cells from the epithelium. This effect was not observed with PIV3 or several other respiratory paramyxoviruses that target ciliated cells. Once shed, RSV-infected epithelial cells became incorporated into airway secretions, underwent apoptosis, and were then transported across the airway surface by coordinated cilia beat.

The use of RSV gene-deletion mutants demonstrated that these effects were dependent on the expression of the RSV NS2 protein. Specifically, whereas ciliated cells infected by RSV became rounded, ciliated cells infected with RSVΔNS2 remained columnar and embedded within the intact epithelium. Because PIV3 also targeted ciliated cells but did not cause the cell rounding phenotype, we used PIV3 as a vector to express RSV genes in ciliated cells. Infection of ciliated cells in vitro with PIV3 engineered to express RSV NS2 (PIV3-NS2) resulted in infected cell morphologic changes indistinguishable from ciliated cells infected by RSV, whereas cells infected with PIV3 or PIV3-NS1 remained columnar. Findings from both RSV deletion mutants and PIV3 expressing individual RSV genes indicated that the induction of this novel ciliated cell morphologic phenotype was unique to RSV, and that expression of RSV NS2 in the context of an RSV or PIV3 infection was sufficient to induce this phenotype in ciliated cells.

To identify the functional domain within NS2 responsible for cell rounding, we infected HAE with RSV containing sequential deletion mutations within the NS2 protein. Viruses with deletion of amino acids 30-40, 40-50, 50-60, and 84-94, relative to the N-terminus of NS2, are unable to induce cell rounding and retain the native columnar morphology, identical to cells infected with RSVΔNS2. Although NS2 expression following infection of HEp2 cells with these RSV deletion mutants has been confirmed by western blot, we have not yet confirmed expression in ciliated cells. Thus, it is also possible that deletion of internal sections of the NS2 protein resulted in protein degradation or malfunction, resulting in complete loss of NS2 function. Deletion of the first 5 or 10 amino acids from the C-terminus of NS2 also results in a loss of cell rounding. Little is known about the functional domains within the NS2 protein, although Swedan and coworkers demonstrated that deletion of the C-terminal 10 amino acid residues of NS2 abrogated the ability of NS2 to decrease STAT2 levels and impaired the NS2-mediated response to

exogenous IFNβ (95). Because the C-terminus of NS1 and NS2 are relatively well conserved, with both containing the same DNLP amino acid tetramer followed by an aromatic residue (F/Y), it would be interesting if these regions had differing signaling functions in the context of infection. Future studies of these mutants to determine differences in NS2 expression, viral replication, and NS2 function will contribute to the understanding of the functions of NS2 in infected ciliated cells.

Previous studies have demonstrated that the RSV NS proteins enhance viral replication. Recombinant RSV deleted for one or both NS genes resulted in viruses with severely attenuated growth in vitro and in vivo (93, 107, 219). Deletion of either the NS1 or NS2 gene attenuated human RSV in chimpanzees (106, 107). The NS proteins have also been shown to interfere with a number of antiviral host responses aimed at reducing the extent of virus replication, most notably type I and III interferon (IFN) pathways. The mechanisms by which NS1 and NS2 inhibit IFN responses are complex, involving both coordinated and independent functions of the NS proteins (93-95, 98, 100). Both proteins have also been implicated in inhibiting apoptosis (92) and RSV NS2 was reported to enhance induction of NF-kB (104). Although some effects of the NS proteins appear to involve synergy between NS1 and NS2, this did not appear to be the case in the present study. Here, the cell morphologic and shedding phenotype attributed to RSV NS2 appeared to be independent of, and unaffected by, NS1. While the precise mechanism of NS2-induced morphologic consequences remains unknown, we speculate that these events are not directly related to the ability of NS2 to modify interferon responses.

Destruction of apical cilia structures and shedding of infected cells following RSV infection resulted in a net decline in the epithelial surface area with active cilia. Coordinated cilia beat is required for effective transport of particles across the airway surface and, as expected, a marked decline in mucociliary transport (MCT) rate was observed following RSV

infection. Interestingly, MCT rate began to decline prior to loss of ciliated epithelium, where, at day 4 pi, although ~60% of the epithelium displayed active cilia, MCT rate was drastically reduced. We therefore suggest that two processes modulated the RSV-mediated decline in MCT rate. First, RSV infection of an individual ciliated cell leads to degradation of the cilia apparatus before the infected cell is extruded from the epithelium. Ciliary dyskinesia and asynchronous cilia beat of infected cells disrupt unidirectional flow, resulting in local decreases in mucociliary transport. Second, as infection spreads, increased numbers of cells experience ciliary dyskinesia and the process of cell shedding removes ciliated cells from the epithelium. As fewer uninfected ciliated cells are available to provide for cilia beat, noted by a decrease in percentage of ciliated epithelium, MCT is abolished and RSV-infected HAE are unable to transport shed cells across the airway epithelium. These factors are also likely to impair mucociliary clearance in vivo.

Unusual epithelial cell morphology and sloughing of virus antigen positive cells has been described for RSV-infected humans and bovine RSV-infected calves (116, 119, 161). The loss of cilia and disorganization of cilia basal bodies was reported in a bovine model of RSV infection, as we have noted in human ciliated cells infected by RSV and PIV3-NS2 (116). Ciliary dyskinesia and damage have also been reported in RSV-infected primary human ciliated cultures (175). Thus, in in vivo models of RSV infection and retrospective analysis of RSV-infected human lung tissue, shedding of virus infected epithelial cells and degradation of the cilia apparatus appear to be a characteristic of RSV infection.

The mechanism by which RSV NS2 exerts its effects on epithelial cell rounding and shedding remains to be explored. Comparison of PIV3-NS2 infection of epithelial cell-line monolayers with PIV3 or PIV3-NS1 did not reveal a morphological phenotype specific to RSV NS2 (data not shown), suggesting the differentiated state of the columnar airway epithelial cells is a critical component of RSV N2-induced cell rounding. The use of

differentiated airway models such as HAE will therefore be critical in understanding how RSV NS2 modifies airway epithelial cells, resulting in shedding of infected cells into the airway lumen.

The innate inflammatory response plays a critical role in RSV disease and recruitment of leukocytes to regions of infection occurs following secretion of chemoattractants, including IL-8, CXCL10, and RANTES. These cytokines are detected at elevated levels in nasophyngeal secretion and bronchoalveolar aspirates of infants experiencing RSV-associated bronchiolitis (143, 181). Elevated IL-8 levels in nasal washes are associated with more severe disease (144) and neutrophils, recruited by IL-8, are the major type of leukocyte detected in the airway of RSV-infected infants (180). Although these cytokines are secreted by a number of cell types, upreglation of IL-8, CXCL10, and RANTES gene expression in HAE following RSV infection suggests that ciliated cells play an important role in the recruitment of leukocytes. Interestingly, PIV3-NS2 infection of HAE results in more robust upregulation of IL-8 gene expression compared to PIV3 at 18 hours pi, suggesting a role for RSV NS2 in upregulation of IL-8. IL-1β secretion in nasophryngeal washes has also been positively correlated with RSV disease severity (133). In HAE, IL-1β gene transcription is elevated only a single timepoint, 4 days pi, suggesting other cell types, such as macrophages, may responsible for this increase. However, because we determined gene transcription, rather than protein secretion, cleavage of endogenous IL-1β precursor and secretion of mature IL-1β from the epithelium may occur in the absence of gene signal changes. In infected HAE, proinflammatory cytokine secretion may occur from infected cells as a direct result of viral replication or following paracrine activation of uninfected surrounding cells. These message studies do not differentiate between gene transcription in infected versus uninfected cells and we therefore cannot unequivocally determine the infection status and cell type responsible for driving cytokine secretion following RSV

infection. Regardless, these findings provide addition evidence for the central role of airway epithelial cells in modulating the inflammatory response following RSV infection.

In summary, we present evidence that infection of ciliated cells in a model of the human airway epithelium by RSV, but not by several other common respiratory paramyxoviruses, results in cell rounding, disruption of the cilia apparatus, active shedding of individual infected cells, and delay of apoptosis until infected cells are shed from the epithelium. We also demonstrate that infection of HAE results in increased gene transcription of proinflammatory cytokines associated with severe RSV-associated bronchiolitis. Thus, the consequences of RSV infection of HAE reflect several important characteristic hallmarks of RSV disease in infants. By performing loss-of-function and gain-of-function experiments, we attribute these consequences of infection to the RSV NS2 protein. We suggest that the NS2 protein is an important pathogenesis factor for RSV disease and may represent a therapeutic target to dampen disease severity.

3.5 Materials and Methods

Cells

Human airway epithelial cells were isolated by the UNC Cystic Fibrosis Center Cell Culture and Tissue Procurement Core from tracheobronchial airway specimens obtained from patients provided by the National Disease Research Interchange (NDRI, Philadelphia, PA) or as excess tissue following lung transplantation. All protocols were approved by the University of North Carolina at Chapel Hill Institutional Review Board. Primary epithelial cells derived from single patient sources were plated on permeable Transwell-Col supports (12-mm diameter, Corning, Inc.) and grown in custom media at an air-liquid interface for 8 to 10 weeks to form differentiated, polarized cultures as previously described (211). HEp2 cells (ATCC) were maintain in MEM (Gibco) supplemented with 10% fetal bovine serum. LLC-

MK2 cells (ATCC) were maintained in DMEM (Gibco) supplemented with 10% fetal bovine serum.

Viruses

All viruses used in this study were derived from cDNA (recombinant) and contain a GFP insertion as an additional gene unless otherwise stated.

Recombinant human metapneumovirus (HMPV; strain CAN97-83), parainfluenza virus 5 (PIV5; strain W3A), and Sendai virus (SeV) were described previously (214, 220, 221) and were provided by Drs. Peter Collins, Robert Lamb, and Daniel Kolakofsky, respectively. RSV Memphis 37 strain was isolated from a pediatric case of bronchiolitis and has been described previously (178). This virus is a primary low-passage clinical isolate, not a recombinant virus, and does not express GFP. This virus was provided by Dr. John DeVincenzo.

Wild-type RSV, RSVΔNS1, RSVΔNS2, and RSVΔNS1/2 are derivatives of the A2 strain and were constructed and described previously (105, 106, 212, 213). These viruses were provided by Dr. Peter Collins. Each of these RSV constructs express the green fluorescent protein (GFP) gene as an additional gene inserted between the RSV phosphoprotein (P) and matrix (M) genes. Wild-type RSV and all mutants were amplified in HEp2 cells stably expressing the V gene from SV5 (210).

RSV viruses containing deletions of the NS2 gene are derivatives of the A2 strain and were constructed and provided by Michael Teng. An HA tag has been added to the N-terminus of the NS2 gene in each of these constructs. These viruses were amplified in HEp2 cells and do not contain a GFP gene insertion.

PIV3 is a derivative of the JS strain engineered to express the GFP gene as an additional gene inserted between the PIV3 phosphoprotein (P) and matrix (M) genes, as has been described previously (81, 222). Codon-optimized RSV NS1 or NS2 genes were

synthesized (DNA2.0) and inserted into the PIV3 viral genome between the hemagglutinin-neuraminidase (HN) and viral polymerase (L) genes using cloning methods similar to those previously used to express CFTR and rhAFP in this genome region (223, 224). A unique EagI restriction site was generated in the non-coding region downstream of the HN gene in the PIV3 subgenomic cDNA. The NS1 or NS2 coding sequence was amplified by RT-PCR from plasmids expressing codon-optimized NS1 or NS2 , cloned into a pCR-Blunt II-TOPO vector (Invitrogen), and sequenced. The following primer sets were used: NS1 sense (5'-CCGCGGCCACCATGGGCAGCAATAGTCTC-3'), NS1 antisense (5'-GGGCCCGAGTTATGGGTTCAGGTCAA-3'), NS2 sense (5'-CCGCGGCCACAATGGATACCACGC-3'), and NS2 antisense (5'-GGGCCCCTCGAGTCAAGGGTTCAA-3'). The underlined portions represent SacII and ApaI restriction sites. Using the SacII and ApaI restriction sites, NS1 or NS2 was inserted into a vector following a linker sequence consisting of the PIV3 gene-end, intergenic, and gene-start transcription regions, flanked at both ends by EagI sites. This cassette was then inserted using the EagI sites into the full-length PIV3GFP antigenomic cDNA and the resulting genomes were designated PIV3-NS1 or PIV3-NS2. A PIV3 genome expressing both NS1 and NS2 was also generated by inserting the RSV NS1 and NS2 genes together into PIV3 between the HN and L genes using similar methods. From the linker vector containing NS1, a sequence consisting of the EagI restriction site, PIV3 linker region, and NS1 gene was PCR amplified using the NS1 sense primer (5'-CGAATTGGCGGCCGAAAATA-3') and the NS1 antisense primer (5'-CAGGAGTTCAGCACGATGGGGGCCCGAGTTATGGGT-3'), destroying the 3' EagI site and creating an 18bp overhang. From the linker vector containing NS2, a sequence consisting of the PIV3 linker region, the NS2 gene, and the EagI restriction site was amplified using the NS2 sense primer (5'-

GCTGAACTCCTGCATCGTAAAATAAGAAAAACTTAG-3') and the NS2 antisense primer (5'-ACTTGGCCCAAGCTTGAGTA-3'), destroying the 5' EagI site and adding the complementary 18bp overhang. These 2 fragments were combined in a fusion reaction using the NS1 sense and NS2 antisense primers and the resulting fragment was cloned into a pCRBluntII TOPO vector (Invitrogen) and sequenced. The final fragment consisted of a PIV3 linker region, the RSV NS1 gene, a second PIV3 linker region, and the RSV NS2 gene, flanked by EagI sites. This cassette was then inserted using the EagI sites into the full-length PIV3GFP antigenomic cDNA, creating PIV3-NS1/2. Each insert was designed to retain the "rule of six" required for PIV3 genome replication. All viruses were rescued and amplified in LLC-MK2 cells using methods described previously (222) and sequenced.

Viral inoculations and growth

The apical surfaces of HAE were rinsed with PBS to remove excess airway secretions. Virus inoculum diluted in serum-free DMEM (Gibco; 100 µl per 12 mm well) was applied to the apical surface of HAE for 2 hrs at 37°C then removed by aspiration and the apical surfaces rinsed with PBS, and cultures incubated at 37°C. Viral growth kinetics were determined by performing apical surface washes with 300 µl of serum-free DMEM which were harvested after 30 min at 37°C and stored at −80°C until analysis. RSV viral titers in the apical washes were determined on HEp2 cells by titration and counting GFP-positive cells 24 h post-inoculation. PIV3 viral titers were determined by a 50% tissue culture infectious dose ($TCID_{50}$) assay on LLC-MK2 cell monolayers, with positive wells scored by GFP expression. *En face* fluorescent images of GFP-positive cells in HAE were captured using a Leica DMIRB Inverted Fluorescent Microscope equipped with a Retiga 1300 CCD camera (Q-Imaging). The proportion of the surface area of epithelium positive for GFP was determined by pixilating a black-and-white image and calculating the percentage of black pixels using ImageJ software (NIH) for five fields per culture and averaging the results.

Histology and immunoprotocols

Tight junctions were visualized by fixing HAE in 4% paraformaldehyde in PBS followed by permeabilization with 1.5% Triton-X100 in PBS. Immunodetection of ZO-1 was performed by blocking cultures in 3% bovine serum albumin (BSA) in PBS followed by incubation with a primary antibody against ZO-1 (mouse monoclonal, Invitrogen). Immunoreactivity was detected using an anti-mouse secondary conjugated to Alexafluor 594 (Molecular Probes). *En face* images were captured on a Leica SP5 confocal microscope.

For histological analysis, HAE fixed in 4% paraformaldehyde in PBS were paraffin embedded and 5 μm thick histological sections prepared. Sections were stained with hematoxylin and eosin (H&E) or Richardson's stain. Immunodetection of RSV antigen and β-tubulin IV was performed by blocking sections in 3% bovine serum albumin (BSA) in PBS followed by incubation with primary antibodies against GFP (rabbit polyclonal; Abcam) and β-tubulin IV (mouse monoclonal; Sigma). Immunoreactivity was detected using an anti-rabbit IgG conjugated to Alexafluor 488 and an anti-mouse IgG conjugated to Alexafluor 594 (Molecular Probes). In cases when we wished to preserve and visualize apical secretions of HAE, cultures were fixed in the alcohol-based fixative Omnifix (FR Chemical) as previously described (225) and stained with H&E. Immunohistochemistry for viral antigen were performed by blocking sections in 3% BSA and incubation with primary antibodies against RSV (anti-RSV goat polyclonal; Meridian Life Sciences) or PIV3 (anti-PIV3 rabbit serum raised against sucrose-gradient-purified PIV3; (226)). Immunoreactivity was detected using anti-goat or anti-rabbit secondary antibodies conjugated to horseradish peroxidase (HRP), visualized using 3,3'-diaminobenzidine (Sigma), and counterstained with hematoxylin. For transmission electron microscopy studies, HAE were fixed in glutaraldehyde solution followed by an osmium tetroxide solution to preserve the hydrated external environment of the HAE, as previously described (225), and visualized using standard TEM techniques.

Morphometric analysis of cell height and airway occlusion

XZ confocal images were acquired using a Leica SP5 confocal microscope. XZ images through the tallest region of a GFP-positive infected cell in fixed but unprocessed HAE cultures were imported into ImageJ software (NIH) where pixel height was measured and converted to microns using the electronic magnification measurement bar from the confocal image. A minimum of 100 infected cells were measured from at least 3 individual donors.

qRT-PCR

Cytokine gene expression at the mRNA level was determined by quantitative reverse transcription PCR (qRT-PCR). HAE were harvested at time points indicated and stored in RNAzol at −80°C until analysis. Total intracellular RNA was isolated from HAE samples using the RNeasy RNA Isolation kit (Qiagen). Complimentary DNA was generated using Oligo(dT) primers and SuperScript II reverse transcriptase (Invitrogen). Real-time PCR was performed using Taqman gene expression assays and an Applied Biosystems 7500 Fast Real-Time PCR System (Applied Biosystems). Input cDNA was normalized to GAPDH and signals were expressed as a ratio to mock-infected HAE signals.

Cell shedding

Cell shedding was quantified by determining the amount of double-stranded DNA (dsDNA) in apical washes of HAE using the Quant-It PicoGreen dsDNA kit (Invitrogen). Apical washes were performed with 300 µl serum-free DMEM for 30 min at 37°C. Washes were harvested and stored at −80°C prior to analysis. Samples were diluted five-fold in Tris-EDTA buffer and dsDNA was measured in duplicate following manufacturer's instructions using a 96-well plate format. dsDNA concentration per sample was calculated based on fluorescence of a titrated dsDNA standard.

Percentage area ciliated

Following removal of apical washes for titer and cell shedding assays, HAE were allowed to come to room temperature for 15 min to normalize cilia beat frequency and 100 µl PBS was added apically. HAE were placed on an inverted phase contrast microscope (TE2000; Nikon) using a 20x objective and high speed (125Hz) video images were captured with an eight-bit b/w camera (GS-310 Turbo; Megaplus). The analog signal was digitized via an analog-to-digital converter board (A/D; National Instruments). A digital computerized analysis system was used to analyze the acquired video images, using software based on Sisson-Ammons Video Analysis (227).

Mucociliary transport rates

Following removal of apical washed for titer and shedding assays, green fluorescent microspheres (0.02% v/v, 1µm; Invitrogen) were added to the apical surface and HAE were incubated at 37^{o}C. Time-lapse fluorescent images were obtained for 3 s using a Leica DMIRB Inverted Fluorescent Microscope equipped with a Retiga 1300 CCD camera (Q-Imaging). The rate of microsphere displacement was calculated as previously described (223).

Statistical analysis

Unpaired t-test and one-way analysis of variance (ANOVA) with Tukey's post-test was performed as indicated. Statistical significance was defined as $P<0.05$ unless otherwise noted.

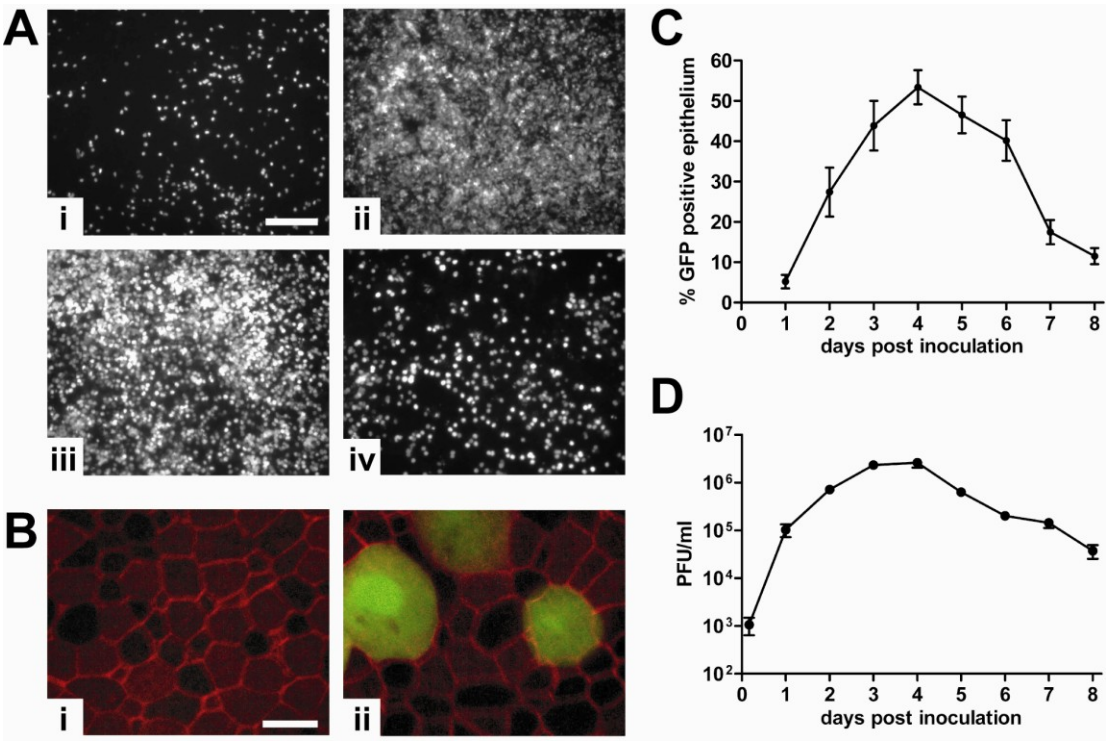

Figure 3.1. RSV-GFP infection, replication, and clearance in HAE cultures. (A) Representative *en face* fluorescent images of GFP-positive cells in HAE infected with RSV expressing GFP at 1 (i), 3 (ii), 5 (iii), and 7 (iv) days post-inoculation. Scale bar represents 200 μm. **(B)** Representative *en face* images of uninfected (i) or RSV infected (ii) HAE at 1d pi. Infected cells are detected by GFP fluorescence (green) and tight junctions are detected using an antibody against ZO-1 (red). Scale bar represents 10 μm. **(C)** The number of RSV infected cells in HAE over time quantified as the percentage of the epithelium surface area positive for GFP fluorescence. **(D)** Virus titers present in the airway surface fluid over time. Data (mean ± SEM) are representative of independent experiments utilizing at least n = 4 cultures per donor obtained from 3 different donors.

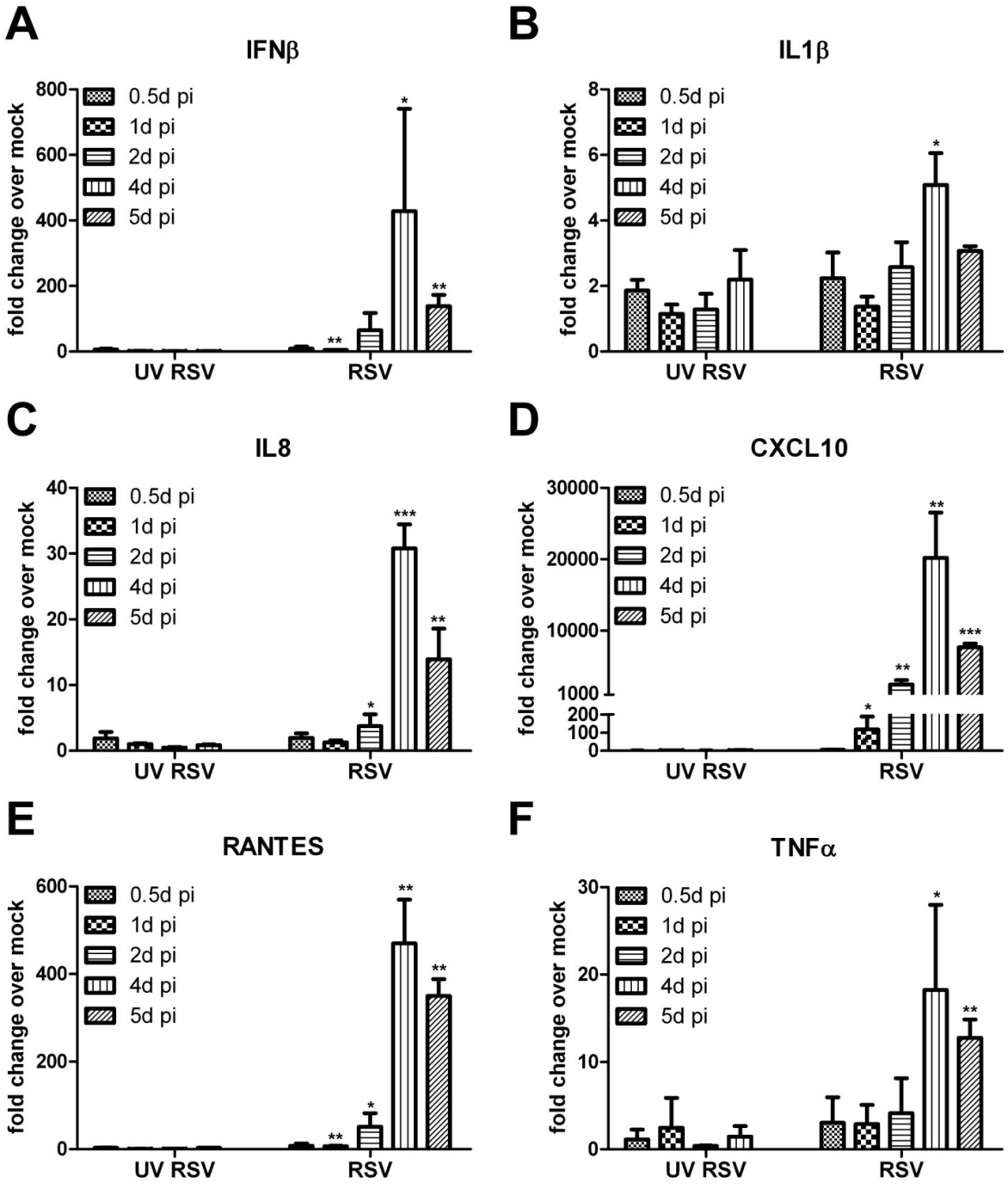
A
IFNβ
fold change over mock
800
600
400
200
0
0.5d pi
1d pi
2d pi
4d pi
5d pi
UV RSV
RSV
B
IL1β
8
6
4
2
0
C
IL8
40
30
20
10
0
D
CXCL10
30000
20000
10000
1000
200
100
0
E
RANTES
600
400
200
0
F
TNFα
30
20
10
0

Figure 3.2. IFN and cytokine production in HAE following infection with RSV-GFP. Expression levels of IFNβ **(A)**, IL-1β **(B)**, IL-8 **(C)**, CXCL10 **(D)**, RANTES **(E)**, and TNFα **(F)** were determined in RSV and UV-inactivated RSV infected HAE. Total RNA was extracted from infected HAE at 12h pi and days 1, 2, 4, and 5 pi and gene expression levels were measured by qRT-PCR. Each sample was internally normalized to GAPDH and is expressed as fold change compared to mock-inoculated culture. Data (mean ± SD) represent n=3 cultures. Significant changes in mRNA levels of RSV relative to UV-inactivated RSV were determined for each time point by unpaired *t* test. Unmarked: not significant; **P*<0.05, ***P*<0.01, ****P* < 0.001.

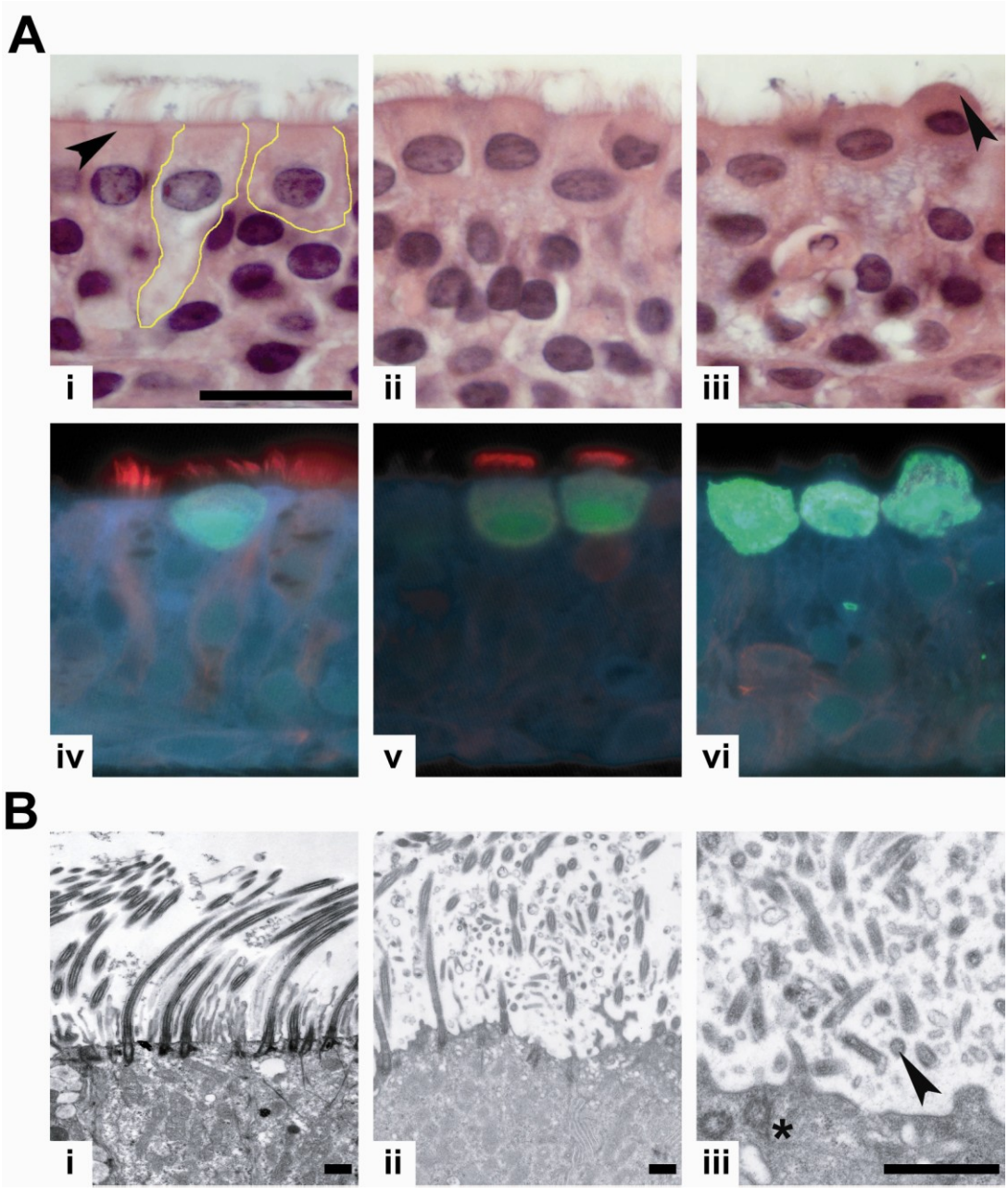
A
i
ii
iii
iv
v
vi
B
i
ii
iii
*

Figure 3.3. Morphologic and structural changes in RSV-infected ciliated columnar cells. (A) Representative histologic sections of HAE inoculated with RSV expressing GFP and counterstained with H&E (i-iii) or immunoprobed for GFP (green) and beta-tubulin IV (red) (iv-vi) at 1 (i, iv), 3 (ii, v), and 5 (iii, vi) days pi. Yellow outlines in (Ai) depict the different ciliated cell morphologies seen in RSV infected HAE, where non-infected ciliated cells are columnar and RSV infected ciliated cells exhibit rounded morphology. Arrowheads indicate robust apical terminal web in non-infected ciliated cells (i) which thins in RSV-infected ciliated cells with rounded morphology (iii). Images are representative of independent experiments with 4 different donor cultures. Scale bar represents 10 μm. **(B)** Representative transmission electron micrographs of cross-sections of the apical surfaces of non-infected (i) and RSV-GFP-infected (ii, iii) HAE. Arrowhead indicates particulates showing virus-like morphology. Star indicates disorganized basal bodies. Scale bar represents 1 μm.

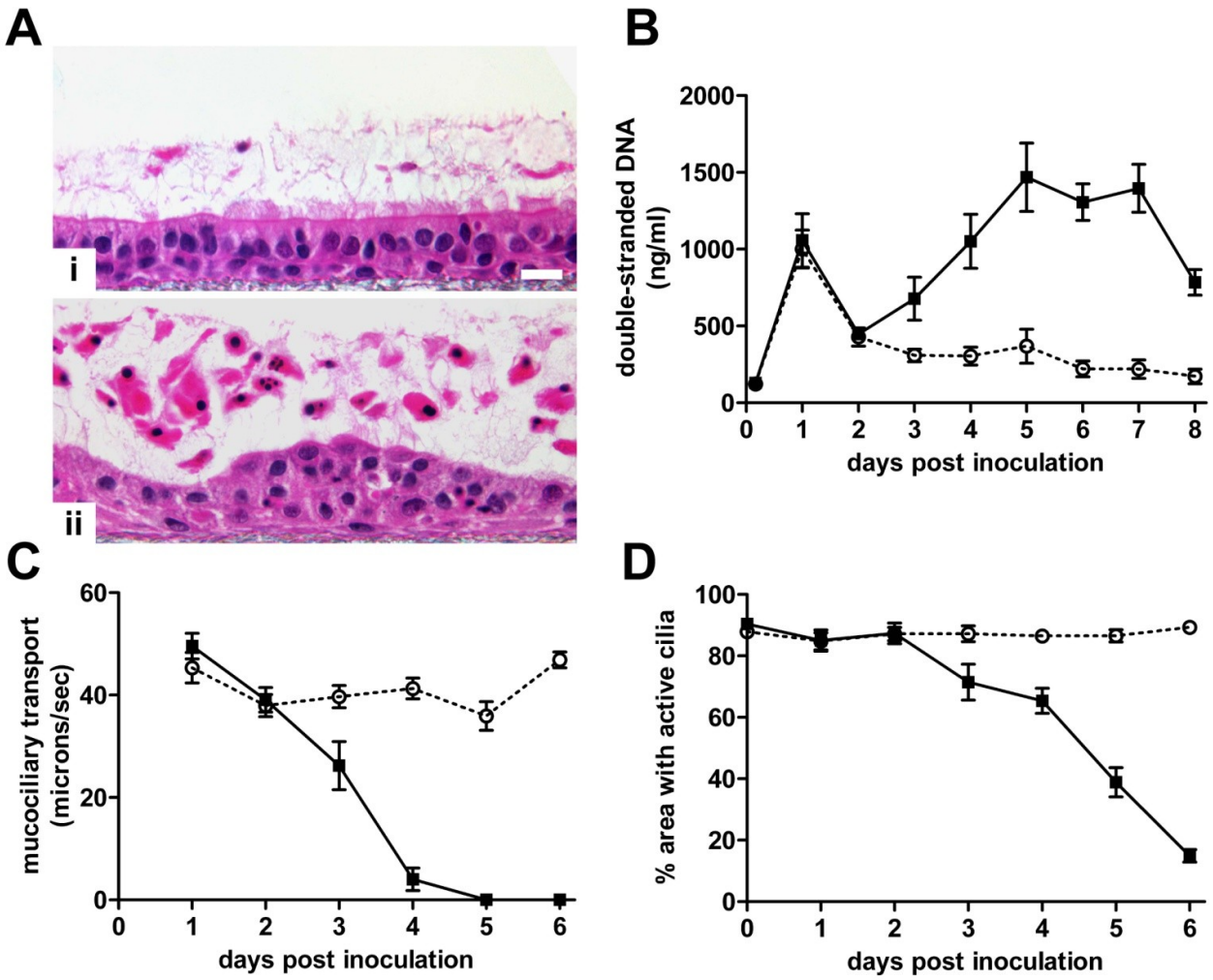
A
i
ii
B
double-stranded DNA (ng/ml)
2000
1500
1000
500
0
0 1 2 3 4 5 6 7 8
days post inoculation
C
mucociliary transport (microns/sec)
60
40
20
0
0 1 2 3 4 5 6
days post inoculation
D
% area with active cilia
100
80
60
40
20
0
0 1 2 3 4 5 6
days post inoculation

Figure 3.4. Ciliated cell shedding and loss of cilia activity during RSV-GFP infection of HAE. (A) Representative images of histological cross-sections of non-infected (i) or HAE infected with RSV expressing GFP (ii) fixed at 5 days pi using a fixation protocol to preserve the content and depth of airway surface secretions. Scale bar represents 20 μm. **(B)** Concentration of dsDNA as an index for numbers of shed cells present in apical washes harvested every 24 h from non-infected (open circles) or RSV-infected (closed squares) HAE. Data (mean ± SEM) are derived from n = 4 cultures per donor for 4 different donors. **(C)** Fluorescent bead velocity as an index of mucus transport rates on the apical surfaces of non-infected (open circles) or RSV-infected (closed squares) HAE at indicated times post-inoculation. Data (mean ± SEM) represent n = 3-6 cultures per donor for 3 different donors. **(D)** Surface area of active cilia beat on non-infected (open circles) or RSV-infected (closed squares) HAE. Data (mean ± SEM) represent n = 4. Data in panels (B) – (D) show significant differences at 3d pi ($P<0.05$) and at all time-points thereafter ($P<0.001$), as determined by unpaired *t* test.

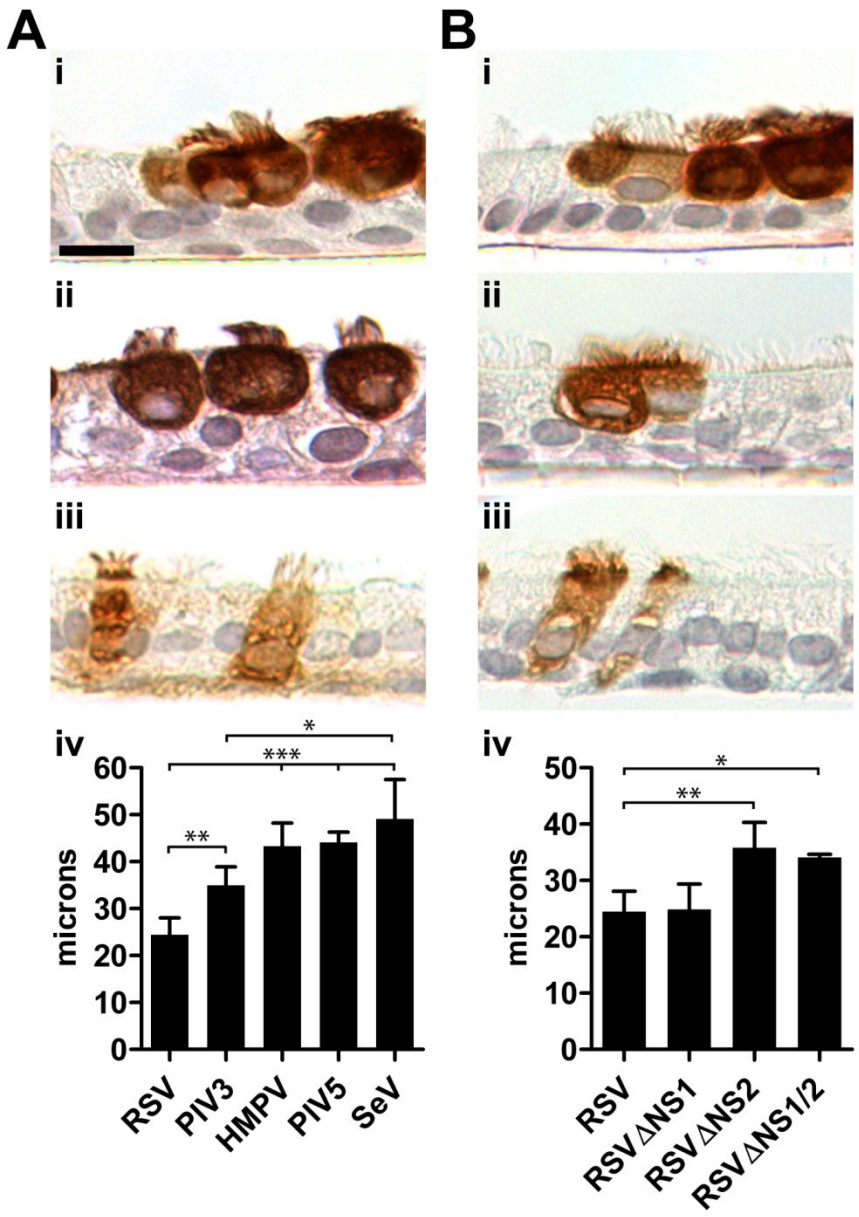
A
B
i
ii
iii
iv
microns
RSV
PIV3
HMPV
PIV5
SeV
RSV
RSVΔNS1
RSVΔNS2
RSVΔNS1/2

Figure 3.5. RSV-induced ciliated cell rounding is unique to RSV infection and due to expression of the RSV NS2 protein. (A) Representative images of histologic cross-sections of fixed and paraffin embedded HAE infected with recombinant RSV-GFP (i), low passage clinical isolate RSV Memphis 37 (ii), or recombinant PIV3-GFP (iii). Infected cells were detected at 3 days pi using an anti-RSV antibody (i, ii) or anti-PIV3 antibody (iii). Scale bar represents 10 μm. Height of infected ciliated cells (mean ± SD) was determined by confocal microscopy of fixed but unprocessed HAE infected with RSV, PIV3, human metapneumovirus (HMPV), parainfluenza virus 5 (PIV5), or Sendai virus (SeV) (iv). All viruses express GFP. At least 100 infected cells in cultures obtained from 3 different donors were measured. **(B)** Representative images of histologic cross-sections of HAE infected with RSV (i), or gene deletion mutants RSVΔNS1 (ii) and RSVΔNS2 (iii). All viruses express GFP. Height of infected cells (mean ± SD) was determined as in (Aiv). **P*<0.05, ***P*<0.01, ****P* < 0.001, one-way ANOVA with Tukey's post-test.

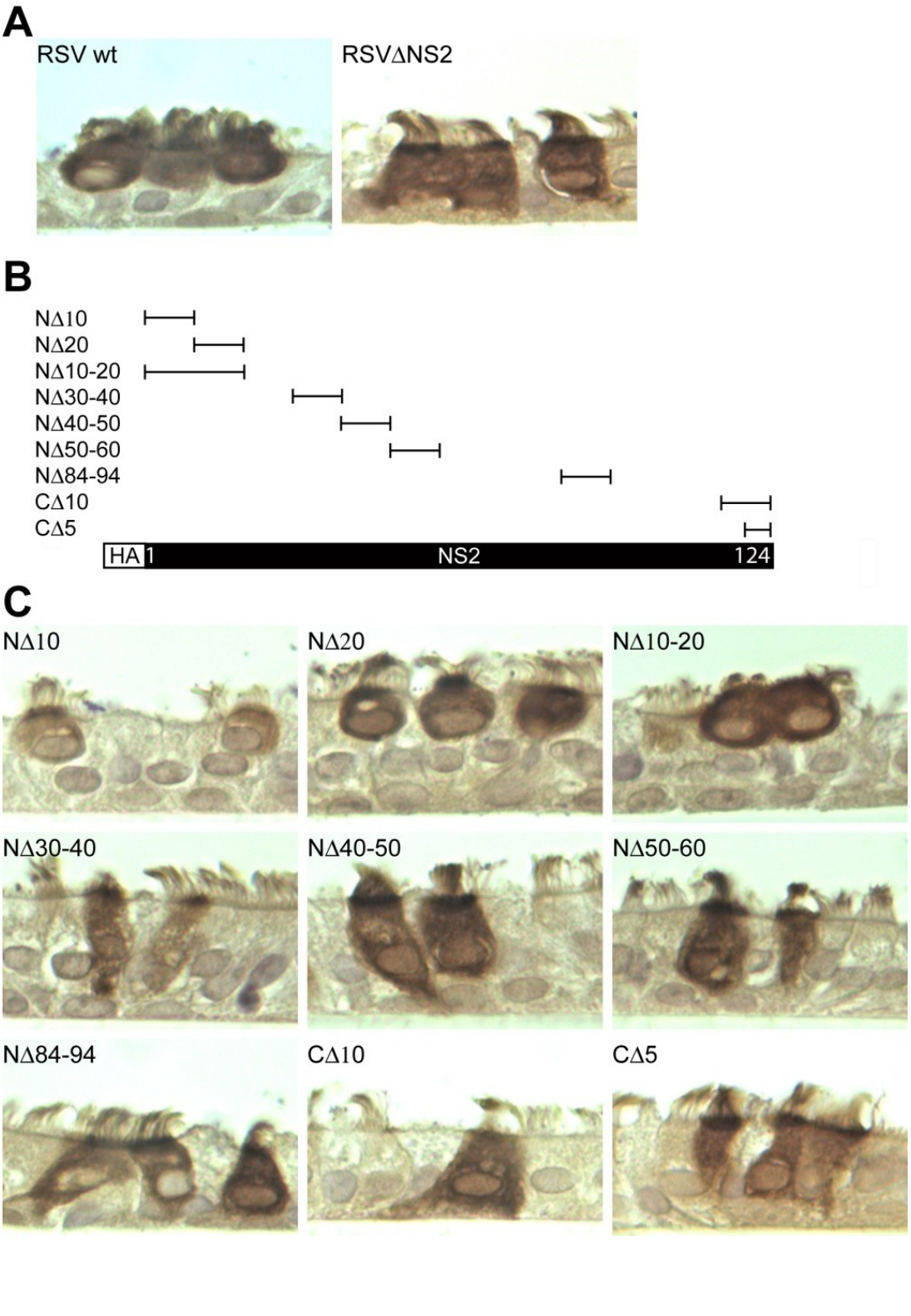
A
RSV wt
RSVΔNS2
B
NΔ10
NΔ20
NΔ10-20
NΔ30-40
NΔ40-50
NΔ50-60
NΔ84-94
CΔ10
CΔ5
HA
1
NS2
124
C
NΔ10
NΔ20
NΔ10-20
NΔ30-40
NΔ40-50
NΔ50-60
NΔ84-94
CΔ10
CΔ5

Figure 3.6. RSV-induced cell rounding is ablated by mutations within the NS2 protein. **(A)** Representative images of histologic cross sections of HAE infected with RSV or RSVΔNS2. **(B)** Schematic of sequential deletions of the NS2 protein. The NS2 ORF of RSV rA2 strain was replaced by a codon-optimized NS2 ORF with an N-terminal HA tag. Deletions were synthesized into the NS2 ORF, cloned into the RSV antigenome (A2 strain), and virus was rescued as previously described (105). Virus nomenclature indicates amino acid deletions in NS2 relative to the indicated C- or N-terminus. All viruses were amplified in HEp2 cells. **(C)** Representative images of histologic cross sections of HAE infected with the indicated RSV mutant virus. Infected cells were detected at 3 days pi using an antibody against RSV. Equal levels of NS2, N, P, and M proteins were detectable by western blot of lysates from HEp2 cells infected with each virus (not shown).

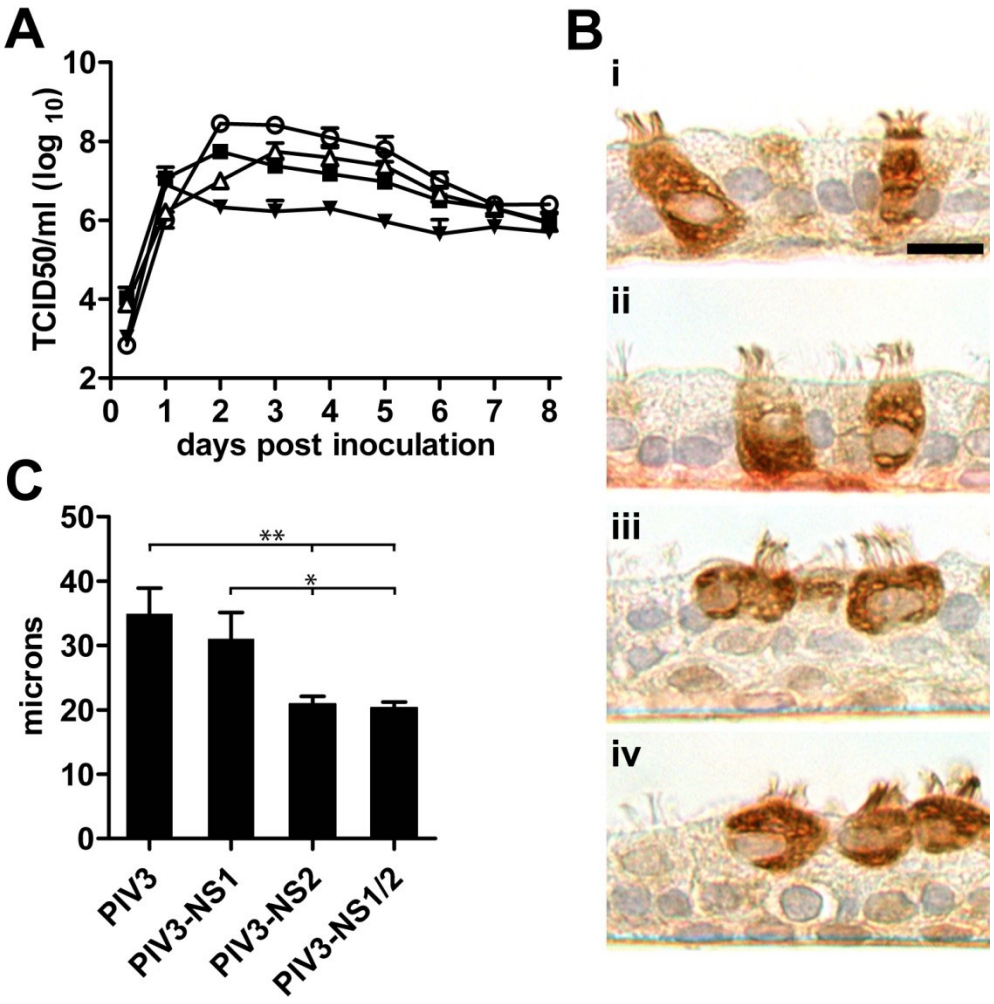

Figure 3.7. Expression of RSV NS2 in HAE ciliated cells using PIV3 results in infected cell rounding. (A) Growth kinetics of recombinant PIV3 (open circles) and PIV3 expressing either RSV NS1 (PIV3-NS1, closed squares), NS2 (PIV3-NS2, open triangles) or both NS1 and NS2 (PIV3-NS1/2, closed triangles). All viruses express GFP. Virus titers in apical washes were assessed at 24 h intervals. Data (mean ± SEM) represent n = 4 cultures per donor with cultures from 3 different donors. **(B)** Representative images of histologic cross-sections of HAE infected with PIV3 (i), PIV3-NS1 (ii), PIV3-NS2 (iii), or PIV3-NS1/2 (iv). Infected cells were detected with an anti-PIV3 antibody. Scale bar indicates 10 μm. **(C)** Height of infected cells (mean ± SD) was determined as described in Figure 4. **P*<0.05, ***P*<0.01, one-way ANOVA with Tukey's post-test.

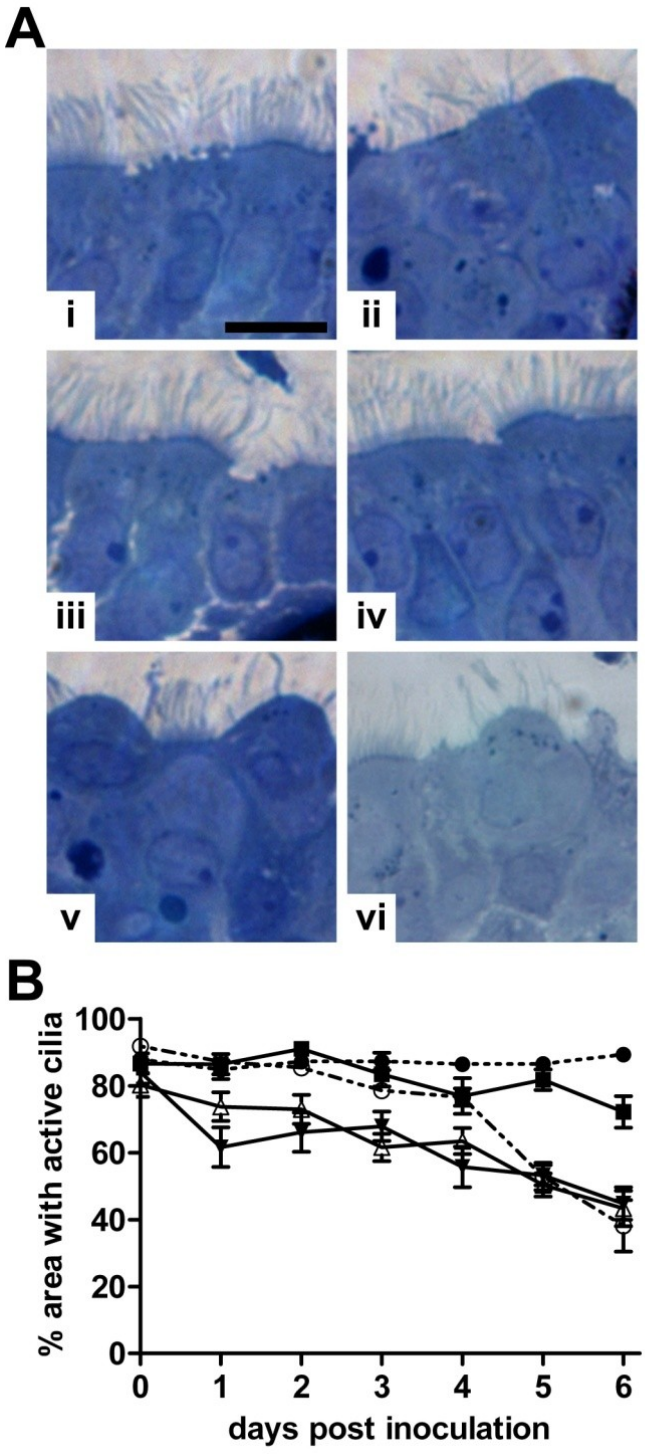
A
i
ii
iii
iv
v
vi
B
% area with active cilia
100
80
60
40
20
0
0
1
2
3
4
5
6
days post inoculation

Figure 3.8. Expression of RSV NS2 by PIV3 in HAE cultures mimics RSV-induced cytopathology at the apical surface of ciliated cells. (A) Representative images of histologic sections of non-infected HAE (i), or HAE fixed 2d post-inoculation by RSV (ii), PIV3 (iii), PIV3-NS1 (iv), PIV3-NS2 (v), or PIV3-NS1/2 (vi) showing similar apical membrane disruption in ciliated cells infected by RSV, PIV3-NS2, and PIV3-NS1/2. Richardson's counter stain. Scale bar represents 10 μm. **(B)** Surface area of active cilia beat on non-infected (closed circles, dotted line), PIV3 (open circles), PIV3-NS1 (closed squares), PIV3-NS2 (open triangles), or PIV3-NS1/2 (closed triangles) infected HAE. Data (mean ± SEM) represent quadruplicate cultures. All viruses express GFP.

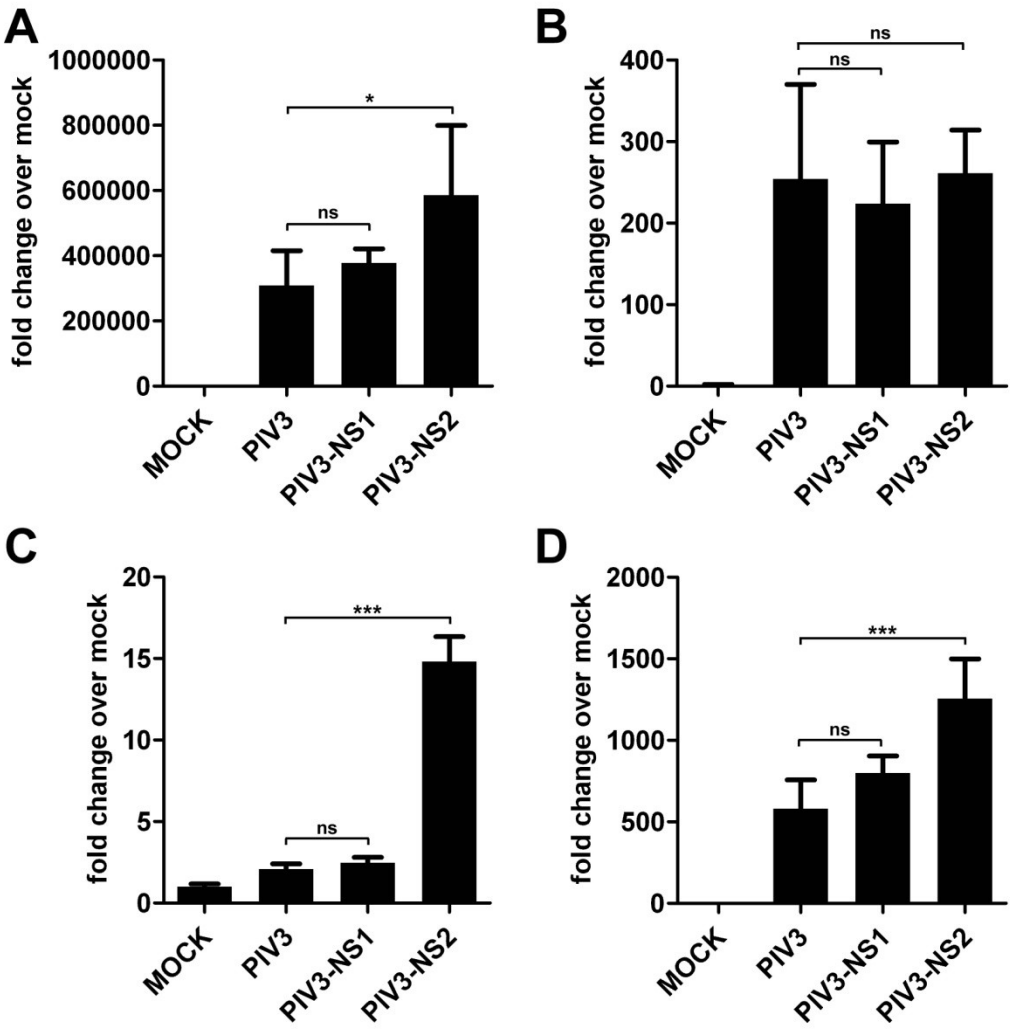

Figure 3.9. IFN and cytokine changes following infection of HAE with PIV3, PIV3-NS1, or PIV3-NS2. HAE were mock inoculated or infected with PIV3, PIV3-NS1, or PIV3-NS2. At 18 hours pi, cultures were harvested and message levels were determined by qRT-PCR for PIV3 N **(A)**, IFN-β **(B)**, IL-8 **(C)**, and CXCL10 **(D)**. Each sample was internally normalized to GAPDH and are expressed as fold change over mock inoculated culture. Data (mean ± SD) represent n=4 cultures. ns: not significant, **P*<0.05, ****P*<0.001, one way ANOVA with Tukey's post-test.

CHAPTER IV

RSV NS2 PROTEIN PROMOTES EPITHELIAL CELL SHEDDING AND DISTAL AIRWAY OBSTRUCTION

4.1 Overview

Respiratory syncytial virus (RSV) infection is the major cause of bronchiolitis in young children. The factors contributing to an increased propensity of RSV-induced distal airway disease compared to other commonly encountered respiratory viruses remain unclear. Here, we identify the RSV non-structural 2 (NS2) protein as a unique viral genetic determinant for initiating RSV-induced distal airway obstruction. Using recombinant respiratory viruses and the hamster in vivo model of infection, we show RSV NS2 promotes shedding of infected cells, resulting in two effects. First, epithelial cell shedding accelerated clearance of virus titers, presumably by clearing virus-infected cells from airway mucosa. Second, epithelial cell shedding resulted in accumulation of detached, pleomorphic epithelial cells in the narrow diameter bronchiolar airway lumen, resulting in acute distal airway obstruction. We propose that this study reveals a novel consequence of RSV infection of the airway epithelium, where NS2-promoted epithelial cell shedding accelerates viral clearance but also causes acute distal airway obstruction, possibly serving as the initiating event for bronchiolitis. Our studies identify a mechanism that may explain why RSV is the dominant virus causing bronchiolitis in young children and identify RSV NS2 as a novel therapeutic target for reducing the severity of disease.

Sections of this chapter are under review for publication in the Journal of Clinical Investigation.

4.2 Introduction

Human respiratory syncytial virus (RSV) is a nonsegmented, negative-sense, single-stranded RNA virus belonging to the family *Paramyxoviridae,* subfamily *Pneumovirinae*. RSV is the most common virus causing acute and severe lower airway disease in infants and young children, with nearly all children experiencing at least one RSV infection by the age of 2 years (1). While most RSV infections present with mild to moderate self-limiting pulmonary symptoms, in ~2% of cases, especially in infants who are very young (< 3 months), premature, or who have underlying immunodeficiency or cardiopulmonary disease, lower airway disease is severe enough to require hospitalization (5). Worldwide, an estimated 34 million new pediatric cases of RSV-associated lower airway disease occur annually accounting for approximately 200,000 deaths, almost all occurring in developing countries with reduced access to standardized care (4).

Despite significant impact of RSV infection on infant morbidity and mortality, treatment options remain limited to supportive care, poorly efficacious pharmacologic agents, and passively administered neutralizing antibodies. Supportive care including supplemental oxygen and ultimately, mechanical ventilation, remains the best available therapeutic approach. Ribavirin is the only anti-viral drug currently approved for treating RSV infections, but issues of efficacy, delivery, and potential side-effects in neonates restrict its use to immunocompromised patients (54). Bronchodilators and anti-inflammatory steroids are widely used to dampen inflammatory consequences of RSV infection despite evidence these treatments provide little to no clinical benefit (56, 57, 60). Passively administered neutralizing antibodies against RSV are used prophylactically to reduce the severity of RSV-induced pulmonary disease in susceptible populations (47). However, these antibody treatments rely on expensive monthly injections and therefore are restricted to at-risk infants (228). Licensed RSV vaccines are currently unavailable, although actively under development. The high incidence of RSV infection and the potential for severe distal airway

disease in vulnerable young children combined with limited availability of therapeutic options identifies a significant clinical global need to reduce the burden of RSV infection and disease in infants and young children.

RSV infects the mucosal epithelium lining the human respiratory tract, predominantly targeting the columnar epithelial cells of the conducting airways. The columnar airway epithelium serves a critical role in maintaining lung sterility by providing a physical barrier to systemic penetration of pathogens and generating and secreting antimicrobials. Additionally, the airway epithelium regulates mucus content, viscosity, and hydration to facilitate mechanical clearance of inhaled pathogens. Air-trapping and increased airway resistance are hallmarks of severe RSV-associated disease in the infant, although the factors contributing to these symptoms are unclear. Histologic analyses of lung tissues obtained post-mortem from RSV-infected infants describe epithelial cells positive for RSV antigen sloughed into the lumens of the infected airways (117, 119, 161). It was speculated that these intralumenal accumulations of infected and necrotic epithelial cells could contribute to airway obstruction and inflammation, exacerbating airway disease. Whether sloughing of airway epithelial cells was a direct consequence of RSV-induced epithelial cell cytopathology or a bystander effect of the robust infiltration and activation of inflammatory cells into the infected airways has been difficult to decipher in the complex in vivo environment of the lung.

We have previously described an in vitro model of RSV infection of human cartilaginous airway epithelium (HAE) that recapitulates the cellular distribution and physiology of the human differentiated airway epithelium. Using this model, we and others have shown that RSV infects and spreads in HAE by preferentially infecting ciliated epithelial cells while sparing mucin-containing Goblet cells and the underlying basal epithelial cells (114, 115). These in vitro findings are supported by histologic studies of cartilaginous airways from RSV-infected patients that also demonstrate the preferential

tropism of RSV for ciliated cells (117). Tropism for ciliated cells is not unique to RSV, as other RNA viruses including paramyxoviruses, coronaviruses, and avian influenza viruses have been shown to preferentially infect ciliated cells in the HAE model (125, 229, 230).

Previous studies have sought to determine the fate of RSV-infected ciliated cells over time in an in vitro primary differentiated model of the human airway epithelium. We demonstrated that infection of ciliated cells with RSV results in rounding of the infected cell, a unique consequence we attributed to expression of the RSV NS2 protein. Following a transition from a columnar to a rounded cell morphology, RSV infection of ciliated cells resulted in destruction of the cilia apparatus, loss of cilia function, and extrusion of the infected cell from the airway epithelium into lumenal secretions of HAE. Gain of function experiment using recombinant parainfluenza virus (PIV3-GFP) engineered to express RSV NS2 protein (PIV3-NS2) demonstrated that ciliated cells infected by PIV3-NS2, but not PIV3, became rounded and morphologically indistinguishable from RSV-infected ciliated cells.

We now expand our in vitro studies to explore potential in vivo functions of RSV NS2 expression. In this study, we compared the consequences of infection in the airways of Golden Syrian hamsters and show that PIV3-NS2, but not PIV3, caused rapid shedding of infected epithelial cells from the airway epithelium and accelerated clearance of virus infection from the lung. However, these studies also revealed PIV3-NS2 induced shedding of infected cells into the narrower diameter bronchiolar airways resulted in acute obstruction of the small airway lumens. Further, PIV3-NS2 infection causes earlier and more robust neutrophil influx in the lower airways of infected animals. These findings suggest the acute, distal airway obstruction, a common feature of RSV infection in infants, may be due to the rapid shedding of bronchiolar epithelial cells into the airway lumen and that this event is a direct consequence of RSV NS2 expression. These studies provide the first description of the unique fate of RSV-infected columnar airway epithelial cells and identify the expression of a single RSV protein, RSV NS2, as promoting this event.

4.3 Results

Effects of PIV3-NS2 on the infection of the hamster nasal cavity and lower airways

To determine the effects of RSV NS proteins in vivo, we used PIV3 as a vector to express NS1 and NS2. Among the convenient experimental animal models available, mice are not useful for PIV3 because of very poor virus replication in the airway epithelium, whereas Golden Syrian hamsters are semi-permissive to PIV3 infection and provide a useful model for infection. For these studies, we first focused on the airway epithelium of the hamster nasal cavity, as the nasal respiratory epithelium is a pseudostratified columnar epithelium with densities of ciliated and mucin-containing (Goblet) cells similar to those of HAE cultures and human cartilaginous airway epithelium in vivo. Hamsters were inoculated intranasally with PIV3, PIV3-NS2, or PIV3-NS1 (10^6 PFU). Maximal virus titers were reached in the nasal tissue by 3 days pi and revealed PIV3-NS1 and PIV3-NS2 were equally, but modestly, attenuated for growth compared to PIV3 (Figure 4.1A), similar to attenuation in HAE.

We next identified virus-infected epithelial cells in histologic sections of hamster nasal epithelium by immunodetection of PIV3 antigen at the time point of maximal nasal titers, day 3 pi (Figure 4.1B). As predicted by our HAE studies, all recombinant PIV3 viruses infected ciliated cells but not mucin-containing Goblet cells of the hamster nasal respiratory epithelium. While ciliated cells infected by PIV3 or PIV3-NS1 retained the native columnar cell morphology, cells infected by PIV3-NS2 were rounded and resembled human ciliated cells infected by PIV3-NS2 or RSV in vitro. Morphometric analysis of infected ciliated cell height in histologic sections of hamster nasal respiratory epithelium revealed a significant shortening of ciliated cell infected by PIV3-NS2 compared to those infected by PIV3 or PIV3-NS1 (Figure 4.1C), a phenotype remarkably similar to that seen in human cells in vitro. Occasionally in PIV3-NS2 infected hamster nasal cavities, virus antigen-positive cells were seen extruding from the epithelium and into the airway lumen but, unlike in HAE studies,

accumulations of shed, virus-infected epithelial cells after PIV3-NS2 infection were rarely noted in the nasal cavity, suggesting epithelial cells shed from the epithelium were rapidly and effectively cleared from the nasal cavity airway lumen, presumably by mechanical clearance mechanisms.

Next, we explored the effects of RSV NS2 on PIV3 infection of the lungs of hamsters by comparing the consequences of infection with PIV3 or PIV3-NS2. Because PIV3-NS1-infected cells showed no morphologic differences in HAE cultures or hamster nasal epithelium when compared to PIV3, we focused lung studies solely on the comparison of PIV3 versus PIV3-NS2 infection of hamster lower airways. For PIV3, histologic analysis of whole lungs after 3 days of infection showed viral antigen distributed throughout the conducting airways, predominately in the epithelial cells of the large bronchial and small bronchiolar airway regions (Figure 4.2Ai and 4.2Bi, respectively). Although virus antigen was occasionally detected in cells of the alveolar regions, the majority of infected cells were epithelial cells of the conducting airways. PIV3-infected epithelial cells of large and small airways retained columnar morphology and remained embedded in the epithelium, similar to PIV3-infected epithelial cells in HAE cultures.

In contrast, in PIV3-NS2 inoculated hamsters at 3 days pi, all virus antigen-positive cells detected in the larger diameter airways were rounded and either shedding from or fully detached from the underlying intact epithelium (Figure 4.2Aiii). The smaller-diameter bronchiolar airways similarly showed extensive cell rounding and detachment (Figure 4.2Biii). Remarkably, the narrow lumens of the bronchioles contained large accumulations of shed, virus antigen-positive cells (Figure 4.2Biii). This revealed an intriguing and unpredicted consequence of PIV3-NS2 infection. However, by 5 days pi, almost all evidence of infection and small airway occlusion was gone, suggesting effective clearance of the cell accumulations from the airway lumens (Figure 4.2Biv). The rapid clearance of virus-infected cells from within the bronchiolar airway lumen was also noted in the bronchial airways at 5

days pi (Figure 4.2Aiv). In contrast, the robust infection of the bronchial and bronchiolar airway epithelium in hamsters infected by PIV3 at 3 days pi was largely unaltered by 5 days pi, indicating PIV3-infected cells were not cleared as effectively from the epithelium as PIV3-NS2 infected cells (Figure 4.2Aii and 4.2Bii).

To determine if more effective clearance of virus-infected cells following PIV3-NS2 infection influenced viral load in the lung, we harvested hamster lung tissues inoculated with PIV3-NS2 or PIV3 at 1, 2, 3, 5, and 7 days pi and measured whole lung virus titers. These data revealed a strong temporal correlation between the extent of virus antigen-positive cells and lung viral titers. Specifically, although the lung titers of PIV3 and PIV3-NS2 were very similar at 1 and 2 days pi, PIV3 titers declined by less than 1-log between 3 and 5 days pi, whereas the reduction in PIV3-NS2 titers was markedly accelerated, dropping almost 3-logs during the same 2-day period (Figure 4.3A). Both viruses were completely cleared by 7 days pi. Throughout the experiments, the hamsters showed no clinical signs of illness, as reported in previous studies of PIV3 infection of hamster airways (231). This is not surprising given the semi-permissive nature of PIV3 infection in this non-native host. To determine if infection impacted activity of hamsters, we measured the distance hamsters ran in a 24h period over 6 days of infection. Despite robust infection, neither PIV3 nor PIV3-NS2 infected hamsters ran significantly shorter distances as compared to control animals (Figure 4.3B).

Neutrophil dominated inflammation in PIV3 and PIV3-NS2 infected animals

We next characterized the inflammatory cell profile in both PIV3 and PIV3-NS2 infected animals. Because these studies aim to determine early effects of infection on the ciliated airway epithelium, we focused only on immune cell infiltrates at 3 days pi. Cuffing of airways resulting from inflammatory cell infiltration into the parenchyma surrounding infected airways was evident in PIV3-NS2 infected animals, though such severe cuffing was rarely noted in PIV3 infected animals (Figure 4.4A). To determine the cell types present in the airway lumen, we performed bronchoalveolar lavage (BAL) on mock, PIV3, and PIV3-NS2

infected animals at 3 days pi. Consistent with observed increases in cellularity of PIV3-NS2 infected airway lumens, BAL fluid from PIV3-NS2 infected animals contained roughly twice as many cells as mock or PIV3 infected animals (Figure 4.4 B). The cell types in BAL fluid were determined by morphological criteria and significantly elevated numbers of macrophages and neutrophils were retrieved from PIV3-NS2 infected animals as compared to mock or PIV3-infected animals (Figure 4.4C). Activated neutrophils release numerous effector proteins that contribute to neutrophil-mediated cytoxicity and, in proteomic analysis of cell-free BAL fluid, we detected elevated levels of neutrophil effector proteins. Neutrophil elastase was not detected in either mock or PIV3-infected animals but was present in PIV3-NS2 infected animals (Figure 4.4D). Myeloperoxidase (MPO) was detected in low amounts in mock and PIV3 infected animals and, although not statistically significant, increased MPO was detected in BAL fluid of PIV3-NS2 infected animals (Figure 4.4E). Interestingly, histological analysis of the location of neutrophils in PIV3 or PIV3-NS2 infected animals indicated that, while in PIV3-infected animals neutrophils were associated with the airway epithelium, neutrophils in PIV3-NS2 infected animals were most frequently noted below the basement membrane or within the airway lumen (Figure 4.4F, arrow heads).

Accumulation of shed cells in the distal airway of PIV3-NS2 infected hamsters

In contrast to HAE and hamster nasal epithelium studies in which PIV3 only infected ciliated cells, we noted that PIV3 and PIV3-NS2 infected both ciliated and non-ciliated columnar cells of the small conducting airway regions. We also noted that PIV3-NS2-infected cells shed into the small airways exhibited an unusual pleomorphic morphology compared to cells shed from HAE or the hamster nasal respiratory epithelium. PIV3-NS2-infected cells shedding from small airway epithelium were swollen and at times bi-nucleated, with cell bodies extending from the intact epithelium into the airway lumen (Figure 4.5iv). Using cytokeratin 18 as an immunomarker for epithelial cells, we confirmed that the infected, shedding, and accumulated cells were epithelial cells, as expected (Figure 4.5Avi). The

accumulation of these detached, virus antigen-positive cells in the bronchioles infected by PIV3-NS2 was dramatic and sufficient to cause partial to complete occlusion of the bronchiolar lumens (Figure 4.5C).

To determine the viability of shed cells, we stained airway sections for DNA fragmentation using TUNEL. In PIV3 infected airways, no TUNEL signal was noted in the airway, associated with the epithelium, or in the surrounding parenchyma. In contrast, TUNEL positivity was noted in the lumen and surrounding parenchyma of PIV3-NS2 infected airways, although the relative numbers of TUNEL positive cells were low. The majority of infected cells within the airway lumen were TUNEL negative, consistent with histological observation that the nuclei of shed cells in the airway lumen were morphologically intact. While we did not identify the cell type displaying TUNEL positivity, the location of staining suggests a combination of neutrophils and epithelial cells account for the TUNEL-positive cells of these airways. Additionally, we detected keratin 19 and 8, two major keratin components of the cytoskeletal scaffold of epithelial cells, in proteomic analysis of cell-free BAL fluid from PIV3 and PIV3-NS2 infected hamsters (Figure 4.5D, E). No keratins were detected in mock-inoculated animals. Although both keratins were detected in PIV3 animals, comparison of keratins detected in PIV3 versus PIV3-NS2 revealed a 3-fold increase in keratin 8 and an 8-fold increase in keratin 19 in BAL fluid from PIV3-NS2 infected animals. Analysis was undertaken on cell-free samples, thus the keratins detected in BAL fluid were likely released following necrosis of epithelial cells within the airway lumen. Consistent with this, necrotic debris was noted in histological sections of airway accumulations in the distal airways of PIV3-NS2 infected animals.

Accumulation of infected cells in the distal airways of RSV infected infants

To ascertain whether the morphologic consequences of PIV3-NS2 infection of hamster lower airways were predictive of events in lower airways of humans infected by RSV, we probed histologic sections of autopsy lung tissues obtained from RSV-infected

patients for viral antigen. Assessment of pseudostratified columnar airway epithelium, indicative of larger airway regions, showed clear evidence of RSV antigen-positive epithelial cells embedded in the epithelium, displaying shortened, rounded cell morphology (data not shown). Occasionally, RSV antigen-positive cells were also detected detached in the airway lumen, suggestive of shed, virus-infected cells which had not fully cleared from the airway. Examination of the distal bronchiolar airways revealed bronchiolar lumens partially or fully occluded by pleomorphic epithelial cells positive for RSV antigen and in some cases in the process of shedding into the airway lumen (Figure 4.6). Swollen and bi-nucleated cells were also observed in the airway lumen of these regions. These observations indicated that the morphologic changes, cell shedding, and small airway occlusions observed in hamster distal airways infected by PIV3-NS2 resembled the consequences of RSV infection of human lower airways detected in post-mortem samples.

4.4 Discussion

RSV is the most important viral agent of lower airway disease in infants and young children and is commonly associated with severe bronchiolitis in these populations. In the very young, bronchiolitis caused by RSV is documented to be more severe and prolonged than bronchiolitis caused by other etiologies, including parainfluenza viruses (PIV) or rhinoviruses (9, 10). A recent study of young children with acute respiratory illness found those infected with RSV had twice as many emergency room visits and six times more hospitalizations than those with seasonal influenza virus infections (15). Why RSV has a tendency towards increased frequency and severity of distal small airway disease in infants amongst other etiologies was unknown.

In vitro and in vivo studies have established that ciliated cells of the human large cartilaginous airways are an important target for RSV infection. The ciliated airway epithelium serves an important role in maintaining lung health, as it provides a mechanical

barrier against inhaled pathogens and contributes to clearance by facilitating mucociliary transport. Precisely how RSV infection of the airway epithelium causes disease was poorly defined, but it has previously been attributed to both direct virus-mediated epithelial cell cytopathology and exaggerated host immune responses, especially excessive neutrophil-associated inflammation (181). Other consequences of RSV infection, such as incidence of wheezing and possible skewing of future immune responses, have been reported (34, 36). Although clinical and preclinical studies have increased our understanding of factors involved in RSV disease, the early, initiating aspects of RSV infection of the airway epithelium and the relationship to subsequent airway pathology remained poorly defined.

Investigating the role of the airway epithelium in RSV pathogenesis has been impeded by the scarcity of representative models of polarized and differentiated airway epithelium that are both susceptible to human RSV infection and mimic the outcomes of infection observed in RSV-infected human airways in vivo. Indeed, most experiments modeling RSV infection of the airway epithelium rely on transformed epithelial cell-line monolayers, which do not resemble the differentiated architecture of airway epithelium in vivo. The widely available in vivo models, particularly small rodents, also poorly reproduce the consequences of RSV infection observed in human airways, largely due to low infectivity of the conducting airway epithelial cells. Species-specific RSV equivalents used in appropriate permissive hosts, such as bovine RSV in calves, are useful models for understanding RSV pathogenesis, but differences between the human and animal viruses and the human and animal hosts have been documented and complicate such analyses (209).

In the previous chapter, we assessed the impact of RSV NS2 on the function of the airway epithelium using RSV gene-deletion mutants to infect cultures of primary human pseudostratified airway epithelial cells (HAE) that closely resemble the epithelium of authentic airway tissue. These studies demonstrated that cell rounding and shedding were

dependent on expression of the RSV NS2 protein. However, these gene-deletion mutants lacked the major RSV type I interferon antagonist proteins and are severely attenuated in HAE. Because PIV3 also targets ciliated cells but does not cause the cell rounding phenotype, we used PIV3 as a vector to express RSV genes in ciliated cells. Infection of ciliated cells in vitro with PIV3 engineered to express RSV NS2 (PIV3-NS2) resulted in infected cell morphologic changes indistinguishable from ciliated cells infected by RSV.

In this present study, we used PIV3-NS2 and control viruses to investigate the significance of our in vitro HAE findings in an in vivo hamster model. Evaluation of infection by PIV3-NS2 and control viruses in the hamster nasal respiratory epithelium, which mimics HAE in its distribution of ciliated and non-ciliated Goblet cells, showed that PIV3 recombinant viruses infected only ciliated cells in the respiratory epithelium and that PIV3-NS2 caused the same cell rounding, membrane cytopathology, and shedding phenotypes associated with the expression of RSV NS2 in ciliated cells of HAE.

Similar to outcomes in HAE and hamster nasal ciliated cells, infection of hamster lower airway epithelial cells with PIV3-NS2, but not PIV3, resulted in rounding and shedding of the infected cells from the epithelium into the airway lumen. In contrast, PIV3-infected epithelial cells remained columnar and embedded within the intact epithelium. In the large airways of hamsters infected with PIV3-NS2, infected cells that shed from the epithelium rarely accumulated in the airway lumen, suggesting that the majority of shed cells were rapidly and effectively cleared from the lumen, presumably by mechanical airway clearance mechanisms. In the narrower diameter small airways, shed cells accumulated in the airway lumen, suggesting clearance of shed cells from the small airway lumens was delayed. These effects were most pronounced in the small airways of hamsters 2-3 days after infection by PIV3-NS2, and accumulations of detached virus-antigen-positive cells were easily detected as occlusions in the small airway lumens, reminiscent of bronchiolar airway occlusions frequently observed in the small airways of young infants infected by RSV. We

also note studies with RSV-infected infants describe infection of the larger airways as patches or clusters of infected cells compared to more robust circumferential infection of distal airway epithelial cells (117, 118). Our in vivo studies with PIV3-NS2 suggest patchy infection in the large airways may represent continuous shedding and clearance of infected cells in these regions, while shedding and accumulation may perpetuate infection in the distal airways.

Despite histological evidence of epithelial cells in the airway lumen, few epithelial cells were noted in lavage fluid of PIV3-NS2 infected hamsters. It is possible that occlusions containing epithelial cells are not easily flushed from the airways and were not collected using the lavage technique. Histological sections of lungs post-BAL showed some evidence of occlusions remaining in the airway. Alteranatively, morphologic changes of epithelial cells following infection with PIV3-NS2, especially cell swelling, may have resulted in some epithelial cells being misidentified and counted as macrophages, since cell types were determined by morphological characteristics. Immunodetection of specific cell type markers could be used to complement future analysis of the cell types present in BAL fluid.

The narrower diameter of the small airway lumens likely is a significant factor in the development of airway occlusions. Similarly, narrow airway lumen size is suggested to contribute to the increased frequency of small airway obstruction associated with infants infected by RSV. However, we also noted that cells shedding into the hamster or human small airways exhibited an unusual swollen and pleomorphic morphology compared to cells shedding from HAE, the hamster nasal respiratory epithelium, or the hamster larger airways. These airway region-dependent consequences of PIV3-NS2 infection may reflect a difference in the responses of ciliated cells distributed in the small airways compared to those in the large airways. Alternatively, the swollen pleomorphic cells may represent other epithelial cell-types present in the small airways which are susceptible to PIV3-NS2 infection, such as the non-ciliated columnar club (Clara) cell. In human and hamster lower

airways, club cell numbers increase in density as the conducting airways descend into the distal bronchiolar airway regions (113, 232). Indeed, in our studies in hamster airways, we noted PIV3 and PIV3-NS2 infection of both ciliated and non-ciliated columnar epithelial cells of the distal airways, the latter likely representing club cells. RSV infects both ciliated and non-ciliated cells in the small airways of humans (117, 119) and both cell types are infected in the small airways of calves and lambs experimentally infected with RSV (116, 149). Thus, the apparent morphologic differences in the cells shed into the smaller compared to larger airways might reflect the increased frequency of PIV3-NS2 infection of club cells in the small airways versus infection of ciliated cells in the larger airways. Regardless of the specific epithelial cell-types infected by PIV3-NS2 in the different airway regions, we suggest that the combination of narrower diameter airway lumens in the bronchioles and the expanded volume of cells shed into these airway regions enhances the likelihood that shed cells would accumulate and occlude the smaller diameter airway lumens.

Unusual epithelial cell morphology has been described for RSV-infected humans and bovine RSV-infected calves (116, 119, 161) and sloughing of virus antigen-positive cells caused small airways occlusion in ovine and baboon models of RSV infection (149, 153). In contrast, unusual airway epithelial cell morphologies are rarely noted after RSV inoculation of small animal models, most notably the mouse. Thus, in several appropriate large animal models of RSV infection as well as retrospective analysis of human cases of RSV infection, shedding of pleomorphic, virus antigen-positive epithelial cells, especially in the smaller diameter distal airways, appears to be a characteristic hallmark of RSV infection.

The appearance of cell accumulations and airway lumen occlusions in the small airways of hamsters infected with PIV3-NS2 suggests that the phenomenon of RSV NS2-induced cell shedding might have importance for RSV disease. RSV bronchiolitis has long been associated with small airway obstruction resulting in air-trapping distal to the obstruction, leading to increased airway resistance (233, 234). Classically, the composition

of the obstructive material has been considered to be a mixture of necrotic epithelial cells, mucus secretions, and inflammatory cell exudate. However, the limited number of autopsy specimens now available from RSV-infected patients, including those described in this study, reveal unusual pleomorphic epithelial cells shedding from the airway epithelium and RSV antigen-positive debris accumulating in the lumen of infected airways, with only rare examples of mucus-related airway plugging, further emphasizing the potential significance of shed and accumulated epithelial cells as a major contributor to small airway obstruction after RSV infection.

The present study suggests that RSV, compared to other common respiratory paramyxoviruses, has an unusual ability to induce epithelial cell shedding, and that NS2-induced cell shedding may be an important factor in RSV pathogenesis by contributing to plugging of small airway lumens. However, in the hamster model, the small airway plugging observed in association with PIV3-NS2 infection was transient, as maximal occlusion occurred at 3 days pi but was cleared by 5 days pi. Obstruction of small airways was also not associated with increased clinical disease in hamsters. The lack of disease associated with PIV3 (and RSV) infection in rodent models largely reflects their semi-permissive nature for virus replication, with relatively low whole lung viral titers and relatively short durations of infection. In contrast, RSV infection of humans results in substantially higher virus titers and virus shedding can continue for one or several weeks (178, 235). Primary RSV infection in humans is nearly always symptomatic and, in this more permissive setting, it is reasonable to expect that RSV NS2-promoted occlusion of the small airways would be longer-lived and contribute to disease severity. It also is likely that RSV-induced cytopathology leading to inhibition of mucociliary activity would have a greater effect on mechanical clearance in a more permissive setting, due to longer duration and increased extent of infection, which would further reduce clearance of shed cells.

Interestingly, we also noted an additional effect associated with NS2-induced cell shedding. Specifically, PIV3-NS2 infection was cleared from hamster lungs more rapidly than PIV3. This was evident by histologic analysis, which showed that, despite the extensive infection and airway occlusions associated with PIV3-NS2 on day 3, the infected cells were largely cleared by day 5. In contrast, in animals infected with PIV3, there were abundant infected cells on both days 3 and 5 pi. Consistent with this, quantification of whole lung viral titers confirmed that PIV3-NS2 was cleared more rapidly than PIV3, even though both viruses reached similar peak titers by days 2-3. These data raise the possibility that the cell shedding promoted by RSV NS2 might have a potential beneficial effect for the host, namely to accelerate clearance of virus-infected cells and infection from the airways. This observation, however, is based on indirect evidence, specifically the impact of RSV NS2 on the clearance of PIV3 rather than RSV.

Neutrophils are the primary immune cell type notes in bronchial washes of RSV infected infants (180). Similarly, we noted a large influx of neutrophils at 3 days pi in PIV3-NS2 infected hamsters. At this timepoint, inflammation was minimal around PIV3 infected airways, though present at later timepoints (5 days pi) in these animals. In agreement with histological findings, increased numbers of neutrophils and macrophages were also noted in BAL fluid collected from hamsters infected with PIV3-NS2 at 3 days pi and the neutrophil effector proteins MPO and neutrophil elastase were present in cell-free BAL fluid. While neutrophils were present in and around the airways of both PIV3 and PIV3-NS2 infected airways, albeit at differing levels, histologic examination suggests differential location of neutophils in the distal airway regions of infected animals. Specifically, neutrophils in PIV3 infected airways appeared to be directly associated with the lumenal surface of the airway epithelium. In contrast, neutrophils in PIV3-NS2 infected airways were frequently noted either below the basement membrane, having not yet migrated across the airway epithelium, or within the airway lumen not in contact with the intact airway epithelium. The

presence of neutrophils in the airway lumen, rather than directly associated with the epithelium suggests that neutrophils are associating with the infected, shed cells in PIV3-NS2 infected animals rather than cells within the airway epithelium. Differences in neutrophil location may reflect a protective response of the host, whereby neutrophils associate with shed cells rather than cells within the epithelium, protecting the epithelium from neutrophil-mediated cytotoxicity. Alternatively, cell shedding may represent an immune evasion mechanism of the virus, where removal of the infected cells from the epithelium might decrease the likelihood that infected cells will directly encounter inflammatory cells recruited to site of infection.

At this time, it is not possible to assess the relative importance of the seemingly contrasting effects demonstrated in this study, namely shedding resulting in clogged airways and potentially enhanced disease versus shedding resulting in accelerated clearance and reduced disease. Unfortunately, it is not feasible to evaluate obstruction versus clearance of RSV using NS gene deletion mutants because, as noted, deletion of these proteins has drastic effects on host antiviral responses and causes severe attenuation of the mutants in vivo, which would confound this analysis. However, the central role of airway plugging in RSV pathogenesis in humans suggests that NS2-induced cell shedding and morphological changes are important to the development RSV disease in vivo.

In summary, using PIV3 as a vector for RSV NS2, we confirm the previous in vitro finding that NS2 mediated cell rounding in an in vivo hamster model of infection. We then expand on the previous in vitro studies by demonstrating that expression of RSV NS2 in vivo resulted in accelerated clearance of infection. We propose that NS2-induced cell shedding acts as a novel clearance mechanism to remove infected cells from both the airway epithelium and the lumen. In the narrow diameter distal airways, however, NS2-induced shedding contributed to acute airway obstruction which was strikingly reminiscent of airway plugging that occurs during RSV bronchiolitis in infants. The notion that RSV NS2 may be a

pathogenesis factor increasing the likelihood of small airway obstruction as a precursor to bronchiolitis identifies NS2 as a potential therapeutic target for limiting the severity and frequency of RSV bronchiolitis, particularly in infants. It also suggests that deletion of the NS2 gene may be desirable in live-attenuated RSV vaccine candidates (69). Future studies will be needed to explore how RSV NS2-mediated shedding of infected cells affects the development of immunity to RSV infection and whether manipulation of NS2-promoted epithelial cell shedding in response to RSV infection may serve as a therapeutic target for reducing the severity of distal airway disease in RSV-infected infants.

4.5 Materials and Methods

Animals

In vivo animal studies used Golden Syrian hamsters (Harlan) and all procedures were conducted in accordance with the National Institutes of Health Guide for the Care and Use of Laboratory Animals and using animal study protocols approved by the Animal Care and Use Committee of the National Institute of Allergy and Infectious Diseases and the Institutional Animal Care and Use Committee of the University of North Carolina at Chapel Hill.

Viruses

All viruses used in this study were derived from cDNA (recombinant) and contain a GFP insertion as an additional gene unless otherwise mentioned.

Wild-type RSV is a derivative of the A2 strain and was constructed and described previously (212). This virus expresses the green fluorescent protein (GFP) gene as an additional gene inserted between the RSV phosphoprotein (P) and matrix (M) genes. Wild-type RSV and all mutants were amplified in HEp2 cells stably expressing the V gene from SV5 (210).

PIV3 is a derivative of the JS strain engineered to express the GFP gene as an additional gene inserted between the PIV3 phosphoprotein (P) and matrix (M) genes, as has been described previously (81, 222). Codon-optimized RSV NS1 or NS2 genes were synthesized (DNA2.0) and inserted into the PIV3 viral genome between the hemagglutinin-neuraminidase (HN) and viral polymerase (L) genes using cloning methods similar to those previously used to express CFTR and rhAFP in this genome region (223, 224). A unique EagI restriction site was generated in the non-coding region downstream of the HN gene in the PIV3 subgenomic cDNA. The NS1 or NS2 coding sequence was amplified by RT-PCR from plasmids expressing codon-optimized NS1 or NS2 , cloned into a pCR-Blunt II-TOPO vector (Invitrogen), and sequenced. The following primer sets were used: NS1 sense (5'-CCGCGGCCACCATGGGCAGCAATAGTCTC-3'), NS1 antisense (5'-GGGCCCGAGTTATGGGTTCAGGTCAA-3'), NS2 sense (5'-CCGCGGCCACAATGGATACCACGC-3'), and NS2 antisense (5'-GGGCCCCTCGAGTCAAGGGTTCAA-3'). The underlined portions represent SacII and ApaI restriction sites. Using the SacII and ApaI restriction sites, NS1 or NS2 was inserted into a vector following a linker sequence consisting of the PIV3 gene-end, intergenic, and gene-start transcription regions, flanked at both ends by EagI sites. This cassette was then inserted using the EagI sites into the full-length PIV3GFP antigenomic cDNA and the resulting genomes were designated PIV3-NS1 or PIV3-NS2. A PIV3 genome expressing both NS1 and NS2 was also generated by inserting the RSV NS1 and NS2 genes together into PIV3 between the HN and L genes using similar methods. From the linker vector containing NS1, a sequence consisting of the EagI restriction site, PIV3 linker region, and NS1 gene was PCR amplified using the NS1 sense primer (5'-CGAATTGGCGGCCGAAAATA-3') and the NS1 antisense primer (5'-CAGGAGTTCAGCACGATGGGGGCCCGAGTTATGGGT-3'), destroying the 3' EagI site and creating an 18bp overhang. From the linker vector containing NS2, a sequence

consisting of the PIV3 linker region, the NS2 gene, and the EagI restriction site was amplified using the NS2 sense primer (5'-GCTGAACTCCTGCATCGTAAAATAAGAAAAACTTAG-3') and the NS2 antisense primer (5'-ACTTGGCCCAAGCTTGAGTA-3'), destroying the 5' EagI site and adding the complementary 18bp overhang. These 2 fragments were combined in a fusion reaction using the NS1 sense and NS2 antisense primers and the resulting fragment was cloned into a pCRBluntII TOPO vector (Invitrogen) and sequenced. The final fragment consisted of a PIV3 linker region, the RSV NS1 gene, a second PIV3 linker region, and the RSV NS2 gene, flanked by EagI sites. This cassette was then inserted using the EagI sites into the full-length PIV3GFP antigenomic cDNA, creating PIV3-NS1/2. Each insert was designed to retain the "rule of six" required for PIV3 genome replication. All viruses were rescued and amplified in LLC-MK2 cells using methods described previously (222) and sequenced.

Viral inoculations and growth

Ten- to twelve-week-old female Golden Syrian hamsters (Harlan) were transiently anesthetized (methoxyflurane) and inoculated intranasally with 10^6 pfu of PIV3, PIV3-NS1, or PIV3-NS2 in 100 µl serum-free L-15 Leibovitz medium (Gibco). Animals were euthanized and respiratory tissues harvested at indicated times post-inoculation for analysis of virus titers or histologic assessment. For virus titrations, whole lungs or nasal turbinates were weighed and homogenized in PBS. Viral titers were determined by standard plaque assay of the clarified supernatants as previously described (236).

Histology and immunoprotocols

For histologic examination of hamster tissues, excised nasal turbinates or whole lungs were immersion-fixed in 10% neutral-buffered formalin, embedded in paraffin, and histological sections generated for examination and staining. Sections were stained with H&E. Immunohistochemistry for viral antigen was performed by blocking sections in 3% BSA and incubation with primary antibodies against PIV3 (anti-PIV3 rabbit serum raised against

sucrose-gradient-purified PIV3; (226)). To identify epithelial cells, a cytokeratin 18 antibody was used (mouse monoclonal; Abcam). Immunoreactivity was detected using anti-goat or anti-rabbit secondary antibodies conjugated to horseradish peroxidase (HRP), visualized using 3,3'-diaminobenzidine (Sigma), and counterstained with hematoxylin.

RSV infection in human airways was determined in lung tissue obtained from a patient naturally infected by RSV provided by Dr. Alan Proia is association with the Duke University Pathology Specimen Repository in accordance with Duke University IRB protocols. RSV and cytokeratin 8/18 immunoreactivity was performed on histological sections using a Leica Bond-III automated stainers (Leica Microsystems Inc.). Following antigen retrieval with Novocastra Bond Epitope Retrieval 1 solution (Leica Microsystems), sections were incubated with a primary antibody against RSV antigen (clones 5H5N, 2G12, 5A6, IC3; Vector Laboratories) and detected with the Novocastra Bond Polymer Refine Detection system (Leica Microsystems). Immunostaining for CK 8/18 used a proteinase K epitope retrieval solution (Dako North America, Inc.), the primary antibody Novocastra CK 8/18 monoclonal antibody (clone 5D3, Leica Microsystems), and detection with the Novocastra Bond Polymer Refine Detection system.

Morphometric analysis of cell height and airway occlusion

Height of infected cells in the nasal respiratory tissue was determined by measuring pixel height of infected cells in images from fixed, viral-antigen stained sections using ImageJ software (NIH) and converting to microns.

Occlusion of airways was determined by imaging infected airway regions from fixed, viral-antigen stained sections, converting to black-and-white images, pixilating, and calculating the percentage of black pixels within the airway lumen using ImageJ software. Airway occlusions were measured from 3 individual animals harvested at 3days pi.

Bronchoalveolar lavage

Bronchoalveolar lavages were performed using standardized procedures (237). Hamsters were euthanized by exsanguination under deep Avertin anesthesia. The left main stem bronchus was ligated to perform BAL on the right lobe only. Two ml cold sterile PBS was instilled and retrieved via the trachea three times before collection and cell counting. BAL cells were pelleted by centrifugation at 1000xg for 5min at 4°C and the cell-free fluid (BALF) was collected and stored at -80°C for future analysis. BAL cells were resuspended in PBS and cytospin slides of 30,000-60,000 cells/slide were obtained (StatSpin CytoFuge 2), air dried, and stained with Newcomer's stain for differential cell counts.

Proteomics of BALF

LC-MS/MS identification of proteins in cell-free BAL fluid (BALF) was performed as described previously (238). A total of 100 µl of BALF from each hamster was denatured with 300 µl GuHCL (pH8.0) and proteins were reduced with 20mM dithiothreitol for 30m at 60^{o}C and alkylated with iodoacetamide (Sigma) for 1h at 25^{o}C. Reduced and alkylated BAL samples were buffer-exchanged into a pH 8.0 digestion buffer using a HiTrap Desalting column (GE Healthcare) and digested with 2 µg trypsin at 37^{o}C overnight. The final digest was vacuum dried to remove bicarbonate salts and resolubilized in 20 µl 0.1% formic acid water.

The LC-MS/MS was performed with a Dionex ultimate 3000 RSLCnano system coupled to a hybid quadrupole orbitrap mass spectrometer with a Nano spray source (Q Exactive, Thermo Fisher). For liquid chromatography, one microliter of the sample was loaded into a trap column Acclaim PepMap 2 cm × 75 µm i.d., C18, 3 µm, 100 A (Dionex) at 5 µl/min with aqueous solution containing 0.05 % (v/v) trifluoroacetic acid and 2 % acetonitrile. After 7 minutes, the trap column was set on line with an analytical column Acclaim PepMap RSLC 15 cm × 75 µm i.d., C18, 2 µm, 100 A (Dionex) with a linear gradient of 4-30 % solvent B (99.9% acetonitrile with 0.1% formic acid) over 157 min with a

constant flow of 300 nL/min. Eluted Peptides were analyzed by a data-dependent top 10 method dynamically choosing the most abundant precursor ions from the survey scan (300–1650 Th) for HCD fragmentation. For MS scan, data were acquired at resolution of 70,000 at m/z 200, target AGC value of 1e6, maximum fill times of 80 ms. For the MS/MS scan, data were acquired at resolution of 17,500 at m/z 200, target AGC value of 1e5, maximum fill times of 80 ms. Dynamic exclusion was set to 20 second.

Proteins identified from the BALF were quantified using a label-free method termed the normalized spectral index (SIN) (239). SIN is defined as the cumulative fragment ion intensities for all spectra counted for a protein (SI) normalized by the sum of SI over all proteins and by the length of the protein.

Running wheels

To determine if infection results in decreased activity, a Nalgene activity wheel (Nalge Nunc International) was placed in each hamster cage, equipped with a magnetic switch with an LCD counter that records revolutions, with water and food available ad libitum. Running wheels were place in each cage for 2 days prior to inoculations for baseline recording of activity and to allow for exploration and acclimation. Following inoculation, activity was recorded as number of revolutions per 24 hour period and reported as distance run per day.

Statistical analysis

Unpaired t-test and one-way analysis of variance (ANOVA) with Tukey's post-test was performed as indicated. Statistical significance was defined as $P<0.05$ unless otherwise noted.

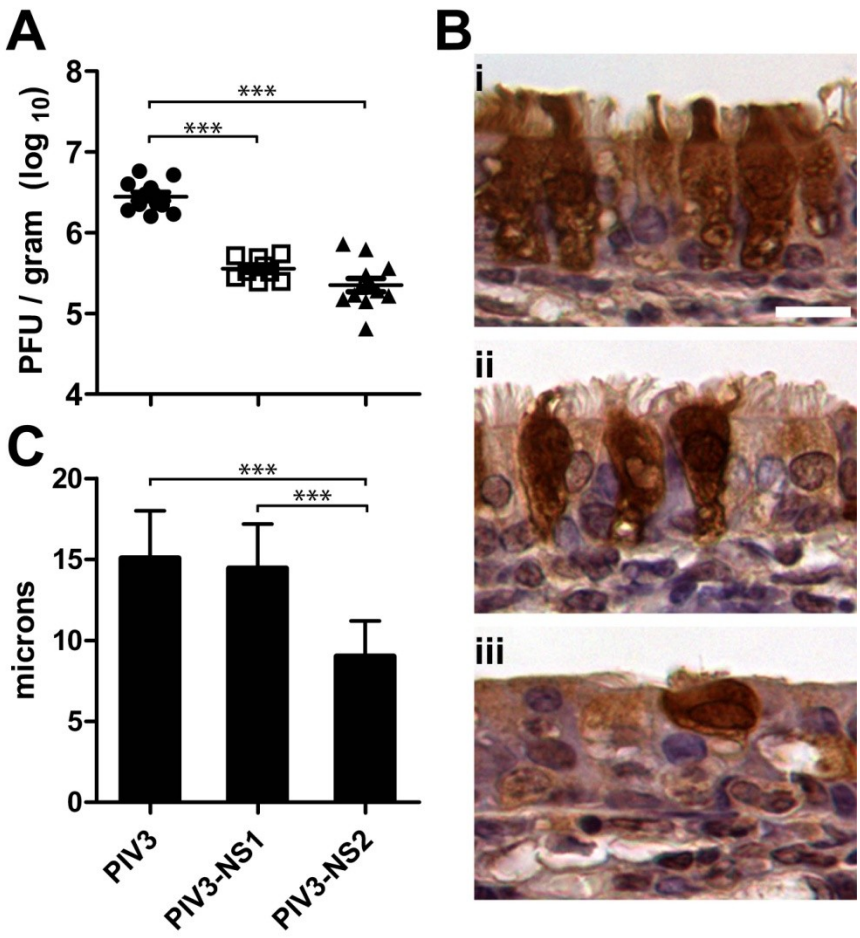

Figure 4.1. PIV3-NS2 causes ciliated cell rounding in the hamster nasal respiratory epithelium in vivo. (A) The nasal epithelium of Golden Syrian hamsters was inoculated with 10^6 PFU of PIV3 (closed circles), PIV3-NS1 (open squares), or PIV3-NS2 (closed triangles) and virus titers in the nasal turbinates was determined at 3 days pi. Data (mean ± SEM) represent 3 independent experiments with total of 9 - 12 animals. **(B)** Representative images of histologic cross-sections of hamster nasal respiratory epithelium infected by PIV3 (i), PIV3-NS1 (ii), or PIV3-NS2 (iii). Virus antigen was detected at 3 days pi with an anti-PIV3 antibody. Scale bar represents 10 μm. **(C)** Height of infected ciliated cells (mean ± SD) was determined by measuring height of virus-antigen positive cells from fixed tissue sections with at least 200 cells analyzed across 3 individual animals. All viruses express GFP. ****P* <0.001, one-way ANOVA with Tukey's post test.

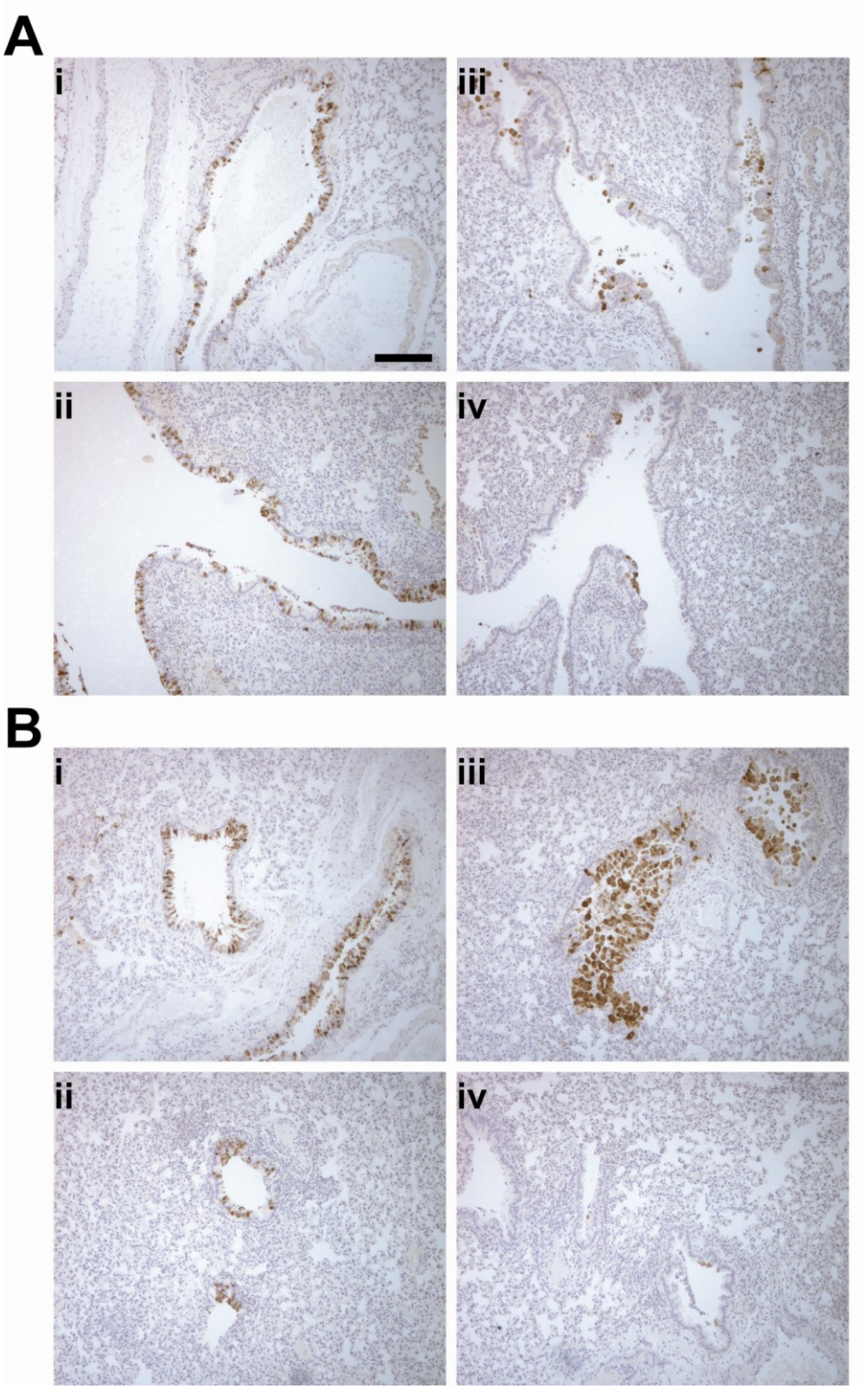
A
i
iii
ii
iv
B
i
iii
ii
iv

Figure 4.2. Accelerated clearance of virus-infected cells in hamsters infected by PIV3-NS2. (A, B) Representative images of histologic cross-sections of hamster large airways **(A)** and small airways **(B)** 3 days (i, iii) and 5 days (ii, iv) after infection with PIV3 (i, ii) or PIV3-NS2 (iii, iv). Note the rapid loss of PIV3-NS2 infected cells from airways at 5 days pi, a time when PIV3 infection remained robust. Scale bar represents 100 μm.

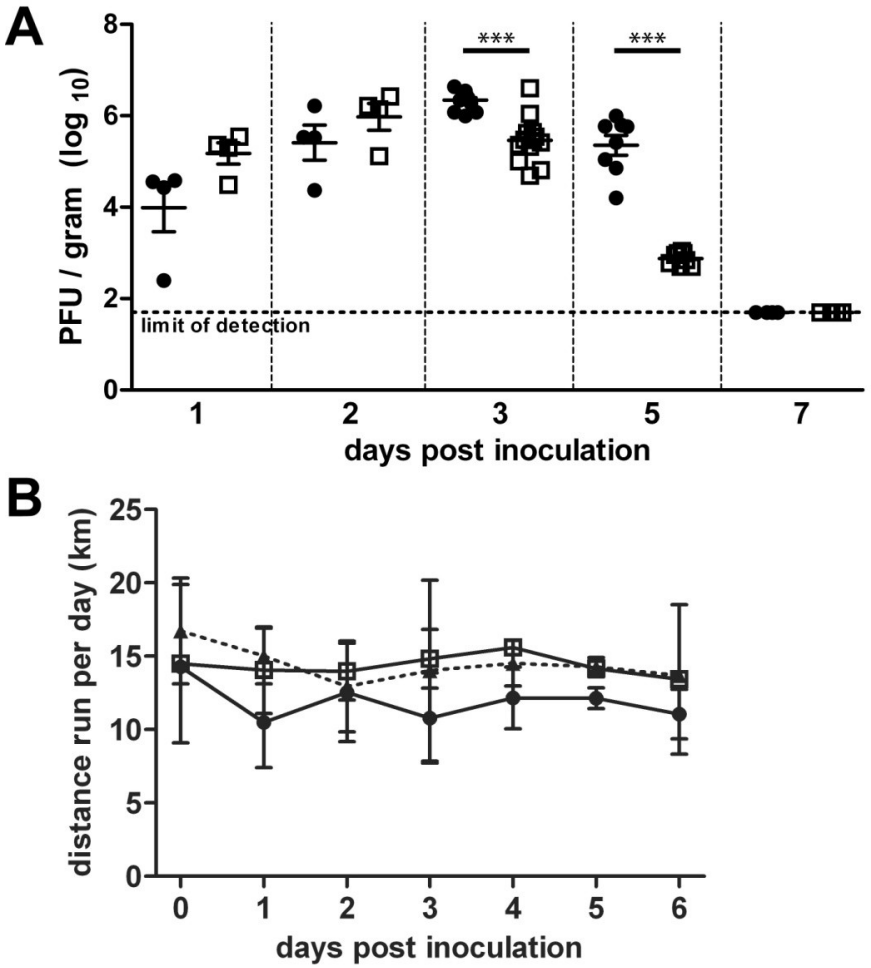

Figure 4.3 Accelerated clearance of viral load in hamsters infected by PIV3-NS2. (A) Whole lung virus loads in hamsters infected with PIV3 (closed circles) or PIV3-NS2 (open squares) measured over time, demonstrating a more rapid clearance of PIV3 infection when the virus expresses RSV NS2. Data (mean ± SEM) represent 3 independent experiments with total of 4 – 9 animals per timepoint. All viruses express GFP. ****P* <0.0001, unpaired *t* test. **(B)** Daily running wheel distance in hamsters mock inoculated (closed triangles, dotted line) or inoculated with PIV3 (closed circles, solid line) or PIV3-NS2 (open squares, solid line). Despite differences in whole lung viral load and lower airway infection, no difference in running distance, an index of clinical disease, was evident. Data represent 2 – 3 animals per timepoint.

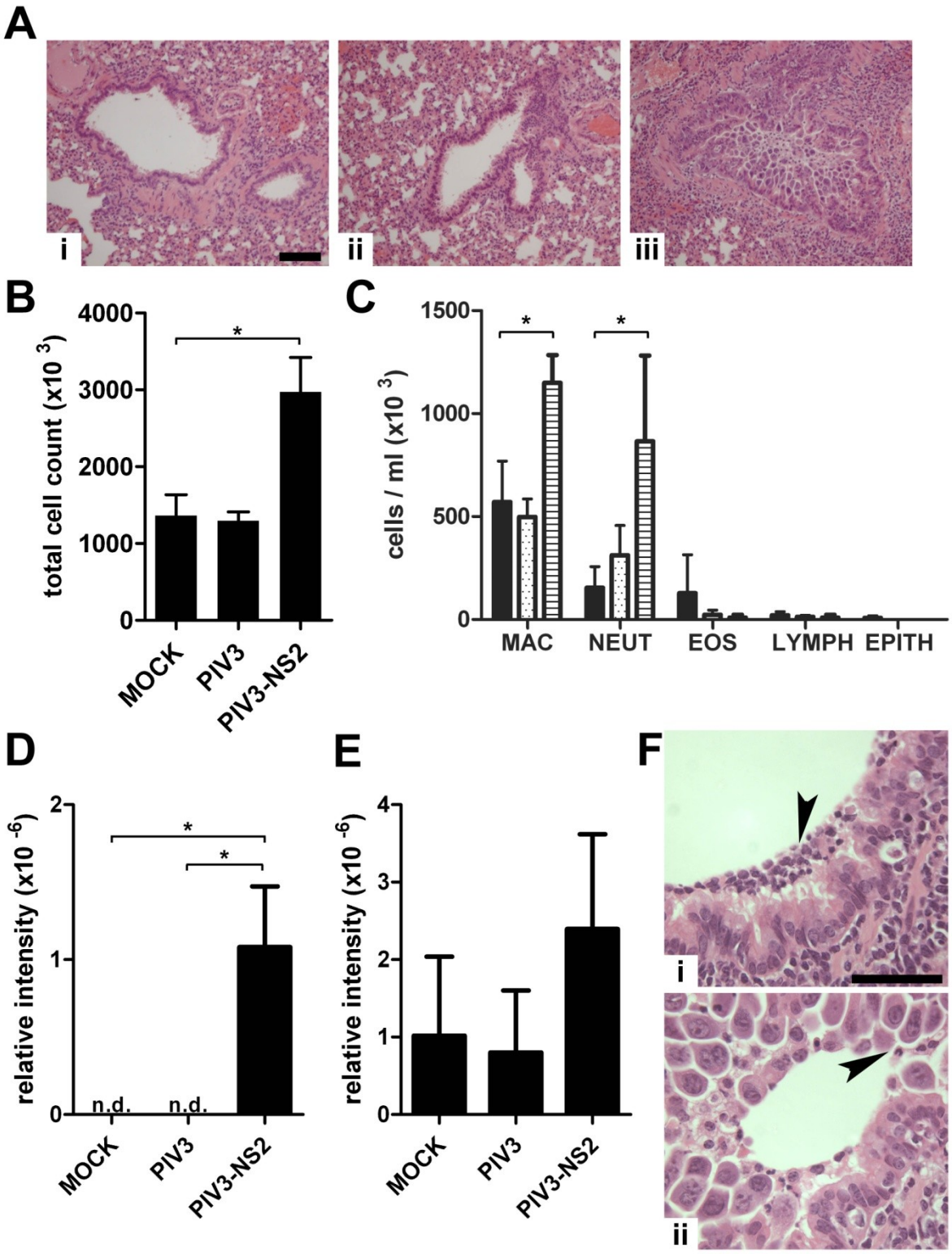
A
i
ii
iii
B
total cell count (x10 3)
4000
3000
2000
1000
0
*
MOCK
PIV3
PIV3-NS2
C
cells / ml (x10 3)
1500
1000
500
0
*
*
MAC
NEUT
EOS
LYMPH
EPITH
D
relative intensity (x10 -6)
2
1
0
*
*
n.d.
n.d.
MOCK
PIV3
PIV3-NS2
E
relative intensity (x10 -6)
4
3
2
1
0
MOCK
PIV3
PIV3-NS2
F
i
ii

Figure 4.4. Neutrophilic inflammation in distal airways of PIV3-NS2 infected hamsters. **(A)** Representative images of H&E stained histologic cross-sections of the smaller airways in hamsters mock inoculated (i) or infected with PIV3 (ii) or PIV3-NS2 (iii) at 3 days pi. Scale bar represents 100 μm. **(B)** Total cell counts in bronchoalveolar lavage (BAL) fluid of infected hamsters at 3 days pi. **(C)** Cytospins of cells from BAL of mock-inoculated hamsters (black bar) or hamsters infected with PIV3 (dotted bar) or PIV3-NS2 (striped bar) were Giemsa stained and cell types (macrophages, neutrophils, eosinophils, lymphocytes, and epithelial cells) were differentiated by morphologic criteria and counted. **(D, E)** Identification and relative abundance of the neutrophil effector proteins neutrophil elastase **(D)** and myeloperoxidase **(E)** were determined in cell free BAL fluid at 3 days pi by LC-MS/MS based identification and label-free quantification using the normalized spectral index method (239). **(F)** Representative images of neutrophils in the lumen of PIV3-infected animals (i) at 5 days pi or PIV3-NS2 infected animals (ii) at 3 days pi, the respective times of peak neutrophil influx. Arrow heads denote examples of neutrophils. Scale bar represents 50 μm. All quantitative data (mean ± SEM) represent n = 4 animals. n.d. not detected *P<0.05, one-way ANOVA with Tukey's post-test.

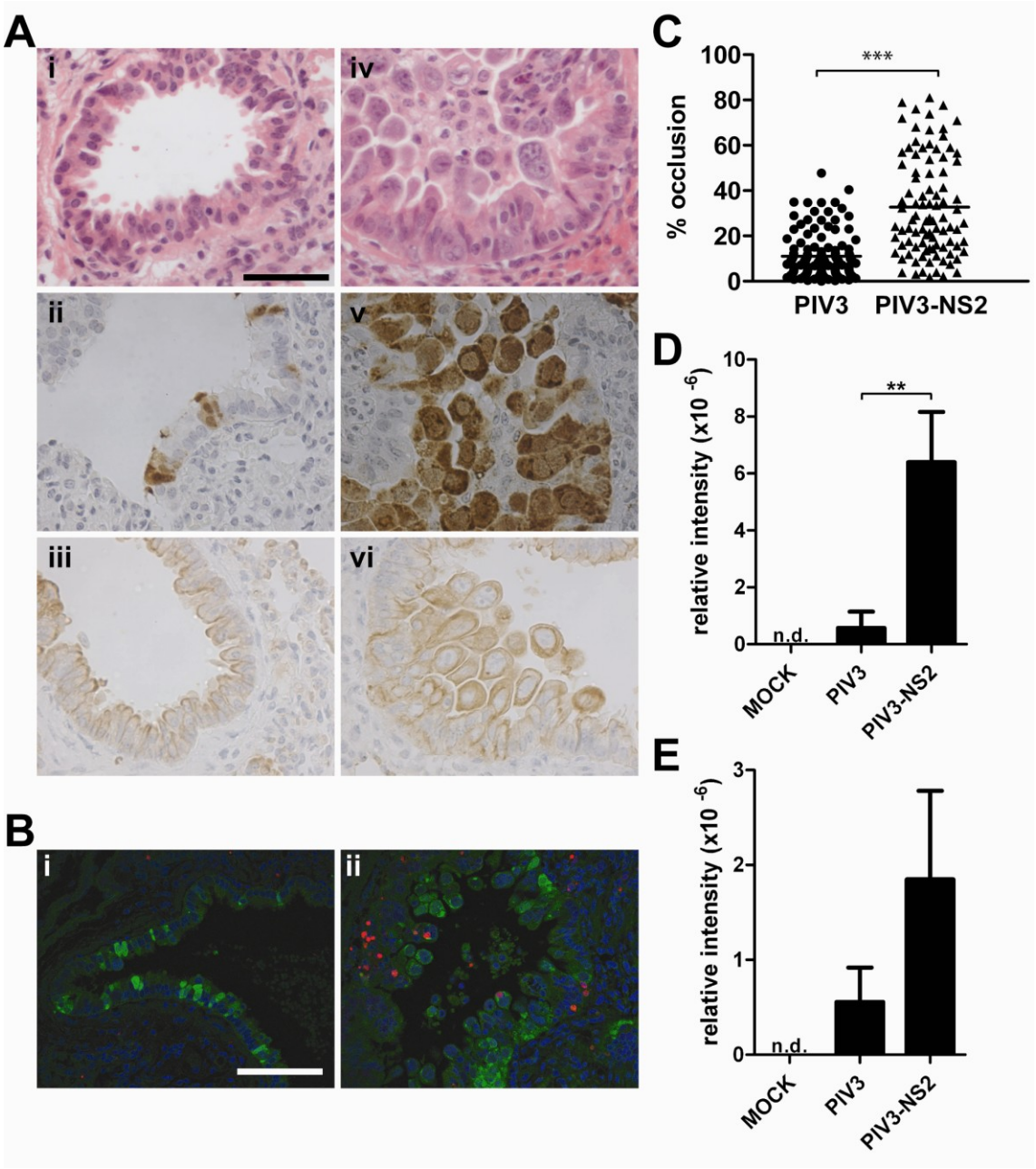
A
i
iv
ii
v
iii
vi
B
i
ii
C
100
80
60
40
20
0
% occlusion
***
PIV3
PIV3-NS2
D
relative intensity (x10 -6)
10
8
6
4
2
0
**
n.d.
MOCK
PIV3
PIV3-NS2
E
relative intensity (x10 -6)
3
2
1
0
n.d.
MOCK
PIV3
PIV3-NS2

Figure 4.5. Shedding of cells infected by PIV3-NS2 but not PIV3 into hamster lower conducting airways. (A) Representative images from histologic cross-sections of hamster distal airways infected with PIV3 (i - iii) and PIV3-NS2 (iv - vi). Sections were stained with H&E (i, iv), or with antibody against PIV3 to identify PIV3-infected cells (ii, v), or with an antibody against cytokeratin 18 to identify epithelial cells (iii, vi) at 3 days pi. Scale bar represents 50 μm. **(B)** Representative images from histologic cross-sections of hamster distal airways infected with PIV3 (i) and PIV3-NS2 (ii). Sections were stained for viral antigen (green) and nuclei (blue). Apoptotic cells were identified by TUNEL staining (red). Note the majority of infected cells in the airway lumen are negative for TUNEL staining. **(C)** Morphometric quantitative analysis of distal airway cell accumulation in hamsters infected with PIV3 or PIV3-NS2 by measuring the percentage of cross-sectional airway lumen surface area occupied by virus antigen-positive cells at 3 days pi. Histologic, antigen-stained whole lung sections from 3 animals were measured and each symbol represents occlusion of an individual airway. ***P <0.0001, unpaired t test. **(D, E)** Identification and relative abundance of the epithelial cell specific proteins keratin 19 **(D)** and keratin 8 **(E)** were determined in cell free bronchoalveolar lavage fluid (BALF) at 3 days pi by LC-MS/MS based identification and label-free quantification using the normalized spectral index method (239). Keratins in cell-free BALF likely originate from apoptotic or necrotic epithelial cells in the airway lumen. Data (mean ± SEM) represent n = 4 animals. n.d. not detected, **P<0.01, one-way ANOVA with Tukey's post-test.

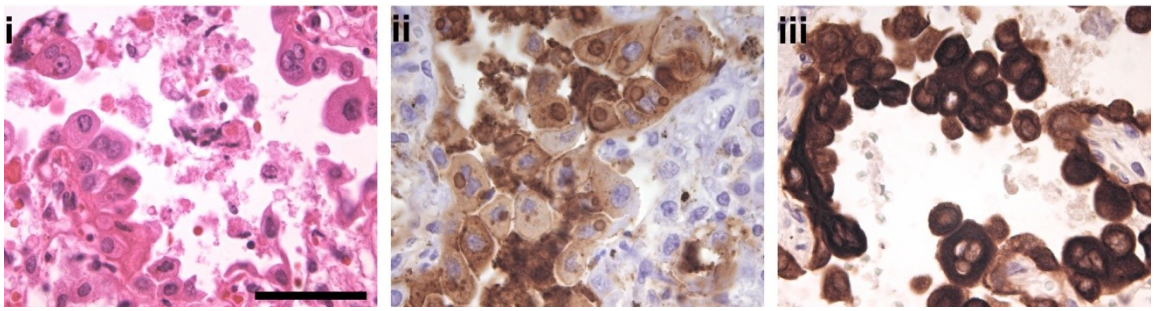

Figure 4.6. Shedding of cells infected by RSV into lower airways of human.

Representative images of histologic cross-sections of human lower airways obtained post-mortem from a patient naturally infected by RSV. Sections were stained with H&E (i), or with an RSV-specific antibody to detect infected cells (ii), or with a cytokeratin 8/18 antibody to detect epithelial cells (iii). Scale bar represents 50 μm. Note the smaller diameter distal airways of humans demonstrate virus antigen-positive cells shedding and accumulation in the lumen, often sufficient to cause airway occlusion, similar to accumulations noted in the hamster distal airways.

CHAPTER V

CONCLUSIONS

Respiratory syncytial virus is a significant pathogen that targets the respiratory mucosa and, in infants, is the most frequent cause of severe lower respiratory tract illness, often presenting as bronchiolitis. The goal of this dissertation was to understand the interactions between RSV and the airway epithelium and to define the cytopathogenic effects of RSV on the primary target of infection, the ciliated cell.

From the studies presented in this dissertation, we conclude the following:

I. RSV infection of human ciliated cells is resolved in vitro by a ciliated cell shedding response.

A. RSV targets columnar ciliated cells of the human airway epithelium and induces cytokine expression associated with severe RSV disease.

RSV demonstrated tropism for ciliated cells in a primary, well-differentiated model of the pseudostratified human airway epithelium (HAE) and infection was not documented in any other cell type, including Goblet cells and basal cells. Efficient initial infection of HAE was dependent upon the presence of the mature form of the RSV glycoprotein protein G, emphasizing the requirement for G in attachment and entry. HAE cultures supported RSV replication and spread, though clearance of infected cells and viral titer was noted at later times after infection. Replication induced increases in gene transcription of common antiviral genes, including IFNβ, IL-1β, IL-8, CXCL10, RANTES, and TNF-α, in a time dependent manner.

RSV tropism for ciliated cells has been previously documented by our group and others (114, 115, 131) and ciliated cell tropism has also been demonstrated a number of additional respiratory viruses, including other myxoviruses (125, 230, 240, 241). As the primary target of RSV infection, ciliated cells are uniquely positioned to initiate and modulate the antiviral response of the airway epithelium. Initiation of antiviral gene transcription likely contributes to limitation of viral replication and recruitment of infiltrating immune cells in the context of in vivo infection.

The innate inflammatory response plays a critical role in RSV disease and proinflammatory cytokines, such as IL-1β and TNF-α, and chemoattractants, such as IL-8, CXCL10, and RANTES, are elevated in nasophryngeal secretions and bronchoalveolar washes of infants with RSV-associated bronchiolitis (132, 136, 142, 143), with increased levels of IL-1β and IL-8 being independently associated with severe disease (118, 133, 144). We provide evidence that airway cells play a central role in modulating the inflammatory response by regulating these cytokines following RSV infection, though the relative contribution of in vivo cytokine secretion from the infected epithelia compared to other cell types such as airway macrophages is unclear.

Interestingly, our studies suggested a role for the RSV NS2 protein in upregulation of IL-8. Consistent with this, previous work has shown that infection of A549 cells with RSV deleted for the NS2 gene resulted in reduced secretion of IL-8 compared to wild-type virus or RSV deleted for the NS1 gene alone (104). The promotor region of the IL-8 gene contains binding site for p65 (242) and NS2 has been previously shown to play a role in p65 translocation to the nucleus (92, 104), suggesting a possible mechanism for NS2-mediated IL-8 upregulation. Furthermore, IL-8 is a major chemoattractant for neutrophils, which are the most predominate type of leukocyte detected in the airways of RSV-infected infants (180). The notion that neutrophilic inflammation may be enhanced by NS2 identifies NS2 as a major pathogenesis factor contributing to disease severity.

B. RSV infection of ciliated cells results in destruction of the cilia apparatus, ciliated cells shedding, and impairment of mucociliary clearance.

Previous studies of ciliated airway epithelial cultures have documented RSV-induced ciliary dyskinesia, a decline in the presence of cilia following RSV infection, and sloughing of cells from infected cultures (114, 124, 175). We confirm these features of RSV infection and expand on previous studies with several important findings. First, we attribute damage to the cilia and cilia structures following RSV infection to expression of the NS2 protein, further emphasizing the role of NS2 in RSV pathogenesis. Next, we demonstrate that clearance of viral infection in vitro is driven by active shedding of infected cells from the epithelium and that, based on histologic criteria, apoptosis of infected cells is delayed until complete extrusion of the cell from the epithelium into the apical compartment. Finally, we demonstrate that the combined effects of cilia degradation and infected cell shedding abolished the ability of the epithelium to perform mucociliary transport following RSV infection and these factors are likely to significantly impair mucociliary clearance in vivo.

We speculate that delay of apoptosis until cells are fully detached from the epithelium is an important ciliated cell response that, in vivo, serves to dampen the inflammatory response and decrease potential damage to the barrier function of the airway epithelium. Apoptotic cells shed from the epithelium are subsequently available for phagocytosis or mechanical clearance. Viruses frequently evade or delay apoptosis to allow for enhanced replication and the RSV life-cycle likely benefits from delay of cell shedding and retention of the ciliated cell in the airway epithelium. The RSV NS1 and NS2 proteins delay apoptosis in tissue culture cells lines through activation of cellular anti-apoptotic NF-kB and AKT pathways and these same pathways may be important for suppression of apoptosis in ciliated epithelial cells (92). Interestingly, infection of ciliated cells with PIV3 expressing NS1 results in no visible effect on apical surface structures and minimal cell

shedding, despite robust infection, potentially identifying a more important role in the pro-survival pathway for the NS1 protein as compared to NS2.

Mucociliary clearance is a critical innate defense mechanism of the airway epithelium and coordinated cilia beat is of utmost importance to maintenance of the mucociliary escalator function of the human airway. Therefore, the cytopathogenic effects of RSV on cilia function and mucociliary clearance likely have profound clinical implications. Shedding of cells into the airway lumen combined with impaired mucociliary clearance may contribute to the accumulation of antigen-positive cells noted in the airway lumen of RSV infected animals and infants (116-118, 153). In the large airways, where patchy and noncontiguous infection is often noted, mucociliary clearance may be maintained by surrounding regions of airways with healthy epithelia, allowing for clearance of infected cell debris. However, in the smaller airways where ciliated cells are fewer in number and infection is often noted as circumferential (117), it is possible that RSV infection leads to greater loss of ciliated cells and a more significant decline in mucotransport ability that may result in accumulation of infected cells in the airway lumen. Intralumenal accumulations of cells and debris likely contribute to airway obstruction and inflammation, potentially exacerbating RSV disease.

II. RSV-induced retraction of the ciliated cell tail is attributable to the RSV NS2 protein.

In the pseudostratified airway epithelium of the cartilaginous airway regions, ciliated cells are columnar in morphology, spanning the length of epithelium with the cilia on the apical surface extending into the airway lumen while the ciliated cell tail remains embedded within the underlying basal cell layer. Infection of ciliated columnar cells with RSV results in a transition from the native columnar morphology to a rounded morphology and this morphologic phenotype is unique to RSV, as no other viruses tested in our airway model underwent cell rounding as a result of infection. Because recent studies have identified phenotypic differences between highly passaged laboratory strains of RSV, such as the A2

strain used in these studies, and clinical isolates (243), we confirmed that the recently isolated clinical strain of RSV (Memphis 37) caused morphological changes in infected cells similar to cells infected with the recombinant GFP-expressing RSV. Cell rounding also occurred following infection of HAE with a recombinant RSV without GFP, the biological-derived RSV from which the recombinant was generated, and a wild-type subgroup B RSV, identifying cell rounding as unique consequence specific to RSV infection of ciliated cells. Using gene deletion mutants, we attribute the rounding function to the RSV NS2 protein.

Morphological changes in RSV infected cells have been frequently noted in animal models of RSV disease and histological examination of tissue from RSV-infected infants (116, 119, 153, 161, 244). Retrospective investigation of tissue sections from children with lower respiratory illness demonstrated RSV antigen-positive multi-nucleated epithelial cells and giant cell proliferation in the airway lumen (161). The earliest studies describe these lesions as a “bizarre derangement of the epithelium” and note a “mass of cytoplasm attached by a thread to the epithelial basement” (161). Similarly, in calves infected with bovine RSV, large irregular cytoplasmic projects and hyperplastic epithelial cells were described (116). We suggest that the rounding morphology of RSV infected ciliated cells in vitro, driven by expression of the NS2 protein, directly correlates to the abnormal morphological changes noted in previous studies of RSV infection in vivo.

The mechanism of NS2-induced ciliated cell rounding is currently unclear. Comparison of cell monolayers infected with RSV, RSVΔNS2, PIV3, and PIV3-NS2 did not reveal a morphological phenotype specific to the NS2 protein (data not shown), suggesting the polarized and differentiated state of the ciliated airway epithelium is a critical component of RSV-mediated cell rounding. Cellular pathways known to modulate morphological features of polarized cells are future avenues of exploration and represent a potentially unidentified pathway of interaction with the RSV NS2 protein. Notably, RSV has been shown to modify actin filaments and keratin intermediate filaments during viral assembly and egress

(245-248). Cytoskeletal scaffolds comprised of keratin intermediate filaments (KIFs) are essential for the cell-cell adhesion and structural integrity of cells, and post-translational modification of KIFs, by phosphorylation or O-glycosylation, occurs in response to cellular stress. Cleavage and reorganization of keratin 18 (K18), a primary KIF of ciliated cells, occurs during apoptosis (249) and increased phosphorylation of K18 leads to keratin reorganization, differential localization, and changes in protein association (250-252). A role for NS2-mediated modification of keratin intermediate filaments to promote or enable epithelial cell shedding represents an intriguing hypothesis.

III. Expression of RSV NS2 dramatically alters PIV3 infection kinetics in vivo.

A. RSV NS2 enhances shedding of PIV3-infected cells into the airway lumen and accelerates mechanical airway clearance of infection in vivo.

We next used the hamster model of paramyxovirus infection to evaluate the significance of in vitro findings related to the cytopathic effect of NS2 on ciliated cells. The hamster nasal respiratory epithelium is comprised of similar cell types as HAE and similar outcomes were observed in this region following infection with PIV3-NS2. Both PIV3 and PIV3-NS2 specifically target ciliated cells for infection and no viral antigen was noted in goblet or basal cells. As in HAE, PIV3-NS2 infection of ciliated cells resulted in rounding, cilia cytopathology, and shedding of infected cells, leaving the underlying epithelium intact. In contrast, PIV3-infected cells retained the native columnar morphology and remained embedded within the epithelium. Similarly, in the larger airways, PIV3-NS2 infection resulted in cell rounding and shedding, and viral antigen positive cells were most frequently located within the airway lumen. Over time, shed cells in large airways of PIV3-NS2 infected animals were likely cleared by mucociliary clearance mechanisms. PIV3 infected similar numbers of cells, although cells remained columnar and embedded in the epithelium, with viral-antigen positive cells or cellular debris rarely noted in the airway lumen. Additionally, we found that PIV3-NS2 was cleared from the hamster lungs more rapidly than PIV3. These data raise the

possibility that cell shedding may accelerate clearance of virus-infected cells and viral antigen from the airways, representing a protective cellular response triggered by the NS2 protein.

B. RSV NS2 enhanced shedding of infected cells in the small airways results in acute airway obstruction.

Although cell shedding may promote accelerated clearance in the large airways, shedding of infected cells into the narrower diameter distal airways resulted in accumulation of cells in the airway lumen. In many airways, sufficient cell accumulation resulted in partial to complete obstruction of the airway lumen and occlusions were composed primarily of intact antigen positive epithelial cells, with little contribution of necrotic debris and immune infiltrates. PIV3-NS2 infected cells in the small airways of hamsters displayed an unusual swollen and pleomorphic morphology, exaggerating the morphological changes noted in infected cells in HAE, the hamster nasal epithelium, and the hamster larger airways. Notably, distal airway obstruction associated with PIV3-NS2 was transient and was not associated with clinical signs of disease.

We suggest that enlarged and pleomorphic infected cells in the distal airway may reveal cell-type specific differences in NS2-mediated morphological phenotype. These swollen pleomorphic cells may represent infection of another cell type present in the smaller airway regions, such as the non-ciliated club (Clara) cell. In the human and hamster airways, club cells increase in density as the conducting airways descend into the distal airway region (113, 232). Infection of both ciliated and non-ciliated epithelial cells was noted in the hamster distal airways, the latter likely representing club cells. Similarly, RSV infection of both ciliated and non-ciliated cells has been observed in the small airways of humans, calves, and lambs (116-119, 153). The apparent morphologic difference in shed cells within different regions of the airway may reflect the increased frequency of PIV3-NS2 infection of club cells in the smaller airway compared to ciliated cells in the larger airway. We suggest

that the combination of narrower diameter airway lumens and expanded volume of cells shed into these regions enhances the likelihood that shed cells would accumulate and occlude the smaller diameter airway lumens.

Distal airway obstructions in PIV3-NS2 infected animals were strikingly reminiscent of bronchiolar airway occlusions observed in the small airways of infects with RSV-associated bronchiolitis and we speculate that RSV NS2-induced cell shedding has important implications for RSV disease. RSV bronchiolitis has long been associated with small airway obstruction resulting in air-trapping distal to the regions of obstruction, leading to decreased pulmonary function and increased airway resistance. Tissue sections from RSV-infected patients and studies of large animal models of infection reveal accumulation of RSV antigen-positive debris in the lumen of infected airways, further emphasizing the potential significance of shed and accumulated epithelial cells as a major contributor to small airway obstruction after RSV infection. Furthermore, RSV-associated bronchiolitis is known to be more severe than bronchiolitis associated with other respiratory pathogens such as rhinovirus and parainfluenza viruses (9, 10). Non-RSV bronchiolitis is characterized by pulmonary edema and inflammatory infiltrates, resulting in constriction of the bronchiolar airways. Additional bronchiolar involvement and occlusion due to accumulation of shed RSV-infected cells may account for the more severe consequences associated with RSV bronchiolitis.

We speculate that epithelial cell shedding promoted by NS2 may also provide unique evolutionary benefits to the RSV life-cycle. Shedding of virus-infected cells may, for example, contribute to the spread of infection throughout the respiratory tract, such as by pulmonary aspiration of upper airway secretions laden with shed infected cells into the lower respiratory tract. Shed cells in the large and small airways appear viable and viral replication and shedding may continue as these cells are transported within the respiratory tract. It is

also possible that occlusion of airways may contribute to prolonging disease, thereby increasing the opportunity for viral transmission to secondary contacts.

C. RSV NS2 exaggerates neutrophil recruitment to distal airways.

In hamsters infected with PIV3-NS2, histological evidence indicated earlier and more robust neutrophil recruitment to infected airways, and both neutrophils and proteins secreted by neutrophils were elevated bronchoalveolar lavage fluid of PIV3-NS2 infected animals at 3 days pi. Furthermore, analysis of inflammation in histological sections revealed an intriguing difference in the location of neutrophils in airways of PIV3 and PIV3-NS2 infected animals. PIV3 infection resulted in neutrophil recruitment into the airway lumen at later time points (5 days pi), and neutrophils were frequently noted to be associated with the epithelium, presumably at locations of infection. In contrast, although PIV3-NS2 animals had larger numbers of inflammatory cells at earlier time points (3 days pi), neutrophils were often observed below the basement membrane, having not yet migrated across the airway epithelium, or within the airway lumen, not directly associated with the respiratory epithelium, suggesting that neutrophils are associating with the infected, shed cells in PIV3-NS2 infected animals rather than the airway epithelium.

Neutrophil infiltration is characteristic of RSV infection and neutrophils make up a high percentage of infiltrating leuokocytes in both human studies and animal models of infection (116, 180). Studies in mice suggested that neutrophils were recruited by CD8+ T lymphocytes (253), however more recent evidence indicated that neutrophil recruitment is mediated by cytokine release from the infected airway epithelium. In HAE, we found that airway epithelial cells upregulated IL-8 and CXCL10, major neutrophil recruitment cytokines, in response to RSV and PIV3-NS2 infection, suggesting that infected epithelial cells play a significant role in recruitment of neutrophils to site of infection.

Neutrophil location may have several implications for RSV pathogenesis. RSV infected cells display the neutrophil adhesion protein ICAM-1 at the cell surface (191, 193,

194) and shedding of these infected cells may have a protective effect for the host, where neutrophils in the airway lumen adhere to shed cells, rather than cells within the airway epithelium. In this case, release of cytotoxic neutrophil effector proteins, such as elastase and MPO, in the lumen, rather than directly at the epithelium, may decrease damage to the epithelium and help maintain barrier integrity. Conversely, cell shedding may represent an immune evasion mechanism of the virus, where removal of the infected cell from the epithelium might decrease the likelihood that infected cells will directly encounter inflammatory cells recruited to site of infection. In this scenario, shedding of the infected cell into the airway lumen might reduce neutrophil migration across the respiratory epithelium, as neutrophils in the parenchyma can no longer interact with ICAM-1 on the infected cell to facilitate migration across the respiratory mucosa. Clearance of shed cells would further dampen recruitment signals to site of infection. Virus infected cells that remain in the epithelium, such as occurs in PIV3 infection, likely recruit inflammatory infiltrates and enable direct interactions between infiltrates and infected cells. In the context of RSV, cell shedding resulting in reduction of interactions between immune cells and virus-infected cells may significantly impact the development of immunity to RSV.

Summary

These studies present evidence for a critical role of ciliated cells in development of RSV disease. The observations reported in this dissertation provide new insight into the viral and cellular mechanisms of RSV infection of ciliated cells and define a novel role for the RSV NS2 protein in modulating key pathogenic changes in RSV-infected cells. Use of a well-differentiated model of the human airway allowed for identification of morphological consequence of RSV infection not present in cell line monolayers, namely transition of infected ciliated cells from the native columnar morphology to a rounded morphology. Further, we identify in vivo correlates of in vitro observations using recombinant viruses and the hamster model of infection. In the hamster, we identify two key outcomes of NS2-

mediated morphological changes and cell shedding. In the larger airways, RSV NS2 promotes enhanced clearance of viral infection mediated by clearance of virally infected, shed cells. In the smaller airways, RSV NS2 enhances acute airway obstruction due to narrower airway diameter and increased size of shed cells. Addtionally, we demonstrate early and robust neutrophil influx in the distal airway regions, mediated by the NS2 protein in the context of a viral infection. Acute airway obstruction is a key feature in severe RSV-associated bronchiolitis and these studies identify the NS2 protein as the primary mediator of early airway obstruction. We suggest that NS2-mediated cell shedding and obstruction represent a critical initiating event that contributes to airway pathology associated with severe RSV-mediated bronchiolitis.

REFERENCES

1. **Glezen, W. P., Taber, L. H., Frank, A. L. , and Kasel, J. A.** Risk of primary infection and reinfection with respiratory syncytial virus. *Am J Dis Child*. 1986;140(6):543-546.

2. **Simoes, E. A.** Respiratory syncytial virus infection. *Lancet*. 1999;354(9181):847-852.

3. **CDC**. Respiratory syncytial virus--United States, July 2007-June 2011. *MMWR Morb Mortal Wkly Rep*. 2011;60(35):1203-1206.

4. **Nair, H., Nokes, D. J., Gessner, B. D., Dherani, M., Madhi, S. A., Singleton, R. J., O'Brien, K. L., Roca, A., Wright, P. F., Bruce, N., et al.** Global burden of acute lower respiratory infections due to respiratory syncytial virus in young children: a systematic review and meta-analysis. *Lancet*. 2010;375(9725):1545-1555.

5. **Hall, C. B., Weinberg, G. A., Iwane, M. K., Blumkin, A. K., Edwards, K. M., Staat, M. A., Auinger, P., Griffin, M. R., Poehling, K. A., Erdman, D., et al.** The burden of respiratory syncytial virus infection in young children. *N Engl J Med*. 2009;360(6):588-598.

6. **Shay, D. K., Holman, R. C., Newman, R. D., Liu, L. L., Stout, J. W. , and Anderson, L. J.** Bronchiolitis-associated hospitalizations among US children, 1980-1996. *JAMA*. 1999;282(15):1440-1446.

7. **Hon, K. L., Leung, T. F., Cheng, W. Y., Ko, N. M., Tang, W. K., Wong, W. W., Yeung, W. H. , and Chan, P. K.** Respiratory syncytial virus morbidity, premorbid factors, seasonality, and implications for prophylaxis. *J Crit Care*. 2012;27(5):464-468.

8. **Roberts, S. R., Compans, R. W. , and Wertz, G. W.** Respiratory syncytial virus matures at the apical surfaces of polarized epithelial cells. *J Virol*. 1995;69(4):2667-2673.

9. **Hervas, D., Reina, J., Yanez, A., del Valle, J. M., Figuerola, J. , and Hervas, J. A.** Epidemiology of hospitalization for acute bronchiolitis in children: differences between RSV and non-RSV bronchiolitis. *Eur J Clin Microbiol Infect Dis*. 2012;31(8):1975-1981.

10. **Garcia, C. G., Bhore, R., Soriano-Fallas, A., Trost, M., Chason, R., Ramilo, O. , and Mejias, A.** Risk factors in children hospitalized with RSV bronchiolitis versus non-RSV bronchiolitis. *Pediatrics*. 2010;126(6):e1453-1460.

11. **Stang, P., Brandenburg, N. , and Carter, B.** The economic burden of respiratory syncytial virus-associated bronchiolitis hospitalizations. *Arch Pediatr Adolesc Med*. 2001;155(1):95-96.

12. **Leader, S. , and Kohlhase, K.** Respiratory syncytial virus-coded pediatric hospitalizations, 1997 to 1999. *Pediatr Infect Dis J*. 2002;21(7):629-632.

13. **Bezerra, P. G., Britto, M. C., Correia, J. B., Duarte Mdo, C., Fonceca, A. M., Rose, K., Hopkins, M. J., Cuevas, L. E. , and McNamara, P. S.** Viral and atypical bacterial detection in acute respiratory infection in children under five years. *PLoS One*. 2011;6(4):e18928.

14. **Checchia, P. A., Nalysnyk, L., Fernandes, A. W., Mahadevia, P. J., Xu, Y., Fahrbach, K. , and Welliver, R. C., Sr.** Mortality and morbidity among infants at high risk for severe respiratory syncytial virus infection receiving prophylaxis with palivizumab: a systematic literature review and meta-analysis. *Pediatr Crit Care Med*. 2011;12(5):580-588.

15. **Bourgeois, F. T., Valim, C., McAdam, A. J. , and Mandl, K. D.** Relative impact of influenza and respiratory syncytial virus in young children. *Pediatrics*. 2009;124(6):e1072-1080.

16. **Thompson, W. W., Shay, D. K., Weintraub, E., Brammer, L., Cox, N., Anderson, L. J. , and Fukuda, K.** Mortality associated with influenza and respiratory syncytial virus in the United States. *Jama*. 2003;289(2):179-186.

17. **Boyce, T. G., Mellen, B. G., Mitchel, E. F., Jr., Wright, P. F. , and Griffin, M. R.** Rates of hospitalization for respiratory syncytial virus infection among children in medicaid. *J Pediatr*. 2000;137(6):865-870.

18. **Laing, I., Reidel, F., Yap, P. L. , and Simpson, H.** Atopy predisposing to acute bronchiolitis during an epidemic of respiratory syncytial virus. *Br Med J (Clin Res Ed)*. 1982;284(6322):1070-1072.

19. **El Saleeby, C. M., Bush, A. J., Harrison, L. M., Aitken, J. A. , and Devincenzo, J. P.** Respiratory syncytial virus load, viral dynamics, and disease severity in previously healthy naturally infected children. *J Infect Dis*. 2011;204(7):996-1002.

20. **Cherukuri, A., Patton, K., Gasser, R. A., Jr., Zuo, F., Woo, J., Esser, M. T. , and Tang, R. S.** Adults 65 years old and older have reduced numbers of functional memory T cells to respiratory syncytial virus fusion protein. *Clin Vaccine Immunol*. 2013;20(2):239-247.

21. **Nicholson, K. G., Kent, J., Hammersley, V. , and Cancio, E.** Acute viral infections of upper respiratory tract in elderly people living in the community: comparative, prospective, population based study of disease burden. *Bmj*. 1997;315(7115):1060-1064.

22. **Walsh, E. E., Peterson, D. R. , and Falsey, A. R.** Risk factors for severe respiratory syncytial virus infection in elderly persons. *J Infect Dis*. 2004;189(2):233-238.

23. **Falsey, A. R., Hennessey, P. A., Formica, M. A., Cox, C. , and Walsh, E. E.** Respiratory syncytial virus infection in elderly and high-risk adults. *N Engl J Med*. 2005;352(17):1749-1759.

24. **Falsey, A. R., Cunningham, C. K., Barker, W. H., Kouides, R. W., Yuen, J. B., Menegus, M., Weiner, L. B., Bonville, C. A. , and Betts, R. F.** Respiratory syncytial virus and influenza A infections in the hospitalized elderly. *J Infect Dis*. 1995;172(2):389-394.

25. **Walsh, E. E., Falsey, A. R. , and Hennessey, P. A.** Respiratory syncytial and other virus infections in persons with chronic cardiopulmonary disease. *Am J Respir Crit Care Med*. 1999;160(3):791-795.

26. **Bowden, R. A.** Respiratory virus infections after marrow transplant: the Fred Hutchinson Cancer Research Center experience. *Am J Med*. 1997;102(3A):27-30; discussion 42-23.

27. **Harrington, R. D., Hooton, T. M., Hackman, R. C., Storch, G. A., Osborne, B., Gleaves, C. A., Benson, A. , and Meyers, J. D.** An outbreak of respiratory syncytial virus in a bone marrow transplant center. *J Infect Dis*. 1992;165(6):987-993.

28. **Champlin, R. E. , and Whimbey, E.** Community respiratory virus infections in bone marrow transplant recipients: the M.D. Anderson Cancer Center experience. *Biol Blood Marrow Transplant*. 2001;7 Suppl:8S-10S.

29. **Ghosh, S., Champlin, R. E., Englund, J., Giralt, S. A., Rolston, K., Raad, I., Jacobson, K., Neumann, J., Ippoliti, C., Mallik, S., et al.** Respiratory syncytial virus upper respiratory tract illnesses in adult blood and marrow transplant recipients: combination therapy with aerosolized ribavirin and intravenous immunoglobulin. *Bone Marrow Transplant*. 2000;25(7):751-755.

30. **Nichols, W. G., Gooley, T. , and Boeckh, M.** Community-acquired respiratory syncytial virus and parainfluenza virus infections after hematopoietic stem cell transplantation: the Fred Hutchinson Cancer Research Center experience. *Biol Blood Marrow Transplant*. 2001;7 Suppl:11S-15S.

31. **Casey, J., Morris, K., Narayana, M., Nakagaki, M. , and Kennedy, G. A.** Oral ribavirin for treatment of respiratory syncitial virus and parainfluenza 3 virus infections post allogeneic haematopoietic stem cell transplantation. *Bone Marrow Transplant*. 2013.

32. **Pelaez, A., Lyon, G. M., Force, S. D., Ramirez, A. M., Neujahr, D. C., Foster, M., Naik, P. M., Gal, A. A., Mitchell, P. O. , and Lawrence, E. C.** Efficacy of oral ribavirin in lung transplant patients with respiratory syncytial virus lower respiratory tract infection. *J Heart Lung Transplant*. 2009;28(1):67-71.

33. **Bont, L., Steijn, M., Van Aalderen, W. M., Brus, F., Th Draaisma, J. M., Van Diemen-Steenvoorde, R. A., Pekelharing-Berghuis, M. , and Kimpen, J. L.** Seasonality of long term wheezing following respiratory syncytial virus lower respiratory tract infection. *Thorax*. 2004;59(6):512-516.

34. **Sigurs, N., Aljassim, F., Kjellman, B., Robinson, P. D., Sigurbergsson, F., Bjarnason, R. , and Gustafsson, P. M.** Asthma and allergy patterns over 18 years after severe RSV bronchiolitis in the first year of life. *Thorax*. 2010;65(12):1045-1052.

35. **Stein, R. T., Sherrill, D., Morgan, W. J., Holberg, C. J., Halonen, M., Taussig, L. M., Wright, A. L. , and Martinez, F. D.** Respiratory syncytial virus in early life and risk of wheeze and allergy by age 13 years. *Lancet*. 1999;354(9178):541-545.

36. **Blanken, M. O., Rovers, M. M., Molenaar, J. M., Winkler-Seinstra, P. L., Meijer, A., Kimpen, J. L. , and Bont, L.** Respiratory syncytial virus and recurrent wheeze in healthy preterm infants. *N Engl J Med*. 2013;368(19):1791-1799.

37. **Simoes, E. A., Carbonell-Estrany, X., Rieger, C. H., Mitchell, I., Fredrick, L. , and Groothuis, J. R.** The effect of respiratory syncytial virus on subsequent recurrent wheezing in atopic and nonatopic children. *J Allergy Clin Immunol*. 2010;126(2):256-262.

38. **Bont, L., Steijn, M., van Aalderen, W. M. , and Kimpen, J. L.** Impact of wheezing after respiratory syncytial virus infection on health-related quality of life. *Pediatr Infect Dis J*. 2004;23(5):414-417.

39. **Hall, C. B., Hall, W. J., Gala, C. L., MaGill, F. B. , and Leddy, J. P.** Long-term prospective study in children after respiratory syncytial virus infection. *J Pediatr*. 1984;105(3):358-364.

40. **Stensballe, L. G., Kristensen, K., Simoes, E. A., Jensen, H., Nielsen, J., Benn, C. S. , and Aaby, P.** Atopic disposition, wheezing, and subsequent respiratory syncytial virus hospitalization in Danish children younger than 18 months: a nested case-control study. *Pediatrics*. 2006;118(5):e1360-1368.

41. **Lagos, R., DeVincenzo, J. P., Munoz, A., Hultquist, M., Suzich, J., Connor, E. M. , and Losonsky, G. A.** Safety and antiviral activity of motavizumab, a respiratory syncytial virus (RSV)-specific humanized monoclonal antibody, when administered to RSV-infected children. *Pediatr Infect Dis J*. 2009;28(9):835-837.

42. **Malley, R., DeVincenzo, J., Ramilo, O., Dennehy, P. H., Meissner, H. C., Gruber, W. C., Sanchez, P. J., Jafri, H., Balsley, J., Carlin, D., et al.** Reduction of respiratory syncytial virus (RSV) in tracheal aspirates in intubated infants by use of humanized monoclonal antibody to RSV F protein. *J Infect Dis*. 1998;178(6):1555-1561.

43. **Wu, H., Pfarr, D. S., Johnson, S., Brewah, Y. A., Woods, R. M., Patel, N. K., White, W. I., Young, J. F. , and Kiener, P. A.** Development of motavizumab, an ultra-potent antibody for the prevention of respiratory syncytial virus infection in the upper and lower respiratory tract. *J Mol Biol*. 2007;368(3):652-665.

44. **Boeckh, M., Berrey, M. M., Bowden, R. A., Crawford, S. W., Balsley, J. , and Corey, L.** Phase 1 evaluation of the respiratory syncytial virus-specific monoclonal antibody palivizumab in recipients of hematopoietic stem cell transplants. *J Infect Dis*. 2001;184(3):350-354.

45. **Carbonell-Estrany, X., Simoes, E. A., Dagan, R., Hall, C. B., Harris, B., Hultquist, M., Connor, E. M., Losonsky, G. A. , and Motavizumab Study, G.** Motavizumab for prophylaxis of respiratory syncytial virus in high-risk children: a noninferiority trial. *Pediatrics*. 2010;125(1):e35-51.

46. **Feltes, T. F., Cabalka, A. K., Meissner, H. C., Piazza, F. M., Carlin, D. A., Top, F. H., Jr., Connor, E. M. , and Sondheimer, H. M.** Palivizumab prophylaxis reduces hospitalization due to respiratory syncytial virus in young children with hemodynamically significant congenital heart disease. *J Pediatr*. 2003;143(4):532-540.

47. **Null, D., Jr., Pollara, B., Dennehy, P. H., Steichen, J., Sanchez, P. J., Givner, L. B., Carlin, D., Landry, B., Top, F. H., Jr. , and Connor, E.** Safety and immunogenicity of palivizumab (Synagis) administered for two seasons. *Pediatr Infect Dis J*. 2005;24(11):1021-1023.

48. **Resch, B., Sommer, C., Nuijten, M. J., Seidinger, S., Walter, E., Schoellbauer, V. , and Mueller, W. D.** Cost-effectiveness of palivizumab for respiratory syncytial virus infection in high-risk children, based on long-term epidemiologic data from Austria. *Pediatr Infect Dis J*. 2012;31(1):e1-8.

49. **Hruska, J. F., Bernstein, J. M., Douglas, R. G., Jr. , and Hall, C. B.** Effects of ribavirin on respiratory syncytial virus in vitro. *Antimicrob Agents Chemother*. 1980;17(5):770-775.

50. **Krilov, L. R., Mandel, F. S., Barone, S. R. , and Fagin, J. C.** Follow-up of children with respiratory syncytial virus bronchiolitis in 1986 and 1987: potential effect of ribavirin on long term pulmonary function. The Bronchiolitis Study Group. *Pediatr Infect Dis J*. 1997;16(3):273-276.

51. **Moler, F. W., Steinhart, C. M., Ohmit, S. E. , and Stidham, G. L.** Effectiveness of ribavirin in otherwise well infants with respiratory syncytial virus-associated respiratory failure. Pediatric Critical Study Group. *J Pediatr*. 1996;128(3):422-428.

52. **Ohmit, S. E., Moler, F. W., Monto, A. S. , and Khan, A. S.** Ribavirin utilization and clinical effectiveness in children hospitalized with respiratory syncytial virus infection. *J Clin Epidemiol*. 1996;49(9):963-967.

53. **Ventre, K. , and Randolph, A. G.** Ribavirin for respiratory syncytial virus infection of the lower respiratory tract in infants and young children. *Cochrane Database Syst Rev*. 2007(1):CD000181.

54. **Krilov, L. R.** Safety issues related to the administration of ribavirin. *Pediatr Infect Dis J*. 2002;21(5):479-481.

55. **Glanville, A. R., Scott, A. I., Morton, J. M., Aboyoun, C. L., Plit, M. L., Carter, I. W. , and Malouf, M. A.** Intravenous ribavirin is a safe and cost-effective treatment for respiratory syncytial virus infection after lung transplantation. *J Heart Lung Transplant*. 2005;24(12):2114-2119.

56. **Garrison, M. M., Christakis, D. A., Harvey, E., Cummings, P. , and Davis, R. L.** Systemic corticosteroids in infant bronchiolitis: A meta-analysis. *Pediatrics*. 2000;105(4):E44.

57. **Davison, C., Ventre, K. M., Luchetti, M. , and Randolph, A. G.** Efficacy of interventions for bronchiolitis in critically ill infants: a systematic review and meta-analysis. *Pediatr Crit Care Med*. 2004;5(5):482-489.

58. **Patel, H., Platt, R., Lozano, J. M. , and Wang, E. E.** Glucocorticoids for acute viral bronchiolitis in infants and young children. *Cochrane Database Syst Rev*. 2004(3):CD004878.

59. **Somers, C. C., Ahmad, N., Mejias, A., Buckingham, S. C., Carubelli, C., Katz, K., Leos, N., Gomez, A. M., DeVincenzo, J. P., Ramilo, O., et al.** Effect of dexamethasone on respiratory syncytial virus-induced lung inflammation in children: results of a randomized, placebo controlled clinical trial. *Pediatr Allergy Immunol*. 2009;20(5):477-485.

60. **van Woensel, J. B., Vyas, H. , and Group, S. T.** Dexamethasone in children mechanically ventilated for lower respiratory tract infection caused by respiratory syncytial virus: a randomized controlled trial. *Crit Care Med*. 2011;39(7):1779-1783.

61. **Kim, H. W., Canchola, J. G., Brandt, C. D., Pyles, G., Chanock, R. M., Jensen, K. , and Parrott, R. H.** Respiratory syncytial virus disease in infants despite prior administration of antigenic inactivated vaccine. *Am J Epidemiol*. 1969;89(4):422-434.

62. **Delgado, M. F., Coviello, S., Monsalvo, A. C., Melendi, G. A., Hernandez, J. Z., Batalle, J. P., Diaz, L., Trento, A., Chang, H. Y., Mitzner, W., et al.** Lack of antibody affinity maturation due to poor Toll-like receptor stimulation leads to enhanced respiratory syncytial virus disease. *Nat Med*. 2009;15(1):34-41.

63. **Murphy, B. R. , and Walsh, E. E.** Formalin-inactivated respiratory syncytial virus vaccine induces antibodies to the fusion glycoprotein that are deficient in fusion-inhibiting activity. *J Clin Microbiol*. 1988;26(8):1595-1597.

64. **Wright, P. F., Karron, R. A., Belshe, R. B., Thompson, J., Crowe, J. E., Jr., Boyce, T. G., Halburnt, L. L., Reed, G. W., Whitehead, S. S., Anderson, E. L., et al.** Evaluation of a live, cold-passaged, temperature-sensitive, respiratory syncytial virus vaccine candidate in infancy. *J Infect Dis*. 2000;182(5):1331-1342.

65. **Bernstein, D. I., Malkin, E., Abughali, N., Falloon, J., Yi, T. , and Dubovsky, F.** Phase 1 study of the safety and immunogenicity of a live, attenuated respiratory syncytial virus and parainfluenza virus type 3 vaccine in seronegative children. *Pediatr Infect Dis J*. 2012;31(2):109-114.

66. **Garg, R., Latimer, L., Simko, E., Gerdts, V., Potter, A. , and van Drunen Littel-van den Hurk, S.** Induction of mucosal immunity and protection by intranasal immunisation with a novel respiratory syncytial virus vaccine formulation. *J Gen Virol*. 2013.

67. **Karron, R. A., Thumar, B., Schappell, E., Buchholz, U. J. , and Collins, P. L.** Attenuation of live respiratory syncytial virus vaccines is associated with reductions in levels of nasal cytokines. *J Infect Dis*. 2013;207(11):1773-1779.

68. **Luongo, C., Winter, C. C., Collins, P. L. , and Buchholz, U. J.** Increased genetic and phenotypic stability of a promising live-attenuated respiratory syncytial virus vaccine candidate by reverse genetics. *J Virol*. 2012;86(19):10792-10804.

69. **Luongo, C., Winter, C. C., Collins, P. L. , and Buchholz, U. J.** Respiratory syncytial virus modified by deletions of the NS2 gene and amino acid S1313 of the L polymerase protein is a temperature-sensitive, live-attenuated vaccine candidate that is phenotypically stable at physiological temperature. *J Virol*. 2013;87(4):1985-1996.

70. **Karron, R. A., Buonagurio, D. A., Georgiu, A. F., Whitehead, S. S., Adamus, J. E., Clements-Mann, M. L., Harris, D. O., Randolph, V. B., Udem, S. A., Murphy, B. R., et al.** Respiratory syncytial virus (RSV) SH and G proteins are not essential for viral replication in vitro: clinical evaluation and molecular characterization of a cold-passaged, attenuated RSV subgroup B mutant. *Proc Natl Acad Sci U S A*. 1997;94(25):13961-13966.

71. **Techaarpornkul, S., Barretto, N. , and Peeples, M. E.** Functional analysis of recombinant respiratory syncytial virus deletion mutants lacking the small hydrophobic and/or attachment glycoprotein gene. *J Virol*. 2001;75(15):6825-6834.

72. **Teng, M. N. , and Collins, P. L.** Identification of the respiratory syncytial virus proteins required for formation and passage of helper-dependent infectious particles. *J Virol*. 1998;72(7):5707-5716.

73. **Teng, M. N., Whitehead, S. S. , and Collins, P. L.** Contribution of the respiratory syncytial virus G glycoprotein and its secreted and membrane-bound forms to virus replication in vitro and in vivo. *Virology*. 2001;289(2):283-296.

74. **Mastrangelo, P. , and Hegele, R. G.** The RSV fusion receptor: not what everyone expected it to be. *Microbes Infect*. 2012;14(13):1205-1210.

75. **Tayyari, F., Marchant, D., Moraes, T. J., Duan, W., Mastrangelo, P. , and Hegele, R. G.** Identification of nucleolin as a cellular receptor for human respiratory syncytial virus. *Nat Med*. 2011;17(9):1132-1135.

76. **Hallak, L. K., Spillmann, D., Collins, P. L. , and Peeples, M. E.** Glycosaminoglycan sulfation requirements for respiratory syncytial virus infection. *J Virol*. 2000;74(22):10508-10513.

77. **Techaarpornkul, S., Collins, P. L. , and Peeples, M. E.** Respiratory syncytial virus with the fusion protein as its only viral glycoprotein is less dependent on cellular glycosaminoglycans for attachment than complete virus. *Virology*. 2002;294(2):296-304.

78. **Feldman, S. A., Audet, S. , and Beeler, J. A.** The fusion glycoprotein of human respiratory syncytial virus facilitates virus attachment and infectivity via an interaction with cellular heparan sulfate. *J Virol*. 2000;74(14):6442-6447.

79. **Krusat, T. , and Streckert, H. J.** Heparin-dependent attachment of respiratory syncytial virus (RSV) to host cells. *Arch Virol*. 1997;142(6):1247-1254.

80. **Duan, D., Yue, Y., Yan, Z., McCray, P. B., Jr. , and Engelhardt, J. F.** Polarity influences the efficiency of recombinant adenoassociated virus infection in differentiated airway epithelia. *Hum Gene Ther*. 1998;9(18):2761-2776.

81. **Zhang, L., Bukreyev, A., Thompson, C. I., Watson, B., Peeples, M. E., Collins, P. L. , and Pickles, R. J.** Infection of ciliated cells by human parainfluenza virus type 3 in an in vitro model of human airway epithelium. *J Virol*. 2005;79(2):1113-1124.

82. **Monzon, M. E., Casalino-Matsuda, S. M. , and Forteza, R. M.** Identification of glycosaminoglycans in human airway secretions. *Am J Respir Cell Mol Biol*. 2006;34(2):135-141.

83. **Wertz, G. W., Collins, P. L., Huang, Y., Gruber, C., Levine, S. , and Ball, L. A.** Nucleotide sequence of the G protein gene of human respiratory syncytial virus reveals an unusual type of viral membrane protein. *Proc Natl Acad Sci U S A*. 1985;82(12):4075-4079.

84. **Wertz, G. W., Krieger, M. , and Ball, L. A.** Structure and cell surface maturation of the attachment glycoprotein of human respiratory syncytial virus in a cell line deficient in O glycosylation. *J Virol*. 1989;63(11):4767-4776.

85. **Lambert, D. M.** Role of oligosaccharides in the structure and function of respiratory syncytial virus glycoproteins. *Virology*. 1988;164(2):458-466.

86. **Garcia-Beato, R., Martinez, I., Franci, C., Real, F. X., Garcia-Barreno, B. , and Melero, J. A.** Host cell effect upon glycosylation and antigenicity of human respiratory syncytial virus G glycoprotein. *Virology*. 1996;221(2):301-309.

87. **Garcia-Beato, R. , and Melero, J. A.** The C-terminal third of human respiratory syncytial virus attachment (G) protein is partially resistant to protease digestion and is glycosylated in a cell-type-specific manner. *J Gen Virol*. 2000;81(Pt 4):919-927.

88. **Hendricks, D. A., McIntosh, K. , and Patterson, J. L.** Further characterization of the soluble form of the G glycoprotein of respiratory syncytial virus. *J Virol*. 1988;62(7):2228-2233.

89. **Roberts, S. R., Lichtenstein, D., Ball, L. A. , and Wertz, G. W.** The membrane-associated and secreted forms of the respiratory syncytial virus attachment glycoprotein G are synthesized from alternative initiation codons. *J Virol*. 1994;68(7):4538-4546.

90. **Bukreyev, A., Yang, L. , and Collins, P. L.** The secreted G protein of human respiratory syncytial virus antagonizes antibody-mediated restriction of replication involving macrophages and complement. *J Virol*. 2012;86(19):10880-10884.

91. **Bukreyev, A., Yang, L., Fricke, J., Cheng, L., Ward, J. M., Murphy, B. R. , and Collins, P. L.** The secreted form of respiratory syncytial virus G glycoprotein helps the virus evade antibody-mediated restriction of replication by acting as an antigen decoy and through effects on Fc receptor-bearing leukocytes. *J Virol*. 2008;82(24):12191-12204.

92. **Bitko, V., Shulyayeva, O., Mazumder, B., Musiyenko, A., Ramaswamy, M., Look, D. C. , and Barik, S.** Nonstructural proteins of respiratory syncytial virus suppress premature apoptosis by an NF-kappaB-dependent, interferon-independent mechanism and facilitate virus growth. *J Virol*. 2007;81(4):1786-1795.

93. **Spann, K. M., Tran, K. C., Chi, B., Rabin, R. L. , and Collins, P. L.** Suppression of the induction of alpha, beta, and lambda interferons by the NS1 and NS2 proteins of human respiratory syncytial virus in human epithelial cells and macrophages [corrected]. *J Virol*. 2004;78(8):4363-4369.

94. **Hastie, M. L., Headlam, M. J., Patel, N. B., Bukreyev, A. A., Buchholz, U. J., Dave, K. A., Norris, E. L., Wright, C. L., Spann, K. M., Collins, P. L., et al.** The human respiratory syncytial virus nonstructural protein 1 regulates type I and type II interferon pathways. *Mol Cell Proteomics*. 2012;11(5):108-127.

95. **Swedan, S., Musiyenko, A. , and Barik, S.** Respiratory syncytial virus nonstructural proteins decrease levels of multiple members of the cellular interferon pathways. *J Virol*. 2009;83(19):9682-9693.

96. **Liu, P., Jamaluddin, M., Li, K., Garofalo, R. P., Casola, A. , and Brasier, A. R.** Retinoic acid-inducible gene I mediates early antiviral response and Toll-like receptor 3 expression in respiratory syncytial virus-infected airway epithelial cells. *J Virol*. 2007;81(3):1401-1411.

97. **Rudd, B. D., Burstein, E., Duckett, C. S., Li, X. , and Lukacs, N. W.** Differential role for TLR3 in respiratory syncytial virus-induced chemokine expression. *J Virol*. 2005;79(6):3350-3357.

98. **Ling, Z., Tran, K. C. , and Teng, M. N.** Human respiratory syncytial virus nonstructural protein NS2 antagonizes the activation of beta interferon transcription by interacting with RIG-I. *J Virol*. 2009;83(8):3734-3742.

99. **Lo, M. S., Brazas, R. M. , and Holtzman, M. J.** Respiratory syncytial virus nonstructural proteins NS1 and NS2 mediate inhibition of Stat2 expression and alpha/beta interferon responsiveness. *J Virol*. 2005;79(14):9315-9319.

100. **Ramaswamy, M., Shi, L., Varga, S. M., Barik, S., Behlke, M. A. , and Look, D. C.** Respiratory syncytial virus nonstructural protein 2 specifically inhibits type I interferon signal transduction. *Virology*. 2006;344(2):328-339.

101. **Elliott, J., Lynch, O. T., Suessmuth, Y., Qian, P., Boyd, C. R., Burrows, J. F., Buick, R., Stevenson, N. J., Touzelet, O., Gadina, M., et al.** Respiratory syncytial virus NS1 protein degrades STAT2 by using the Elongin-Cullin E3 ligase. *J Virol*. 2007;81(7):3428-3436.

102. **Straub, C. P., Lau, W. H., Preston, F. M., Headlam, M. J., Gorman, J. J., Collins, P. L. , and Spann, K. M.** Mutation of the elongin C binding domain of human respiratory syncytial virus non-structural protein 1 (NS1) results in degradation of NS1 and attenuation of the virus. *Virol J*. 2011;8:252.

103. **Donnelly, R. P. , and Kotenko, S. V.** Interferon-lambda: a new addition to an old family. *J Interferon Cytokine Res*. 2010;30(8):555-564.

104. **Spann, K. M., Tran, K. C. , and Collins, P. L.** Effects of nonstructural proteins NS1 and NS2 of human respiratory syncytial virus on interferon regulatory factor 3, NF-kappaB, and proinflammatory cytokines. *J Virol*. 2005;79(9):5353-5362.

105. **Teng, M. N. , and Collins, P. L.** Altered growth characteristics of recombinant respiratory syncytial viruses which do not produce NS2 protein. *J Virol*. 1999;73(1):466-473.

106. **Teng, M. N., Whitehead, S. S., Bermingham, A., St Claire, M., Elkins, W. R., Murphy, B. R. , and Collins, P. L.** Recombinant respiratory syncytial virus that does not express the NS1 or M2-2 protein is highly attenuated and immunogenic in chimpanzees. *J Virol*. 2000;74(19):9317-9321.

107. **Whitehead, S. S., Bukreyev, A., Teng, M. N., Firestone, C. Y., St Claire, M., Elkins, W. R., Collins, P. L. , and Murphy, B. R.** Recombinant respiratory syncytial virus bearing a deletion of either the NS2 or SH gene is attenuated in chimpanzees. *J Virol*. 1999;73(4):3438-3442.

108. **Boers, J. E., Ambergen, A. W. , and Thunnissen, F. B.** Number and proliferation of basal and parabasal cells in normal human airway epithelium. *Am J Respir Crit Care Med*. 1998;157(6 Pt 1):2000-2006.

109. **Evans, M. J. , and Plopper, C. G.** The role of basal cells in adhesion of columnar epithelium to airway basement membrane. *Am Rev Respir Dis*. 1988;138(2):481-483.

110. **Spina, D.** Epithelium smooth muscle regulation and interactions. *Am J Respir Crit Care Med*. 1998;158(5 Pt 3):S141-145.

111. **Plopper, C. G.** Comparative morphologic features of bronchiolar epithelial cells. The Clara cell. *Am Rev Respir Dis*. 1983;128(2 Pt 2):S37-41.

112. **Plopper, C. G., Mariassy, A. T., Wilson, D. W., Alley, J. L., Nishio, S. J. , and Nettesheim, P.** Comparison of nonciliated tracheal epithelial cells in six mammalian species: ultrastructure and population densities. *Exp Lung Res*. 1983;5(4):281-294.

113. **Boers, J. E., Ambergen, A. W. , and Thunnissen, F. B.** Number and proliferation of clara cells in normal human airway epithelium. *Am J Respir Crit Care Med*. 1999;159(5 Pt 1):1585-1591.

114. **Villenave, R., Thavagnanam, S., Sarlang, S., Parker, J., Douglas, I., Skibinski, G., Heaney, L. G., McKaigue, J. P., Coyle, P. V., Shields, M. D., et al.** In vitro modeling of respiratory syncytial virus infection of pediatric bronchial epithelium, the primary target of infection in vivo. *Proc Natl Acad Sci U S A*. 2012;109(13):5040-5045.

115. **Zhang, L., Peeples, M. E., Boucher, R. C., Collins, P. L. , and Pickles, R. J.** Respiratory syncytial virus infection of human airway epithelial cells is polarized, specific to ciliated cells, and without obvious cytopathology. *J Virol*. 2002;76(11):5654-5666.

116. **Bryson, D. G., Platten, M. F., McConnell, S. , and McNulty, M. S.** Ultrastructural features of lesions in bronchiolar epithelium in induced respiratory syncytial virus pneumonia of calves. *Vet Pathol*. 1991;28(4):293-299.

117. **Johnson, J. E., Gonzales, R. A., Olson, S. J., Wright, P. F. , and Graham, B. S.** The histopathology of fatal untreated human respiratory syncytial virus infection. *Mod Pathol*. 2007;20(1):108-119.

118. **Welliver, T. P., Garofalo, R. P., Hosakote, Y., Hintz, K. H., Avendano, L., Sanchez, K., Velozo, L., Jafri, H., Chavez-Bueno, S., Ogra, P. L., et al.** Severe human lower respiratory tract illness caused by respiratory syncytial virus and influenza virus is characterized by the absence of pulmonary cytotoxic lymphocyte responses. *J Infect Dis*. 2007;195(8):1126-1136.

119. **Welliver, T. P., Reed, J. L. , and Welliver, R. C., Sr.** Respiratory syncytial virus and influenza virus infections: observations from tissues of fatal infant cases. *Pediatr Infect Dis J*. 2008;27(10 Suppl):S92-96.

120. **Kojima, T., Go, M., Takano, K., Kurose, M., Ohkuni, T., Koizumi, J., Kamekura, R., Ogasawara, N., Masaki, T., Fuchimoto, J., et al.** Regulation of tight junctions in upper airway epithelium. *Biomed Res Int*. 2013;2013:947072.

121. **Cereijido, M., Valdes, J., Shoshani, L. , and Contreras, R. G.** Role of tight junctions in establishing and maintaining cell polarity. *Annu Rev Physiol*. 1998;60:161-177.

122. **Schneeberger, E. E. , and Lynch, R. D.** The tight junction: a multifunctional complex. *Am J Physiol Cell Physiol*. 2004;286(6):C1213-1228.

123. **van Meer, G. , and Simons, K.** The function of tight junctions in maintaining differences in lipid composition between the apical and the basolateral cell surface domains of MDCK cells. *Embo J*. 1986;5(7):1455-1464.

124. **Guo-Parke, H., Canning, P., Douglas, I., Villenave, R., Heaney, L. G., Coyle, P. V., Lyons, J. D., Shields, M. D. , and Power, U. F.** Relative respiratory syncytial virus cytopathogenesis in upper and lower respiratory tract epithelium. *Am J Respir Crit Care Med*. 2013;188(7):842-851.

125. **Zhang, L., Collins, P. L., Lamb, R. A. , and Pickles, R. J.** Comparison of differing cytopathic effects in human airway epithelium of parainfluenza virus 5 (W3A), parainfluenza virus type 3, and respiratory syncytial virus. *Virology*. 2011;421(1):67-77.

126. **Hall, C. B., Douglas, R. G., Jr. , and Simons, R. L.** Interferon production in adults with respiratory syncytial viral infection. *Ann Intern Med*. 1981;94(1):53-55.

127. **Isaacs, D.** Production of interferon in respiratory syncytial virus bronchiolitis. *Arch Dis Child*. 1989;64(1):92-95.

128. **Taylor, C. E., Webb, M. S., Milner, A. D., Milner, P. D., Morgan, L. A., Scott, R., Stokes, G. M., Swarbrick, A. S. , and Toms, G. L.** Interferon alfa, infectious virus, and virus antigen secretion in respiratory syncytial virus infections of graded severity. *Arch Dis Child*. 1989;64(12):1656-1660.

129. **Okabayashi, T., Kojima, T., Masaki, T., Yokota, S., Imaizumi, T., Tsutsumi, H., Himi, T., Fujii, N. , and Sawada, N.** Type-III interferon, not type-I, is the predominant interferon induced by respiratory viruses in nasal epithelial cells. *Virus Res*. 2011;160(1-2):360-366.

130. **Patel, J. A., Kunimoto, M., Sim, T. C., Garofalo, R., Eliott, T., Baron, S., Ruuskanen, O., Chonmaitree, T., Ogra, P. L. , and Schmalstieg, F.** Interleukin-1 alpha mediates the enhanced expression of intercellular adhesion molecule-1 in pulmonary epithelial cells infected with respiratory syncytial virus. *Am J Respir Cell Mol Biol*. 1995;13(5):602-609.

131. **Tristram, D. A., Hicks, W., Jr. , and Hard, R.** Respiratory syncytial virus and human bronchial epithelium. *Arch Otolaryngol Head Neck Surg*. 1998;124(7):777-783.

132. **Laham, F. R., Israele, V., Casellas, J. M., Garcia, A. M., Lac Prugent, C. M., Hoffman, S. J., Hauer, D., Thumar, B., Name, M. I., Pascual, A., et al.** Differential production of inflammatory cytokines in primary infection with human metapneumovirus and with other common respiratory viruses of infancy. *J Infect Dis*. 2004;189(11):2047-2056.

133. **Lindgren, C., Lin, J., Graham, B. S., Gray, M. E., Parker, R. A. , and Sundell, H. W.** Respiratory syncytial virus infection enhances the response to laryngeal chemostimulation and inhibits arousal from sleep in young lambs. *Acta Paediatr*. 1996;85(7):789-797.

134. **Hornsleth, A., Klug, B., Nir, M., Johansen, J., Hansen, K. S., Christensen, L. S. , and Larsen, L. B.** Severity of respiratory syncytial virus disease related to type and genotype of virus and to cytokine values in nasopharyngeal secretions. *Pediatr Infect Dis J*. 1998;17(12):1114-1121.

135. **Matsuda, K., Tsutsumi, H., Okamoto, Y. , and Chiba, C.** Development of interleukin 6 and tumor necrosis factor alpha activity in nasopharyngeal secretions of infants and children during infection with respiratory syncytial virus. *Clin Diagn Lab Immunol*. 1995;2(3):322-324.

136. **McNamara, P. S., Flanagan, B. F., Selby, A. M., Hart, C. A. , and Smyth, R. L.** Pro- and anti-inflammatory responses in respiratory syncytial virus bronchiolitis. *Eur Respir J*. 2004;23(1):106-112.

137. **Arnold, R., Humbert, B., Werchau, H., Gallati, H. , and Konig, W.** Interleukin-8, interleukin-6, and soluble tumour necrosis factor receptor type I release from a human pulmonary epithelial cell line (A549) exposed to respiratory syncytial virus. *Immunology*. 1994;82(1):126-133.

138. **Sheeran, P., Jafri, H., Carubelli, C., Saavedra, J., Johnson, C., Krisher, K., Sanchez, P. J. , and Ramilo, O.** Elevated cytokine concentrations in the nasopharyngeal and tracheal secretions of children with respiratory syncytial virus disease. *Pediatr Infect Dis J*. 1999;18(2):115-122.

139. **Garofalo, R., Mei, F., Espejo, R., Ye, G., Haeberle, H., Baron, S., Ogra, P. L. , and Reyes, V. E.** Respiratory syncytial virus infection of human respiratory epithelial cells up-regulates class I MHC expression through the induction of IFN-beta and IL-1 alpha. *J Immunol*. 1996;157(6):2506-2513.

140. **Mellow, T. E., Murphy, P. C., Carson, J. L., Noah, T. L., Zhang, L. , and Pickles, R. J.** The effect of respiratory synctial virus on chemokine release by differentiated airway epithelium. *Exp Lung Res*. 2004;30(1):43-57.

141. **Bont, L., Heijnen, C. J., Kavelaars, A., van Aalderen, W. M., Brus, F., Draaisma, J. T., Geelen, S. M., van Vught, H. J. , and Kimpen, J. L.** Peripheral blood cytokine responses and disease severity in respiratory syncytial virus bronchiolitis. *Eur Respir J*. 1999;14(1):144-149.

142. **McNamara, P. S., Flanagan, B. F., Hart, C. A. , and Smyth, R. L.** Production of chemokines in the lungs of infants with severe respiratory syncytial virus bronchiolitis. *J Infect Dis*. 2005;191(8):1225-1232.

143. **Noah, T. L., Ivins, S. S., Murphy, P., Kazachkova, I., Moats-Staats, B. , and Henderson, F. W.** Chemokines and inflammation in the nasal passages of infants with respiratory syncytial virus bronchiolitis. *Clin Immunol*. 2002;104(1):86-95.

144. **Smyth, R. L., Mobbs, K. J., O'Hea, U., Ashby, D. , and Hart, C. A.** Respiratory syncytial virus bronchiolitis: disease severity, interleukin-8, and virus genotype. *Pediatr Pulmonol*. 2002;33(5):339-346.

145. **Becker, S. , and Soukup, J. M.** Airway epithelial cell-induced activation of monocytes and eosinophils in respiratory syncytial viral infection. *Immunobiology*. 1999;201(1):88-106.

146. **Murai, H., Terada, A., Mizuno, M., Asai, M., Hirabayashi, Y., Shimizu, S., Morishita, T., Kakita, H., Hussein, M. H., Ito, T., et al.** IL-10 and RANTES are elevated in nasopharyngeal secretions of children with respiratory syncytial virus infection. *Allergol Int*. 2007;56(2):157-163.

147. **Barth, P. J., Wolf, M. , and Ramaswamy, A.** Distribution and number of Clara cells in the normal and disturbed development of the human fetal lung. *Pediatr Pathol*. 1994;14(4):637-651.

148. **Jeffery, P. K. , and Li, D.** Airway mucosa: secretory cells, mucus and mucin genes. *Eur Respir J*. 1997;10(7):1655-1662.

149. **Derscheid, R. J. , and Ackermann, M. R.** Perinatal lamb model of respiratory syncytial virus (RSV) infection. *Viruses*. 2012;4(10):2359-2378.

150. **Manning, C. M., Johnston, C. J., Hernady, E., Miller, J. N., Reed, C. K., Lawrence, B. P., Williams, J. P. , and Finkelstein, J. N.** Exacerbation of lung radiation injury by viral infection: the role of Clara cells and Clara cell secretory protein. *Radiat Res*. 2013;179(6):617-629.

151. **LeVine, A. M., Elliott, J., Whitsett, J. A., Srikiatkhachorn, A., Crouch, E., DeSilva, N. , and Korfhagen, T.** Surfactant protein-d enhances phagocytosis and pulmonary clearance of respiratory syncytial virus. *Am J Respir Cell Mol Biol*. 2004;31(2):193-199.

152. **Wang, S. Z., Rosenberger, C. L., Bao, Y. X., Stark, J. M. , and Harrod, K. S.** Clara cell secretory protein modulates lung inflammatory and immune responses to respiratory syncytial virus infection. *J Immunol*. 2003;171(2):1051-1060.

153. **Olivier, A., Gallup, J., de Macedo, M. M., Varga, S. M. , and Ackermann, M.** Human respiratory syncytial virus A2 strain replicates and induces innate immune responses by respiratory epithelia of neonatal lambs. *Int J Exp Pathol*. 2009;90(4):431-438.

154. **Aoshiba, K., Rennard, S. I. , and Spurzem, J. R.** Cell-matrix and cell-cell interactions modulate apoptosis of bronchial epithelial cells. *Am J Physiol*. 1997;272(1 Pt 1):L28-37.

155. **Frisch, S. M. , and Francis, H.** Disruption of epithelial cell-matrix interactions induces apoptosis. *J Cell Biol*. 1994;124(4):619-626.

156. **Brydon, E. W., Smith, H. , and Sweet, C.** Influenza A virus-induced apoptosis in bronchiolar epithelial (NCI-H292) cells limits pro-inflammatory cytokine release. *J Gen Virol*. 2003;84(Pt 9):2389-2400.

157. **Singhera, G. K., Chan, T. S., Cheng, J. Y., Vitalis, T. Z., Hamann, K. J. , and Dorscheid, D. R.** Apoptosis of viral-infected airway epithelial cells limit viral production and is altered by corticosteroid exposure. *Respir Res*. 2006;7:78.

158. **Sajjan, U., Wang, Q., Zhao, Y., Gruenert, D. C. , and Hershenson, M. B.** Rhinovirus disrupts the barrier function of polarized airway epithelial cells. *Am J Respir Crit Care Med*. 2008;178(12):1271-1281.

159. **Sacco, R. E., McGill, J. L., Palmer, M. V., Lippolis, J. D., Reinhardt, T. A. , and Nonnecke, B. J.** Neonatal calf infection with respiratory syncytial virus: drawing parallels to the disease in human infants. *Viruses*. 2012;4(12):3731-3753.

160. **Sacco, R. E., Nonnecke, B. J., Palmer, M. V., Waters, W. R., Lippolis, J. D. , and Reinhardt, T. A.** Differential expression of cytokines in response to respiratory syncytial virus infection of calves with high or low circulating 25-hydroxyvitamin D3. *PLoS One*. 2012;7(3):e33074.

161. **Shedden, W. I. , and Emery, J. L.** Immunofluorescent Evidence of Respiratory Syncytial Virus Infection in Cases of Giant Cell Bronchiolitis in Children. *J Pathol Bacteriol*. 1965;89:343-347.

162. **Baraniuk, J. N. , and Kim, D.** Nasonasal reflexes, the nasal cycle, and sneeze. *Curr Allergy Asthma Rep*. 2007;7(2):105-111.

163. **Chung, K. F.** Chronic cough: future directions in chronic cough: mechanisms and antitussives. *Chron Respir Dis*. 2007;4(3):159-165.

164. **Chen, T. M. , and Dulfano, M. J.** Mucus viscoelasticity and mucociliary transport rate. *J Lab Clin Med*. 1978;91(3):423-431.

165. **Knowles, M. R. , and Boucher, R. C.** Mucus clearance as a primary innate defense mechanism for mammalian airways. *J Clin Invest*. 2002;109(5):571-577.

166. **Matsui, H., Randell, S. H., Peretti, S. W., Davis, C. W. , and Boucher, R. C.** Coordinated clearance of periciliary liquid and mucus from airway surfaces. *J Clin Invest*. 1998;102(6):1125-1131.

167. **Smith, D. J., Gaffney, E. A. , and Blake, J. R.** Modelling mucociliary clearance. *Respir Physiol Neurobiol*. 2008;163(1-3):178-188.

168. **Button, B. M. , and Button, B.** Structure and function of the mucus clearance system of the lung. *Cold Spring Harb Perspect Med*. 2013;3(8).

169. **Boucher, R. C.** Evidence for airway surface dehydration as the initiating event in CF airway disease. *J Intern Med*. 2007;261(1):5-16.

170. **Button, B., Cai, L. H., Ehre, C., Kesimer, M., Hill, D. B., Sheehan, J. K., Boucher, R. C. , and Rubinstein, M.** A periciliary brush promotes the lung health by separating the mucus layer from airway epithelia. *Science*. 2012;337(6097):937-941.

171. **Bush, A. , and Hogg, C.** Primary ciliary dyskinesia: recent advances in epidemiology, diagnosis, management and relationship with the expanding spectrum of ciliopathy. *Expert Rev Respir Med*. 2012;6(6):663-682.

172. **Noone, P. G., Bali, D., Carson, J. L., Sannuti, A., Gipson, C. L., Ostrowski, L. E., Bromberg, P. A., Boucher, R. C. , and Knowles, M. R.** Discordant organ laterality in monozygotic twins with primary ciliary dyskinesia. *Am J Med Genet*. 1999;82(2):155-160.

173. **Camner, P., Mossberg, B. , and Afzelius, B. A.** Measurements of tracheobronchial clearance in patients with immotile-cilia syndrome and its value in differential diagnosis. *Eur J Respir Dis Suppl*. 1983;127:57-63.

174. **Mata, M., Sarrion, I., Armengot, M., Carda, C., Martinez, I., Melero, J. A. , and Cortijo, J.** Respiratory syncytial virus inhibits ciliagenesis in differentiated normal human bronchial epithelial cells: effectiveness of N-acetylcysteine. *PLoS One*. 2012;7(10):e48037.

175. **Smith, C. M., Kulkarni, H., Radhakrishnan, P., Rutman, A., Bankart, M. J., Williams, G., Hirst, R. A., Easton, A. J., Andrew, P. W. , and O'Callaghan, C.** Ciliary dyskinesia is an early feature of respiratory syncytial virus infection. *Eur Respir J*. 2013;doi: 10.1183/09031936.00205312.

176. **Wong, J. Y., Rutman, A. , and O'Callaghan, C.** Recovery of the ciliated epithelium following acute bronchiolitis in infancy. *Thorax*. 2005;60(7):582-587.

177. **Lekeux, P., Verhoeff, J., Hajer, R. , and Breukink, H. J.** Respiratory syncytial virus pneumonia in Friesian calves: physiological findings. *Res Vet Sci*. 1985;39(3):324-327.

178. **DeVincenzo, J. P., Wilkinson, T., Vaishnaw, A., Cehelsky, J., Meyers, R., Nochur, S., Harrison, L., Meeking, P., Mann, A., Moane, E., et al.** Viral load drives disease in humans experimentally infected with respiratory syncytial virus. *Am J Respir Crit Care Med*. 2010;182(10):1305-1314.

179. **Emboriadou, M., Hatzistilianou, M., Magnisali, C., Sakelaropoulou, A., Exintari, M., Conti, P. , and Aivazis, V.** Human neutrophil elastase in RSV bronchiolitis. *Ann Clin Lab Sci*. 2007;37(1):79-84.

180. **Everard, M. L., Swarbrick, A., Wrightham, M., McIntyre, J., Dunkley, C., James, P. D., Sewell, H. F. , and Milner, A. D.** Analysis of cells obtained by bronchial lavage of infants with respiratory syncytial virus infection. *Arch Dis Child*. 1994;71(5):428-432.

181. **McNamara, P. S., Ritson, P., Selby, A., Hart, C. A. , and Smyth, R. L.** Bronchoalveolar lavage cellularity in infants with severe respiratory syncytial virus bronchiolitis. *Arch Dis Child*. 2003;88(10):922-926.

182. **Smith, P. K., Wang, S. Z., Dowling, K. D. , and Forsyth, K. D.** Leucocyte populations in respiratory syncytial virus-induced bronchiolitis. *J Paediatr Child Health*. 2001;37(2):146-151.

183. **Derscheid, R. J. , and Ackermann, M. R.** The innate immune system of the perinatal lung and responses to respiratory syncytial virus infection. *Vet Pathol*. 2013;50(5):827-841.

184. **Sow, F. B., Gallup, J. M., Krishnan, S., Patera, A. C., Suzich, J. , and Ackermann, M. R.** Respiratory syncytial virus infection is associated with an altered innate immunity and a heightened pro-inflammatory response in the lungs of preterm lambs. *Respir Res*. 2011;12:106.

185. **Abu-Harb, M., Bell, F., Finn, A., Rao, W. H., Nixon, L., Shale, D. , and Everard, M. L.** IL-8 and neutrophil elastase levels in the respiratory tract of infants with RSV bronchiolitis. *Eur Respir J*. 1999;14(1):139-143.

186. **Baggiolini, M., Loetscher, P. , and Moser, B.** Interleukin-8 and the chemokine family. *Int J Immunopharmacol*. 1995;17(2):103-108.

187. **Fiedler, M. A., Wernke-Dollries, K. , and Stark, J. M.** Respiratory syncytial virus increases IL-8 gene expression and protein release in A549 cells. *Am J Physiol*. 1995;269(6 Pt 1):L865-872.

188. **Jagels, M. A., Daffern, P. J., Zuraw, B. L. , and Hugli, T. E.** Mechanisms and regulation of polymorphonuclear leukocyte and eosinophil adherence to human airway epithelial cells. *Am J Respir Cell Mol Biol*. 1999;21(3):418-427.

189. **Zemans, R. L., Colgan, S. P. , and Downey, G. P.** Transepithelial migration of neutrophils: mechanisms and implications for acute lung injury. *Am J Respir Cell Mol Biol*. 2009;40(5):519-535.

190. **Simon, R. H., DeHart, P. D. , and Todd, R. F., 3rd**. Neutrophil-induced injury of rat pulmonary alveolar epithelial cells. *J Clin Invest*. 1986;78(5):1375-1386.

191. **Wang, S. Z., Hallsworth, P. G., Dowling, K. D., Alpers, J. H., Bowden, J. J. , and Forsyth, K. D.** Adhesion molecule expression on epithelial cells infected with respiratory syncytial virus. *Eur Respir J*. 2000;15(2):358-366.

192. **Arnold, R., Konig, B., Galatti, H., Werchau, H. , and Konig, W.** Cytokine (IL-8, IL-6, TNF-alpha) and soluble TNF receptor-I release from human peripheral blood mononuclear cells after respiratory syncytial virus infection. *Immunology*. 1995;85(3):364-372.

193. **Arnold, R., Werchau, H. , and Konig, W.** Expression of adhesion molecules (ICAM-1, LFA-3) on human epithelial cells (A549) after respiratory syncytial virus infection. *Int Arch Allergy Immunol*. 1995;107(1-3):392-393.

194. **Faden, H., Hong, J. J. , and Ogra, P. L.** Interaction of polymorphonuclear leukocytes and viruses in humans: adherence of polymorphonuclear leukocytes to respiratory syncytial virus-infected cells. *J Virol*. 1984;52(1):16-23.

195. **Levine, S., Klaiber-Franco, R. , and Paradiso, P. R.** Demonstration that glycoprotein G is the attachment protein of respiratory syncytial virus. *J Gen Virol*. 1987;68 (Pt 9):2521-2524.

196. **Collins, P. L. , and Mottet, G.** Post-translational processing and oligomerization of the fusion glycoprotein of human respiratory syncytial virus. *J Gen Virol*. 1991;72 (Pt 12):3095-3101.

197. **Fuentes, S., Tran, K. C., Luthra, P., Teng, M. N. , and He, B.** Function of the respiratory syncytial virus small hydrophobic protein. *J Virol*. 2007;81(15):8361-8366.

198. **Karron, R. A., Wright, P. F., Crowe, J. E., Jr., Clements-Mann, M. L., Thompson, J., Makhene, M., Casey, R. , and Murphy, B. R.** Evaluation of two live, cold-passaged, temperature-sensitive respiratory syncytial virus vaccines in chimpanzees and in human adults, infants, and children. *J Infect Dis*. 1997;176(6):1428-1436.

199. **Hallak, L. K., Collins, P. L., Knudson, W. , and Peeples, M. E.** Iduronic acid-containing glycosaminoglycans on target cells are required for efficient respiratory syncytial virus infection. *Virology*. 2000;271(2):264-275.

200. **Martinez, I. , and Melero, J. A.** Binding of human respiratory syncytial virus to cells: implication of sulfated cell surface proteoglycans. *J Gen Virol*. 2000;81(Pt 11):2715-2722.

201. **Collins, P. L. , and Mottet, G.** Oligomerization and post-translational processing of glycoprotein G of human respiratory syncytial virus: altered O-glycosylation in the presence of brefeldin A. *J Gen Virol*. 1992;73 (Pt 4):849-863.

202. **Palomo, C., Garcia-Barreno, B., Penas, C. , and Melero, J. A.** The G protein of human respiratory syncytial virus: significance of carbohydrate side-chains and the C-terminal end to its antigenicity. *J Gen Virol*. 1991;72 (Pt 3):669-675.

203. **Karron, R. A., Wright, P. F., Belshe, R. B., Thumar, B., Casey, R., Newman, F., Polack, F. P., Randolph, V. B., Deatly, A., Hackell, J., et al.** Identification of a recombinant live attenuated respiratory syncytial virus vaccine candidate that is highly attenuated in infants. *J Infect Dis*. 2005;191(7):1093-1104.

204. **Feldman, S. A., Hendry, R. M. , and Beeler, J. A.** Identification of a linear heparin binding domain for human respiratory syncytial virus attachment glycoprotein G. *J Virol*. 1999;73(8):6610-6617.

205. **Gorman, J. J., Ferguson, B. L., Speelman, D. , and Mills, J.** Determination of the disulfide bond arrangement of human respiratory syncytial virus attachment (G) protein by matrix-assisted laser desorption/ionization time-of-flight mass spectrometry. *Protein Sci*. 1997;6(6):1308-1315.

206. **Langedijk, J. P., Schaaper, W. M., Meloen, R. H. , and van Oirschot, J. T.** Proposed three-dimensional model for the attachment protein G of respiratory syncytial virus. *J Gen Virol*. 1996;77 (Pt 6):1249-1257.

207. **Didcock, L., Young, D. F., Goodbourn, S. , and Randall, R. E.** The V protein of simian virus 5 inhibits interferon signalling by targeting STAT1 for proteasome-mediated degradation. *J Virol*. 1999;73(12):9928-9933.

208. **Didcock, L., Young, D. F., Goodbourn, S. , and Randall, R. E.** Sendai virus and simian virus 5 block activation of interferon-responsive genes: importance for virus pathogenesis. *J Virol*. 1999;73(4):3125-3133.

209. **Bossert, B. , and Conzelmann, K. K.** Respiratory syncytial virus (RSV) nonstructural (NS) proteins as host range determinants: a chimeric bovine RSV with NS genes from human RSV is attenuated in interferon-competent bovine cells. *J Virol*. 2002;76(9):4287-4293.

210. **Young, D. F., Andrejeva, L., Livingstone, A., Goodbourn, S., Lamb, R. A., Collins, P. L., Elliott, R. M. , and Randall, R. E.** Virus replication in engineered human cells that do not respond to interferons. *J Virol*. 2003;77(3):2174-2181.

211. **Fulcher, M. L., Gabriel, S., Burns, K. A., Yankaskas, J. R. , and Randell, S. H.** Well-differentiated human airway epithelial cell cultures. *Methods Mol Med*. 2005;107:183-206.

212. **Collins, P. L., Hill, M. G., Camargo, E., Grosfeld, H., Chanock, R. M. , and Murphy, B. R.** Production of infectious human respiratory syncytial virus from cloned cDNA confirms an essential role for the transcription elongation factor from the 5' proximal open reading frame of the M2 mRNA in gene expression and provides a capability for vaccine development. *Proc Natl Acad Sci U S A*. 1995;92(25):11563-11567.

213. **Spann, K. M., Collins, P. L. , and Teng, M. N.** Genetic recombination during coinfection of two mutants of human respiratory syncytial virus. *J Virol*. 2003;77(20):11201-11211.

214. **Iseni, F., Garcin, D., Nishio, M., Kedersha, N., Anderson, P. , and Kolakofsky, D.** Sendai virus trailer RNA binds TIAR, a cellular protein involved in virus-induced apoptosis. *Embo J*. 2002;21(19):5141-5150.

215. **Walsh, E. E. , and Hruska, J.** Monoclonal antibodies to respiratory syncytial virus proteins: identification of the fusion protein. *J Virol*. 1983;47(1):171-177.

216. **Hall, C. B.** Respiratory syncytial virus and parainfluenza virus. *N Engl J Med*. 2001;344(25):1917-1928.

217. **Scull, M. A., Gillim-Ross, L., Santos, C., Roberts, K. L., Bordonali, E., Subbarao, K., Barclay, W. S. , and Pickles, R. J.** Avian Influenza virus glycoproteins restrict virus replication and spread through human airway epithelium at temperatures of the proximal airways. *PLoS Pathog*. 2009;5(5):e1000424.

218. **Schaap-Nutt, A., Liesman, R., Bartlett, E. J., Scull, M. A., Collins, P. L., Pickles, R. J. , and Schmidt, A. C.** Human parainfluenza virus serotypes differ in their kinetics of replication and cytokine secretion in human tracheobronchial airway epithelium. *Virology*. 2012;433(2):320-328.

219. **Wright, P. F., Karron, R. A., Madhi, S. A., Treanor, J. J., King, J. C., O'Shea, A., Ikizler, M. R., Zhu, Y., Collins, P. L., Cutland, C., et al.** The interferon antagonist NS2 protein of respiratory syncytial virus is an important virulence determinant for humans. *J Infect Dis*. 2006;193(4):573-581.

220. **Biacchesi, S., Skiadopoulos, M. H., Tran, K. C., Murphy, B. R., Collins, P. L. , and Buchholz, U. J.** Recovery of human metapneumovirus from cDNA: optimization of growth in vitro and expression of additional genes. *Virology*. 2004;321(2):247-259.

221. **He, B., Paterson, R. G., Ward, C. D. , and Lamb, R. A.** Recovery of infectious SV5 from cloned DNA and expression of a foreign gene. *Virology*. 1997;237(2):249-260.

222. **Durbin, A. P., Hall, S. L., Siew, J. W., Whitehead, S. S., Collins, P. L. , and Murphy, B. R.** Recovery of infectious human parainfluenza virus type 3 from cDNA. *Virology*. 1997;235(2):323-332.

223. **Zhang, L., Button, B., Gabriel, S. E., Burkett, S., Yan, Y., Skiadopoulos, M. H., Dang, Y. L., Vogel, L. N., McKay, T., Mengos, A., et al.** CFTR delivery to 25% of surface epithelial cells restores normal rates of mucus transport to human cystic fibrosis airway epithelium. *PLoS Biol*. 2009;7(7):e1000155.

224. **Zhang, L., Limberis, M. P., Thompson, C., Antunes, M. B., Luongo, C., Wilson, J. M., Collins, P. L. , and Pickles, R. J.** alpha-Fetoprotein gene delivery to the nasal epithelium of nonhuman primates by human parainfluenza viral vectors. *Hum Gene Ther*. 2010;21(12):1657-1664.

225. **Kesimer, M., Ehre, C., Burns, K. A., Davis, C. W., Sheehan, J. K. , and Pickles, R. J.** Molecular organization of the mucins and glycocalyx underlying mucus transport over mucosal surfaces of the airways. *Mucosal Immunol*. 2013;6(2):379-392.

226. **Bukreyev, A., Marzi, A., Feldmann, F., Zhang, L., Yang, L., Ward, J. M., Dorward, D. W., Pickles, R. J., Murphy, B. R., Feldmann, H., et al.** Chimeric human parainfluenza virus bearing the Ebola virus glycoprotein as the sole surface protein is immunogenic and highly protective against Ebola virus challenge. *Virology*. 2009;383(2):348-361.

227. **Sisson, J. H., Stoner, J. A., Ammons, B. A. , and Wyatt, T. A.** All-digital image capture and whole-field analysis of ciliary beat frequency. *J Microsc*. 2003;211(Pt 2):103-111.

228. From the American Academy of Pediatrics: Policy statements--Modified recommendations for use of palivizumab for prevention of respiratory syncytial virus infections. *Pediatrics*. 2009;124(6):1694-1701.

229. **Sims, A. C., Baric, R. S., Yount, B., Burkett, S. E., Collins, P. L. , and Pickles, R. J.** Severe acute respiratory syndrome coronavirus infection of human ciliated airway epithelia: role of ciliated cells in viral spread in the conducting airways of the lungs. *J Virol*. 2005;79(24):15511-15524.

230. **Thompson, C. I., Barclay, W. S., Zambon, M. C. , and Pickles, R. J.** Infection of human airway epithelium by human and avian strains of influenza a virus. *J Virol*. 2006;80(16):8060-8068.

231. **Liu, C., Sharp, E. , and Collins, J.** Studies on the pathogenesis of parainfluenza type 3 virus infection in hamsters. *Arch Gesamte Virusforsch*. 1968;24(3):203-219.

232. **Christensen, T. G., Breuer, R., Hornstra, L. J., Lucey, E. C. , and Snider, G. L.** The ultrastructure of hamster bronchial epithelium. *Exp Lung Res*. 1987;13(3):253-277.

233. **Aherne, W., Bird, T., Court, S. D., Gardner, P. S. , and McQuillin, J.** Pathological changes in virus infections of the lower respiratory tract in children. *J Clin Pathol*. 1970;23(1):7-18.

234. **Simpson, W., Hacking, P. M., Court, S. D. , and Gardner, P. S.** The radiological findings in respiratory syncytial virus infection in children. II. The correlation of radiological categories with clinical and virological findings. *Pediatr Radiol*. 1974;2(3):155-160.

235. **Hall, C. B., Douglas, R. G., Jr. , and Geiman, J. M.** Respiratory syncytial virus infections in infants: quantitation and duration of shedding. *J Pediatr*. 1976;89(1):11-15.

236. **Newman, J. T., Surman, S. R., Riggs, J. M., Hansen, C. T., Collins, P. L., Murphy, B. R. , and Skiadopoulos, M. H.** Sequence analysis of the Washington/1964 strain of human parainfluenza virus type 1 (HPIV1) and recovery and characterization of wild-type recombinant HPIV1 produced by reverse genetics. *Virus Genes*. 2002;24(1):77-92.

237. **Livraghi, A., Grubb, B. R., Hudson, E. J., Wilkinson, K. J., Sheehan, J. K., Mall, M. A., O'Neal, W. K., Boucher, R. C. , and Randell, S. H.** Airway and lung pathology due to mucosal surface dehydration in {beta}-epithelial Na+ channel-overexpressing mice: role of TNF-{alpha} and IL-4R{alpha} signaling, influence of neonatal development, and limited efficacy of glucocorticoid treatment. *J Immunol*. 2009;182(7):4357-4367.

238. **Cao, R., Wang, T. T., DeMaria, G., Sheehan, J. K. , and Kesimer, M.** Mapping the protein domain structures of the respiratory mucins: a mucin proteome coverage study. *J Proteome Res*. 2012;11(8):4013-4023.

239. **Sardiu, M. E. , and Washburn, M. P.** Enriching quantitative proteomics with SI(N). *Nat Biotechnol*. 2010;28(1):40-42.

240. **Bartlett, E. J., Hennessey, M., Skiadopoulos, M. H., Schmidt, A. C., Collins, P. L., Murphy, B. R. , and Pickles, R. J.** Role of interferon in the replication of human parainfluenza virus type 1 wild type and mutant viruses in human ciliated airway epithelium. *J Virol*. 2008;82(16):8059-8070.

241. **Schaap-Nutt, A., Scull, M. A., Schmidt, A. C., Murphy, B. R. , and Pickles, R. J.** Growth restriction of an experimental live attenuated human parainfluenza virus type 2 vaccine in human ciliated airway epithelium in vitro parallels attenuation in African green monkeys. *Vaccine*. 2010;28(15):2788-2798.

242. **Hoffmann, E., Dittrich-Breiholz, O., Holtmann, H. , and Kracht, M.** Multiple control of interleukin-8 gene expression. *J Leukoc Biol*. 2002;72(5):847-855.

243. **Villenave, R., O'Donoghue, D., Thavagnanam, S., Touzelet, O., Skibinski, G., Heaney, L. G., McKaigue, J. P., Coyle, P. V., Shields, M. D. , and Power, U. F.** Differential cytopathogenesis of respiratory syncytial virus prototypic and clinical isolates in primary pediatric bronchial epithelial cells. *Virol J*. 2011;8:43.

244. **Papin, J. F., Wolf, R. F., Kosanke, S. D., Jenkins, J. D., Moore, S. N., Anderson, M. P. , and Welliver, R. C., Sr.** Infant Baboons Infected with Respiratory Syncytial Virus Develop Clinical and Pathologic Changes that Parallel Those of Human Infants. *Am J Physiol Lung Cell Mol Physiol*. 2013.

245. **Burke, E., Dupuy, L., Wall, C. , and Barik, S.** Role of cellular actin in the gene expression and morphogenesis of human respiratory syncytial virus. *Virology*. 1998;252(1):137-148.

246. **Garcia-Barreno, B., Jorcano, J. L., Aukenbauer, T., Lopez-Galindez, C. , and Melero, J. A.** Participation of cytoskeletal intermediate filaments in the infectious cycle of human respiratory syncytial virus (RSV). *Virus Res*. 1988;9(4):307-321.

247. **Kallewaard, N. L., Bowen, A. L. , and Crowe, J. E., Jr.** Cooperativity of actin and microtubule elements during replication of respiratory syncytial virus. *Virology*. 2005;331(1):73-81.

248. **Ulloa, L., Serra, R., Asenjo, A. , and Villanueva, N.** Interactions between cellular actin and human respiratory syncytial virus (HRSV). *Virus Res*. 1998;53(1):13-25.

249. **Caulin, C., Salvesen, G. S. , and Oshima, R. G.** Caspase cleavage of keratin 18 and reorganization of intermediate filaments during epithelial cell apoptosis. *J Cell Biol*. 1997;138(6):1379-1394.

250. **Ku, N. O. , and Omary, M. B.** Identification of the major physiologic phosphorylation site of human keratin 18: potential kinases and a role in filament reorganization. *J Cell Biol*. 1994;127(1):161-171.

251. **Liao, J., Ku, N. O. , and Omary, M. B.** Two-dimensional gel analysis of glandular keratin intermediate filament phosphorylation. *Electrophoresis*. 1996;17(11):1671-1676.

252. **Liao, J., Lowthert, L. A., Ku, N. O., Fernandez, R. , and Omary, M. B.** Dynamics of human keratin 18 phosphorylation: polarized distribution of phosphorylated keratins in simple epithelial tissues. *J Cell Biol*. 1995;131(5):1291-1301.

253. **Cannon, M. J., Openshaw, P. J. , and Askonas, B. A.** Cytotoxic T cells clear virus but augment lung pathology in mice infected with respiratory syncytial virus. *J Exp Med*. 1988;168(3):1163-1168.